

POLITECNICO DI TORINO

Master of Science Course in Mechatronic Engineering

Master Degree Thesis

Initial analysis of the reaction wheels disturbances impact on the attitude control system of a small satellite



Supervisor

PROF. Carlo Novara

Internship Supervisors

DR. Gabriella Caporaletti

PROF. Francesco Donati

Candidate

Stefano Oliva

Academic Year 2019/2020

Contents

Introduction	iv
1 CubeSats and Reaction Wheels	1
1.1 A brief overview on CubeSats	1
1.2 Reaction wheels for attitude control	5
1.2.1 Working principle	5
1.2.2 Marketplace availability nowadays	8
1.2.3 RWs disturbances: state of art and its application	11
2 The attitude control problem	21
2.1 Main goals of the attitude control	22
2.2 A general control scheme and its subsystems	23
2.3 MATLAB/Simulink implementation	44
2.4 EICASLAB implementation	49
3 Benchmark control system	52
3.1 Reference generator and control inputs: specific analysis	53
3.2 Benchmark controller general analysis	55
3.3 MATLAB/Simulink implementation	61
3.4 EICASLAB implementation	64
4 New approach for the control system	68
4.1 Feedback linearisation approach	69
4.2 Linear controller: pole placement design	82
4.3 Non-linear controller: sliding mode design	86
4.4 Reference generator and control inputs: specific analysis	94

<i>CONTENTS</i>	iii
4.5 MATLAB/Simulink implementation	96
4.6 EICASLAB implementation	103
5 Simulation results and comparisons	108
5.1 Simulations without disturbances	109
5.2 Simulation results with disturbances	123
5.3 Comments and comparisons	137
Conclusions and future works	139
Bibliography	141

Introduction

The following work of thesis is aimed to deeply analyse the effects of reaction wheels (RWs) on the attitude control of a small satellite, also known as CubeSat. In particular, it has been studied how the RWs affect the pointing stability of a telescope, mounted on the satellite, when it is necessary performing a photometric analysis of a target star. The strong interest behind the study of the RWs effects is due to their huge impact on the quality of stars observation. Indeed, the RWs tend to induce an oscillating motion on the satellite which strongly influences the telescope pointing stability. Therefore, if the telescope is not stable enough, the measured stars brightness will be strongly different from the real one and this situation compromises the photometric analysis of the target star, which is incredibly useful to study the stellar activity, transiting exoplanets or other astrophysical phenomena. As mentioned before, the telescope is located inside a satellite whose dimensions are really small. The CubeSats are specific types of satellites conceived to significantly reduce in the costs. For this reason, the first element that must be reduced is the dimension. For instance, as it will be described in the following chapter, a $3U$ (three units) CubeSat has the following dimensions: $10 \times 10 \times 30 \text{ cm}$. Therefore, the system under analysis is really compact. Another key element about the costs reduction is the shrunk launch expenses due to the decreased fuel amount related to the low weight of these satellites. Moreover, there is a continuous research of low cost electronic and non-electronic devices, to be put inside the satellite, able to guarantee a good level of quality despite of their cost. This is done to decrease, as much as possible, the expenses related to the satellite.

All the analyses of this thesis has been performed on a $3U$ CubeSat.

The first step towards the final goal is to understand, at first, what reaction

wheels are and how they are employed to control the satellite attitude and, then, what are the effects that strongly influence the pointing performance. A reaction wheel is, basically, a flywheel connected to an electric motor which is suitably supplied to make the wheel rotate. This is one of lots of actuator that can be used to modify the attitude of satellite. However, the reaction wheels are chosen among the other devices, for the application under analysis, because they are cheaper, smaller and lighter and offer a continuous, smooth and moderately intense control action, which allows to obtain a really precise pointing action. The reaction wheels are located inside the satellite according to specific configurations. Their working principle is quite simple since they exploit the angular momentum conservation principle to put the satellite in motion. Indeed, when a RW is activated by the electric motor, through a suitable torque, since the overall angular momentum must not vary, the reaction wheel produces on the CubeSat a torque equal and opposite to the received one and in this way it starts the rotation of the satellite. However, the motion of the RWs is a source of disturbances that modify the desired CubeSat attitude. In particular, they create a kind of oscillating motion, called jitter, which affect the telescope pointing stability. The main reasons behind these disturbances are the shift of the center of mass from the central rotation axis (static unbalance) and the inclination of the principal axis of inertia with respect to the rotation axis (dynamic unbalance). The disturbances model is a bit more complex since they are represented by a sum of sinusoidal waves (harmonic analysis) where the static and dynamic unbalance are defined by the first harmonic, which is the stronger contribution among all the other harmonics.

The characterization of the disturbances is done through a set of forces and pure torques expressed in the wheels reference frames, that are located at the wheels center. These pure moments and the ones coming from the forces are responsible for the attitude modification with respect to an inertial reference frame.

The second step of this work of thesis is to start evaluating the objectives of the control structure and defining all the elements that compose the closed loop system. About the main objectives, it is important to highlight that a disturbance-free analysis of the system has been necessary in order to eval-

uate the basic performance of the control system. In particular, it has been evaluated the value of the RMS pointing error that can be reached before the application of the disturbances. Then, it has been studied the effect of the disturbances on the pointing error with particular attention to the amplitude of the oscillating signal and, therefore, the influence on the overall RMS value. Indeed, if the main objective of the disturbance-free analysis is to try having a small RMS pointing error, the fundamental goal of the disturbances analysis is to reduce the amplitude of the oscillations of the error. As mentioned before, a quite strong oscillation can deeply affect the telescope pointing stability which results in a poor photometric analysis. Moreover, the study of the control system performance can be enriched with the effect of the uncertainty related to some parameters of the CubeSat (Plant). This means that it is possible to evaluate how a variation of the plant characteristic, blinded to the controller, can modify the overall performance and, so, to identify robustness properties of the specific controller. However, this analysis has not been performed in this thesis, but it has been considered as future works.

Instead, about the control system structure, it is really important to highlight that it varies, more or less significantly, according to the kind of controller that is employed in the overall system. It is worth saying that, before studying the controller structure, two important systems has been analysed through their constitutive equations: the satellite (known as plant, with a non-linear dynamic) and the reaction wheels set (actuators). Then, according to the controller type, another fundamental system has been studied i.e the reference generator, which is responsible to generate the signal that must be tracked.

As far as the controller is concerned, it must be noticed that digital controllers have been considered. Actually, the quantization process and its effects have been neglected and only a discrete approach has been evaluated. Therefore, it has been necessary to introduce a zero-order hold to apply the control signal to the actuator, which is a continuous time system.

The starting point has been the analysis of the most used control approach (defined in this thesis as *benchmark controller*), which is, basically, characterized by a non-linear PD controller or a non-linear PD with some feedforward

terms. After a theoretical analysis of the controller contribution to the pointing error and to the disturbances attenuation, according to specific values of the controller parameters, a simulation approach has been considered. In particular, the results coming from two simulation environments has been deeply evaluated. The first one is MATLAB/Simulink, where the simulation scheme is characterized by a set of MATLAB functions plus integrators (when necessary), in order to represent the state equations or in general the characterizing equations of each subsystem. The second one is EICASLAB, which is a software suite produced by the company EICAS Automazione S.p.a where this thesis has been developed. This software was born to allow the implementation of professional controllers for lots of scientific fields, in particular the aerospace one. Its key characteristic is the C-code implementation of all the subsystems that compose the overall control scheme. Therefore, since the controller must be implemented in C-code, this is a quite useful initial step towards a real implementation of the controller on a target board, that can be employed in a real application.

Once the knowledge coming from the benchmark control system has been considered, the core of the work of thesis has been developed. This is the personal contribution to the subject under analysis. Therefore, a new control approach has been studied in order to evaluate its effect on the telescope pointing, with and without reaction wheels disturbances. The new approach is characterized by an input-output feedback linearization controller, which is aimed to cancel the non-linearities of the plant. As it will be deeply discussed, the system under analysis is a MIMO one and the application of the feedback linearization allows to implement a specific decoupling in SISO subsystems. Once this procedure has been completed, another controller responsible for managing the input-output dynamic has been designed, to be placed before the previous one. In particular, two different types of controller has been tested in order to highlight important differences between them and with respect to the benchmark controller. The first one follows the pole placement technique, where the position of the desired closed loop pole is defined. Then, through suitable matrices, a specific linear control law is designed in order to respect the poles position. The second one exploits the sliding mode control theory. This approach leads to the definition of a

non-linear control law due to the presence of a specific non-linear term which, in general, guarantees robustness to the control system. As it will be deeply developed, this approach is based on the formulation of the so called "sliding surface", which is a specific multi-dimensional entity that must be reached by the system trajectory (starting from the initial condition) in order to guarantee the convergence of the outputs to the desired reference signals. Also in this case, after a deep theoretical analysis of the control system behaviour, specific simulations schemes have been developed, in the MATLAB/Simulink and EICASLAB environment, to verify the performance of the control system.

Once all the simulations results have been collected, a careful analysis of each of them and a deep cross-comparison have been conducted to highlight pros and cons of the different control approaches that have been studied. In particular, the simulations results have been useful to evaluate whether the new control approach is worth being implemented in a real application.

Chapter 1

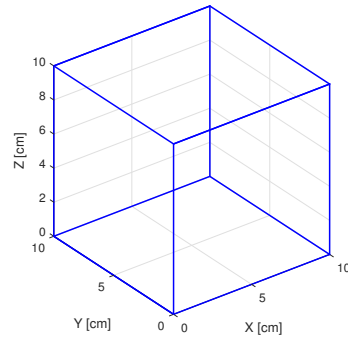
CubeSats and Reaction Wheels

1.1 A brief overview on CubeSats

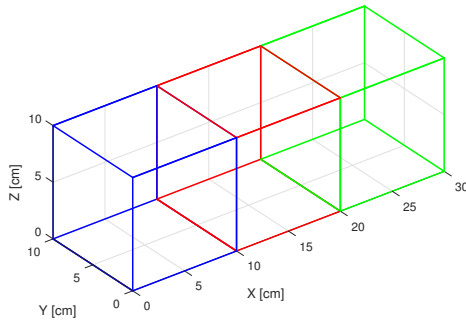
A CubeSat is a kind of small satellite that was initially conceived for educational purposes. However, since 2012 a huge number of CubeSats have been employed for real aerospace applications. There are lots of reasons behind their success. The key element of the CubeSats is saving money. Indeed, in the satellite world, there is a continuous research on how reducing implementations expenses (when this is possible according to the specific application). The first element related to the costs reduction is the decreased dimensions of a CubeSat, which is defined as a small satellite. It is worth noticing that the small satellites classification involves structures whose weight goes from 0.1 g (zepto satellites) to 500 Kg (mini satellites).

The CubeSats are cube-shaped satellites where a specific measurement unit is defined, known as U , that corresponds to a $10\times 10\times 10\text{ cm}$ cube. This is the smallest CubeSat possible. All the other configurations are defined as integer multiples of the unit U and, basically, are built by assembling more cubes together. For example, it is possible to consider a $3U$ or $6U$ satellite, whose dimensions are respectively $10\times 10\times 30\text{ cm}$ and $10\times 20\times 30\text{ cm}$. Figure 2.1 shows a basic representation of CubeSat $1U$, $3U$ and $6U$.

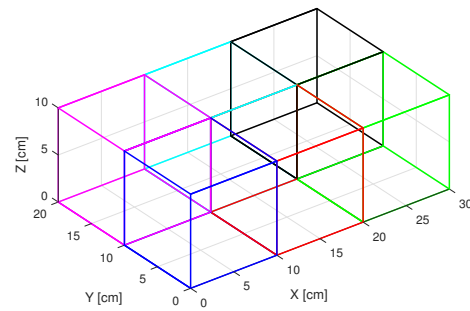
The second element related to the cost reduction is that the launch expenses are significantly shrunk. Indeed, since the CubeSat weight is not so high, it is not necessary a huge amount of fuel to put it in the Earth's orbit. More-



(a) CubeSat 1U



(b) CubeSat 3U



(c) CubeSat 6U

Figure 1.1: Schematic representations of CubeSats

over, in order to be compliant with the cost reduction philosophy, there is a constant research of electronic and non-electronic devices, to be placed in the satellite, characterized by a proper trade off between costs and quality, according to the specific objectives that the missions wants to reach.

The CubeSats are basically composed by six subsystems, as mentioned in [5] and shown in figure 2.2:

- **Structure:** CubeSats are basically composed by aluminium alloys.
- **Communication system:** for ground communications (transmission and reception of signals), CubeSats employ an antenna that exploits bands like VHF, UHF or X.

- **Power system:** it is characterized by solar panels or batteries. Solar panel are more used then batteries since the latter need more space and, in general, they increases the overall system complexity.
- **Control:** the control system is useful to keep the satellite in a specific attitude with respect to a reference frame. It is worth saying that the control subsystem involves also the actuator (like reaction wheels) and attitude determination systems (like star trackers).
- **Computing system:** this system is used for many operations like health monitoring, payload data processing and analysis, etc.
- **Payload:** the characteristics of this subsystem strongly depend on the mission objectives. For instance, it could be a telescope to perform stellar observations.

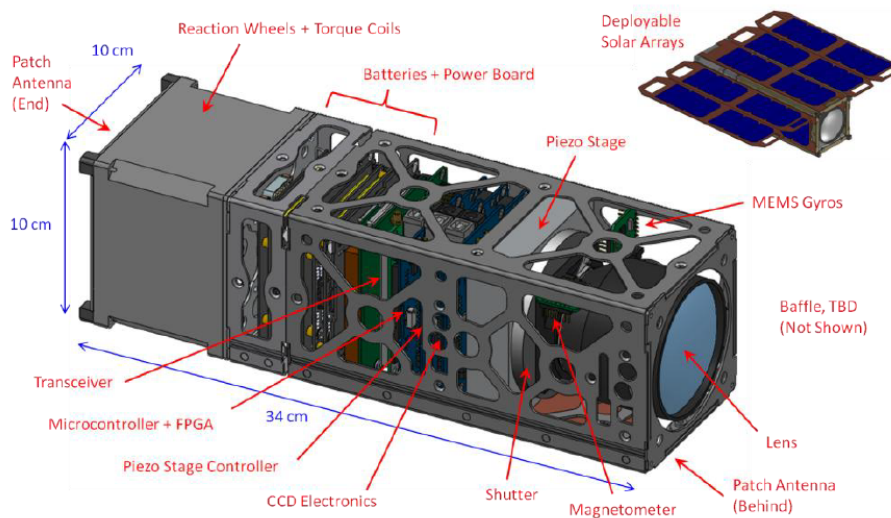


Figure 1.2: A 3U CubeSat with its subsystems [11]

CubeSats are in general placed on a LEO orbit (Low Earth Orbit) whose altitude varies from 160 *Km* to 2000 *Km* with an eccentricity less than 0.25, with an orbital period strictly related to the altitude. An example of CubeSat is the 6U one employed in the NASA/JPL and MIT project known as ASTERIA (Arcsecond Space Telescope Enabling Research in Astrophysics),

shown in figure 2.3. The main goal of the ASTERIA mission was to obtain arcsecond-level pointing error with respect to the desired star, in order to perform a correct photometric analysis, which is a fundamental element to correctly study stellar activities, transiting planets and other astrophysical phenomena. In particular, the ASTERIA mission was able to reach a RMS pointing error of 0.5 arcseconds, over 20 minutes of observation, which is much lower than the preliminary requirement of 5 arcseconds.

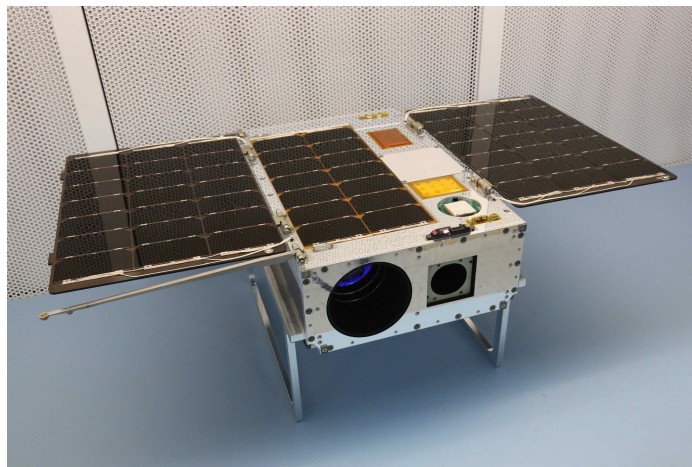


Figure 1.3: ASTERIA 6 *U* CubeSat [13]

1.2 Reaction wheels for attitude control

This section will focus on some important aspects of the reaction wheels that are usually employed in CubeSat. The starting point will be the analysis of some characteristic of these actuators, followed by the explanation of their working principle. Then, it will be introduced a brief overview on the marketplace availability about RWs. Finally, the most important aspect of RWs will be deeply analysed i.e. the disturbances produced by the wheels rotation. In particular, it will be shown the state of art about disturbances modelling and then its application to the specific case analysed in this work of thesis.

1.2.1 Working principle

A reaction wheel is an actuator, placed inside the satellite, responsible for the spacecraft attitude modification with respect to an inertial reference frame. It is composed by a flywheel connected to an electrical motor, in general a DC-Brushless, which makes the wheel rotate, as shown by figure 1.4. They



Figure 1.4: A real reaction wheel [3]

are greatly used in CubeSats due to the reduced dimensions and so weight and their ability of producing a continuous, smooth and moderately intense control action which is fundamental to have a precise pointing action. Moreover, by using a reaction wheel it is completely avoided the problem of using propulsion devices which require a suitable amount of propellant and, therefore, their management is more expensive. Then, since a reaction wheel is in general lighter than other kinds of actuators, the expenses related to the

launch operations are significantly shrunk due to the reduced amount of necessary fuel to put the satellite in the Earth's orbit.

To understand the working principle of a reaction wheel, let's consider the system in figure 1.5, which is composed by a cubic satellite body and a RW, where the vehicle (satellite bus plus RW) body frame is placed in its CoM and the axes coincide with the principal axes of inertia. A reaction wheel exploits the angular momentum conservation principle which states that: "*in absence of external applied moments, the total angular momentum of the system, evaluated in an inertial frame, does not vary*". Therefore, with respect to the system in figure, it is possible to write the following relation:

$$\mathbf{M}_{ext} = \dot{\mathbf{H}}_I = \dot{\mathbf{H}}_I^{(sc)} + \dot{\mathbf{H}}_I^{(w)} \Rightarrow \mathbf{0} = \dot{\mathbf{H}}_I = \dot{\mathbf{H}}_I^{(sc)} + \dot{\mathbf{H}}_I^{(w)} \quad (1.1)$$

or equivalently

$$\mathbf{H}_I = \mathbf{H}_I^{(sc)} + \mathbf{H}_I^{(w)} = const \quad (1.2)$$

where the subscript I defines that the specific quantity is evaluated in the

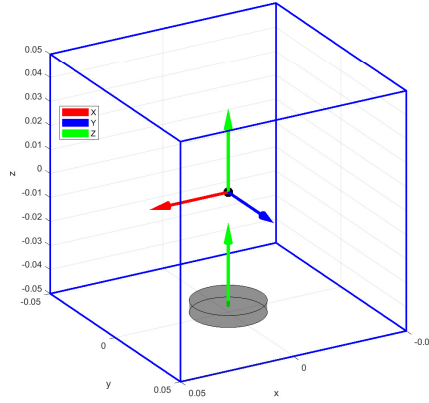


Figure 1.5: Schematic representation of cubic satellite with reaction wheel

inertial reference frame, the superscript (sc) refers to the spacecraft total angular momentum variation and (w) specifies the wheel angular momentum variation. It is really important to highlight that, as discussed in [8], $\mathbf{H}_I^{(sc)}$ defines the total angular momentum of all the rigid body i.e. the spacecraft body plus the reaction wheel mass concentrated at its center of mass. Instead,

$\mathbf{H}_I^{(w)}$ represents the net angular momentum of the reaction wheel about its center of mass. Moreover, both \mathbf{H}_I and $\mathbf{H}_I^{(sc)}$ are referred to the overall system center of mass (spacecraft/satellite body+wheel).

Therefore, when the electric motor of the RW puts in rotation the flywheel, by applying a suitable torque, the latter exerts the same torque in magnitude but opposite in sense to the satellite, since the angular momentum conservation principle must be verified. In this way, the satellite will start rotating, in the opposite sense with respect to the RW one, about an axis parallel to the RW rotation axis and passing through the center of mass (indeed, since the RW applies only a torque, the rotation will necessary be about the CoM). For the situation of figure 1.5, the satellite will start rotating about the body frame x-axis. With this mechanism it is possible to change the attitude of the CubeSat. It is interesting to notice that, the CoM of the satellite bus is very close to the overall spacecraft one, due to the really small contribution coming from the RW mass. So, if we neglect this difference, the CoM of the satellite bus coincides with the spacecraft one. This means that it is not important where the RW is placed (always on a plane parallel to the one in figure), because the spacecraft will rotate always about an axis passing through the CoM.

As it will be shown later, the same approach is considered when more than one RW is placed inside the spacecraft. In general, it is needed at least three reaction wheels (suitably placed) to perform a complete attitude change. For instance, it is possible to have three orthogonal wheels, as shown in figure 1.6, in order to rotate the spacecraft about all its three body axes.

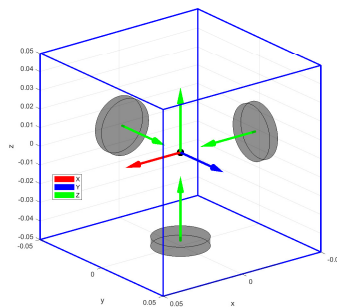


Figure 1.6: Schematic representation of cubic satellite with 3 orthogonal RWs

1.2.2 Marketplace availability nowadays

Nowadays, there are lots of reaction wheel models which can fit every mission objectives. By the way, it is crucial to properly choose the reaction wheels on the basis of the space mission requirements. Indeed, as mentioned by [2], there is a four-steps procedure that must be followed to choose the best reaction wheels.

1. **Specification of the mission parameters:** the complete set of operations that the satellite needs to perform must be clearly defined.
2. **Definition of the satellite design specifications:** it is important to check the design characteristic of the satellite, in order, for instance, to choose the correct size of the RWs with respect to the available volume.
3. **Definition of technological devices:** it is crucial to understand the characteristics of all the satellite components and subsystems. Indeed, the RWs have to properly work together with all the other elements of the satellite.
4. **Specification of the key performance criteria:** it is fundamental to figure out how to evaluate the available RWs on the marketplace with respect to the most relevant criteria for the specific applications.

Some of the key performance criteria are the following ones:

1. Size and weight.
2. Attitude control sensitivity and precision.
3. Redundancy i.e. presence of a fourth wheel

In the following part, it will be shown some of the available reactions wheel in the marketplace, as mentioned in [2].

***RW210* and *RW400* by Hyperion Technologies**

These two kinds of wheels, shown in figure 1.7, have different characteristics that fit well with different types of CubeSats. Indeed, the *RW210* is in general mounted on CubeSats from 1U to 3U. Instead, the *RW400* is used inside bigger satellites like 6 to 12U. By the way, they have specific dimensions and weight that make them suitable only for the above CubeSats. The cage of the *RW210* and *RW400* have respectively the following dimensions and weight: $25 \times 25 \times 15 \text{ mm}$ and about 21 g . Instead, the *RW400* dimensions and weight are about $50 \times 50 \times 27 \text{ mm}$ and 155 g . Consequently, the maximum torque that they can produce is linked to their dimensions. In particular, the *RW210* is able to exert a maximum torque of 0.1 mNm and the *RW400* provides a torque up to 12 mNm . Moreover, both the wheels include a simple dedicated controller.

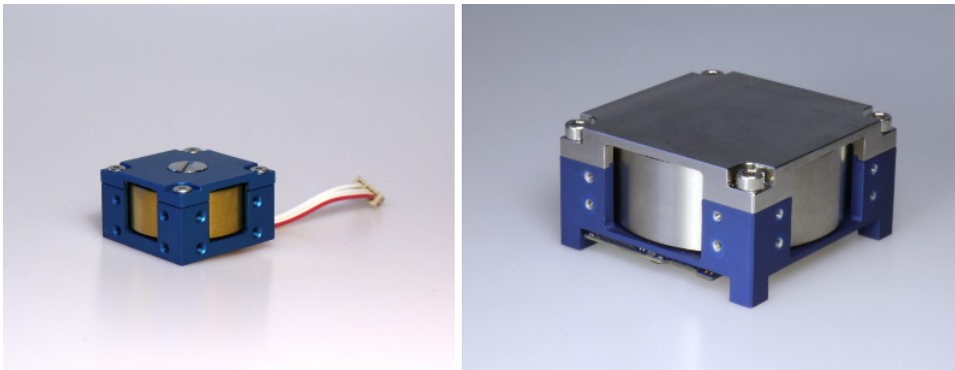


Figure 1.7: *RW210* (left) and *RW400* (right) [2]

***RW-0.01* by Sinclair Interplanetary**

Figure 1.8 shows the *RW-0.01*, whose cage dimensions are $50 \times 50 \times 30 \text{ mm}$ and a weight of 120 g . In this case, the maximum produced torque is about 1 mNm in both directions. Due to its dimensions, it is suitable for CubeSats over 6U. This RW, like all Sinclair Interplanetary's ones, is equipped with a digital processor and it can be commanded by using a serial bus to obtain the desired speed, momentum or torque. Moreover, this wheel is able to provide all the desired telemetric data useful to check the health of the wheel.

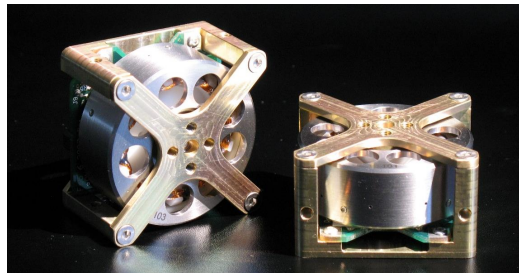


Figure 1.8: Sinclair Interplanetary *RW-0.01* [2]

***MAI-400* by Adcole Maryland Aerospace**

The *MAI-400* reaction wheel, shown by figure 1.9, has a really compact structure characterized by the following dimensions and weight: $33 \times 33 \times 38 \text{ mm}$ and 110 g . According to these dimensions, this RW is suitable for 3U CubeSats. The produced torque is up to 0.635 mNm . The motor drive electronics of this reaction wheel is located on a $1.3 \times 1.3 \text{''}$ PCB, which contains an ARM Cortex CPU.

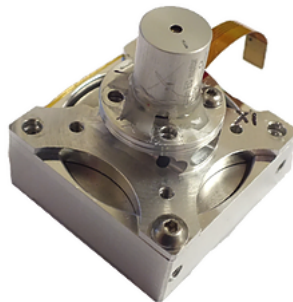


Figure 1.9: *MAI-400* RW [2]

1.2.3 RWs disturbances: state of art and its application

1.2.3.1 State of art about disturbances modelling

The main problem related to the reaction wheels is the presence of some disturbances due to their rotational motion. As it will be deeply analysed, these disturbances are represented by a set of forces (with their moments) and pure moments, which can have a huge impact on the pointing stability of the satellite telescope. Indeed, if there is not an acceptable stability of the telescope with respect to the target star, its photometric study will be strongly inaccurate. This situations will lead, in turns, to an unreliable study about, for example, the stellar activity or transiting exoplanets or other astrophysical phenomena. The following part will analyse the state of art about the reaction wheels disturbances modelling. However, before evaluate how disturbances are modelled, it is crucial to understand how they are produced. The two relevant sources of disturbances are known as static imbalance/unbalance and dynamic imbalance/unbalance.

Static unbalance

The first source is due to an asymmetric distribution of the flywheel mass in radial direction, which leads to a shift of the center of mass with respect to the point where the axis of rotation passes. This situation can be modelled with a symmetric-balanced wheel with an additional mass placed on the lateral surface of the wheel, as shown in figure 1.10. The small cubic mass is known as imbalance/unbalance mass. When the wheel is put in rotation, on the unbalance mass acts a centrifugal force expressed as

$$F_c = m_s a_c = m_s \frac{v^2}{r_s} = m_s r_s \Omega^2 \quad (1.3)$$

where m, r, Ω are respectively the weight of the unbalance mass, its distance from the rotation axis and the angular speed. From this formula is defined the parameter known as static imbalance as $mr = \frac{F_c}{\Omega^2}$. The values of F_c and Ω^2 are determined thorough specific measurements by using a dynamometer. So, the wheel is connected to this dyanamometer and it is put in rotation at different values of speed. Then, a set of force and torques is measured

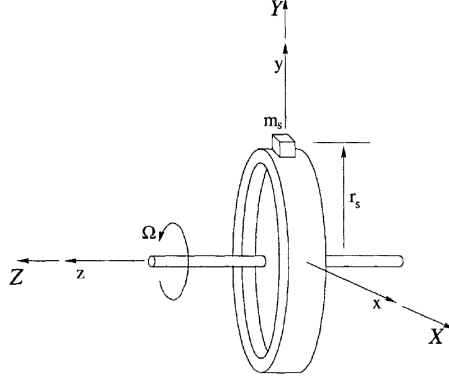


Figure 1.10: Static unbalance modelling [4]

and expressed with respect to the reference frame of the measurement device. Therefore, the obtained signals are expressed as $F_x, F_y, F_z, M_x, M_y, M_z$. These are the disturbances that the reaction wheel produces. However, since the forces and torques must be referenced with respect to the center of wheel, the moments expression must be modified in this way:

$$\mathbf{M}' = \mathbf{M}^{DF} - \mathbf{r}^{DF} \times \mathbf{F}^{DF} \quad (1.4)$$

where $\mathbf{M}', \mathbf{M}^{DF}, \mathbf{r}^{DF}, \mathbf{F}^{DF}$ corresponds to the modified moments, the moments referenced to the dynamometer frame, the distance between the origin of the dynamometer frame and the center of the wheel and the forces with respect to the measurement device frame. So, it is possible to express the new set of forces and moments as $F_x, F_y, F_z, M'_x, M'_y, M'_z$. In particular, the amplitude spectrum of all these quantities is defined by considering different values of wheel speed, in order to build the so called waterfall plot. Now, the F_c of the formula (1.3) is defined as the first harmonic amplitude that can be extracted from the waterfall plot of the signals F_x . In particular, it is evaluated the amplitude of the first harmonic in correspondence of the maximum rotational speed Ω . It is worth noticing that, for each of the measured signals, a specific harmonic analysis is done. This means that, the expression of all the forces and torques is represented by a summation of sinusoidal waves

with specific amplitude and frequency, as mentioned by [12]:

$$F_x(t) = \sum_{i=1}^N F_{x_i}(\Omega(t)) \sin(2\pi h_i \Omega(t)t + \phi_i^{F_{rad}}) \quad (1.5)$$

$$F_y(t) = \sum_{i=1}^N F_{y_i}(\Omega(t)) \sin(2\pi h_i \Omega(t)t + \phi_i^{F_{rad}} + \frac{\pi}{2}) \quad (1.6)$$

$$F_z(t) = \sum_{i=1}^N F_{z_i}(\Omega(t)) \sin(2\pi h_i \Omega(t)t + \phi_i^{F_{axial}}) \quad (1.7)$$

where h_i defines the harmonic coefficient, $\Omega(t)$ is the rotational speed expressed in Hz and $\phi_i^{F_{rad}}$, $\phi_i^{F_{axial}}$ represent random initial phases in the interval $[0, 2\pi)$. Figure 1.11 provides a graphical representation of the first five harmonics related to static imbalance, where each harmonic is defined by a mass placed at a specific radius from the rotation axis and by a rotation frequency expressed through the product $h_i\Omega$. In particular, figure 1.11 depicts the first five contributions of equations (1.5) and (1.6). The X-Y-Z frame is the wheel coordinate system, placed at its center. Moreover, it is interesting to notice the analogy of figure 1.11 with respect to figure 1.10 about the first harmonic contribution i.e. harmonic whose coefficient is 1. Indeed, the contribution coming from the centrifugal force of the unbalance mass m_s is defined by the first harmonic of $F_x(t)$ and $F_y(t)$.

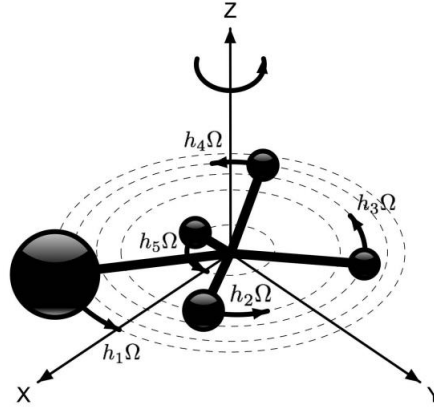


Figure 1.11: Disturbances harmonic model of the static imbalance [12]

Some comments must be done about these expressions. First of all, the amplitude of the sinusoidal waves can be represented by a proportional relation

with respect to Ω^2 as $F(\Omega(t)) = C_i\Omega^2$ where C_i is the specific coefficient related to the i^{th} harmonic, as mentioned by [10]. Then, the contribution coming from the disturbance along the Z-axis can be neglected. Furthermore, as mentioned by [12], the amplitudes of the sinusoidal waves along the X-axis and Y-axis are considered equal i.e. $F_{x_i}(\Omega(t)) = F_{y_i}(\Omega(t))$.

In this work of thesis, it will be considered only the first harmonic (fundamental) contribution, since it is the most relevant one. Finally, it must be pointed out the role that these disturbances will play in the satellite attitude modification. Indeed, the forces F_x and F_y produce moments with respect to the center of mass of the satellite, as it will be discussed in the following part.

Dynamic unbalance

The second source of disturbances is known as dynamic imbalance/unbalance which is determined by the inclination of the principal axis of inertia with respect to rotation axis, caused by an asymmetric mass distribution along the axial direction. This situation can be modelled by two cubic masses m_d placed on the lateral surfaces of the wheel, at r_d distance from the rotation axis and characterized by the h separation between them along the axis of rotation, as shown by figure 1.12. In this situation, the centrifugal forces,

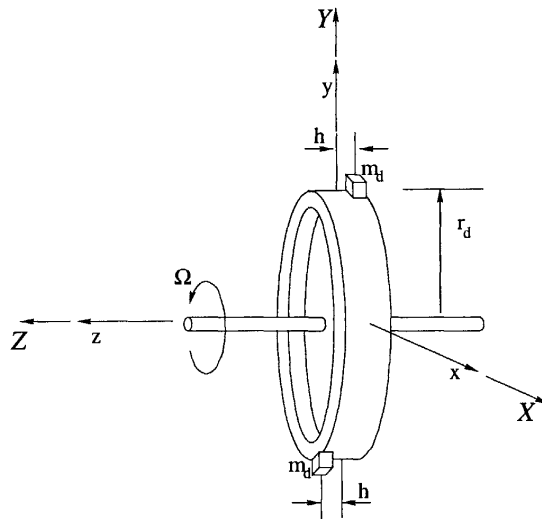


Figure 1.12: Dynamic unbalance modelling [4]

acting on both the masses, produce a couple of forces characterized by the following moment expression (pure moment):

$$\tau = F_c h = m_d a_c h = m_d \frac{v^2}{r_d} h = m_d r_d h \Omega^2 \quad (1.8)$$

From this relation, the dynamic imbalance parameter can be computed as $m_d r_d h = \frac{\tau}{\Omega^2}$ where the values of τ and Ω^2 are taken from the previously mentioned waterfall plot related to the moment along the X-axis M'_x (for notation simplicity expressed as M_x). In particular, as before, it is considered the first harmonic contribution at the maximum wheel speed.

As seen for the static imbalance, also in this case the measured moments M_x, M_y, M_z are expressed through a summation of sinusoidal wave [12], as follows:

$$M_x(t) = \sum_{i=1}^N M_{x_i}(\Omega(t)) \sin(2\pi h_i \Omega(t)t + \phi_i^{M_{rad}}) \quad (1.9)$$

$$M_y(t) = \sum_{i=1}^N M_{y_i}(\Omega(t)) \sin(2\pi h_i \Omega(t)t + \phi_i^{M_{rad}} + \frac{\pi}{2}) \quad (1.10)$$

$$M_z(t) = \sum_{i=1}^N M_{z_i}(\Omega(t)) \sin(2\pi h_i \Omega(t)t + \phi_i^{M_{axial}}) \quad (1.11)$$

where h_i defines the harmonic coefficient, $\Omega(t)$ is the rotational speed expressed in Hz and $\phi_i^{M_{rad}}, \phi_i^{M_{axial}}$ represent random initial phases in the interval $[0, 2\pi)$. Figure 1.13 represents the first three harmonic of the moments related to the dynamic imbalance. In particular, this figure shows the first three harmonic contribution expressed by equations (1.9) and (1.10). Also in this case, it is worth evaluating the analogy of figure 1.12 with respect to figure 1.13 about the first harmonic contribution. Indeed, the contribution coming from the moment of centrifugal forces acting on the unbalance masses m_d is defined by the first harmonic of $M_x(t)$ and $M_y(t)$ (planar contribution). Finally, the same fundamental comments done for the static imbalance about the proportionality relation about the amplitude of sinusoids, the negligible contribution of axial component, the equality of the sinusoids amplitude about X and Y axes and the evaluation of only the fundamental harmonic contribution (due to its relevancy with respect to the other harmonics) can be repeated in this case.

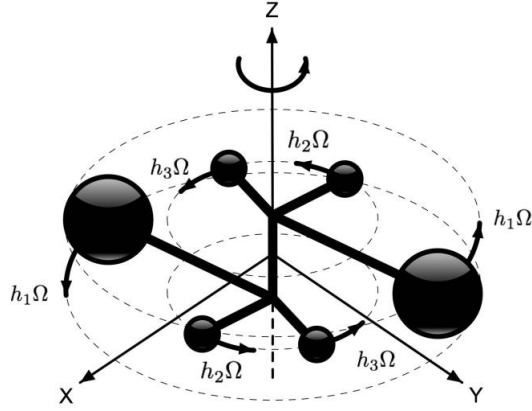


Figure 1.13: Disturbances harmonic model of dynamic imbalance [4]

1.2.3.2 State of art concepts application

In following part, the concepts previously analysed will be applied to the specific case evaluated in this work of thesis. The starting point is the definition of the satellite structure with reaction wheels. Figure 1.14 shows a cubic satellite of $3U$ (10 cm along z -axis, 10 cm along y -axis and 30 cm along x -axis) with three orthogonal reaction wheels attached to the spacecraft bus. This structure differs from the one shown by figure 1.6, about the RWs positions, and it has been considered to make the analysis simpler. As it is easy to see, the rotation axis (Z -axis in green) of the three reaction wheels is aligned with the body frame axes of the bus and this coordinate system is placed in the bus center of mass G .

Now, the expressions of the pure moments and forces (with the relative moments) coming from the static and dynamic imbalance have to be applied to the situation in figure 1.14. So, first of all, it is fundamental to define the rotation matrices that characterize the wheels frame orientation with respect to the bus frame. As it is possible to see, the RF of wheel 1 is rotated clockwise about the y -axis of the body frame of an angle equal to 90° i.e. the rotation angle α is equal to $-\frac{\pi}{2}$. The rotation matrix that describes this situation is given by (1.12). Then, the wheel 2 RF is rotated counter-clockwise about the body x -axis of 90° i.e. $\alpha = \frac{\pi}{2}$ and the relative rotation matrix is (1.13). Finally, the RF of wheel 3 is not subject to any rotation, which means that

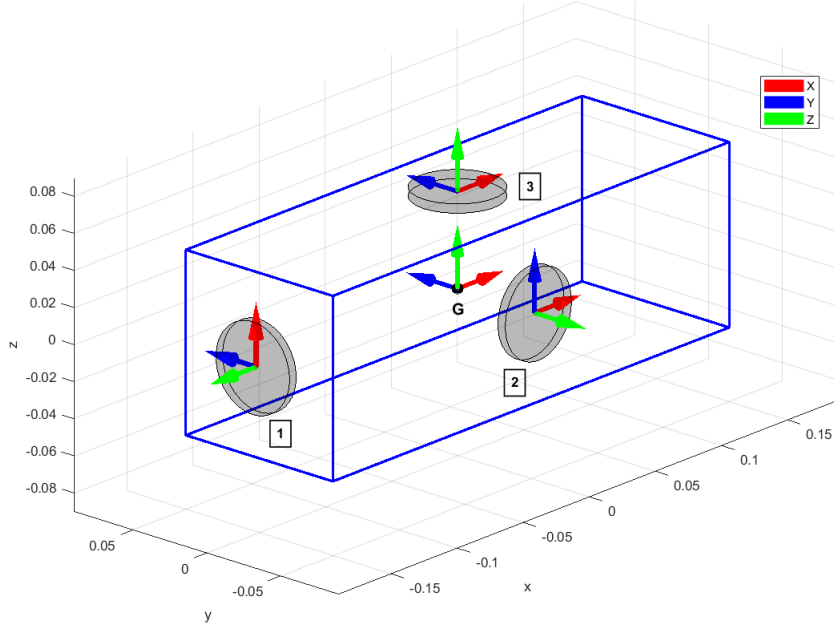


Figure 1.14: Representation of 3U CubeSat with 3 reaction wheels

its rotation matrix coincides with the identity matrix I , as shown by (1.14).

$$\mathbf{R}_{W_1}^B = \begin{bmatrix} \cos(\alpha) & 0 & \sin(\alpha) \\ 0 & 1 & 0 \\ -\sin(\alpha) & 0 & \cos(\alpha) \end{bmatrix} \stackrel{\alpha = -\frac{\pi}{2}}{=} \begin{bmatrix} 0 & 0 & -1 \\ 0 & 1 & 0 \\ 1 & 0 & 0 \end{bmatrix} \quad (1.12)$$

$$\mathbf{R}_{W_2}^B = \begin{bmatrix} 1 & 0 & 0 \\ 0 & \cos(\alpha) & -\sin(\alpha) \\ 0 & \sin(\alpha) & \cos(\alpha) \end{bmatrix} \stackrel{\alpha = \frac{\pi}{2}}{=} \begin{bmatrix} 1 & 0 & 0 \\ 0 & 0 & -1 \\ 0 & 1 & 0 \end{bmatrix} \quad (1.13)$$

$$\mathbf{R}_{W_3}^B = \mathbf{I} = \begin{bmatrix} 1 & 0 & 0 \\ 0 & 1 & 0 \\ 0 & 0 & 1 \end{bmatrix} \quad (1.14)$$

Furthermore, as mentioned in the previous section, only the first harmonic contribute is considered. This means that, for each reaction wheel, the following forces and pure moments expression (in the wheels frame) is evaluated:

$$F_x(t) = C_s \Omega^2 \sin(2\pi h_i \Omega(t)t) + \phi_i^{F_{rad}} \quad (1.15)$$

$$F_y(t) = C_s \Omega^2 \sin(2\pi h_i \Omega(t)t + \phi_i^{F_{rad}} + \frac{\pi}{2}) \quad (1.16)$$

$$M_x(t) = C_d \Omega^2 \sin(2\pi h_i \Omega(t)t + \phi_i^{M_{rad}}) \quad (1.17)$$

$$M_y(t) = C_d \Omega^2 \sin(2\pi h_i \Omega(t)t + \phi_i^{M_{rad}} + \frac{\pi}{2}) \quad (1.18)$$

where $C_s = 170 \text{ mg}\cdot\text{mm}$ and $C_d = 57,000 \text{ mg}\cdot\text{mm}^2$ are the coefficients that represent the static and dynamic imbalance. Their values are defined according to [11].

Now, it is possible to study all the wheel contributions about disturbances, in the reference frame of the satellite bus. However, before starting this analysis, it is important to make the following comment: for the computation of the forces moments, in the expression of the distance between the bus CoM (G) and the wheels center, the height of the wheels has been neglected. Therefore, the distances are simply characterized by the half of the bus dimensions.

Reaction Wheel 1

Reaction wheel 1 is characterized by the following disturbance moments $\mathbf{M}_{W_1} = [M_1^x \ M_1^y \ 0]^T$, expressed in the wheel frame. So, their expression in the bus reference frame is:

$$\begin{bmatrix} M_B^x \\ M_B^y \\ M_B^z \end{bmatrix} = \mathbf{R}_{W_1}^B \mathbf{M}_{W_1} = \begin{bmatrix} 0 & 0 & -1 \\ 0 & 1 & 0 \\ 1 & 0 & 0 \end{bmatrix} \begin{bmatrix} M_1^x \\ M_1^y \\ 0 \end{bmatrix} = \begin{bmatrix} 0 \\ M_1^y \\ M_1^x \end{bmatrix} \quad (1.19)$$

Instead, the disturbance forces in the wheel frame are $\mathbf{F}_{W_1} = [F_1^x \ F_1^y \ 0]^T$. And their specific expression in the bus frame is:

$$\mathbf{F}_{W_1}^B = \begin{bmatrix} F_B^x \\ F_B^y \\ F_B^z \end{bmatrix} = \mathbf{R}_{W_1}^B \mathbf{F}_{W_1} = \begin{bmatrix} 0 & 0 & -1 \\ 0 & 1 & 0 \\ 1 & 0 & 0 \end{bmatrix} \begin{bmatrix} F_1^x \\ F_1^y \\ 0 \end{bmatrix} = \begin{bmatrix} 0 \\ F_1^y \\ F_1^x \end{bmatrix} \quad (1.20)$$

Then, the distance between the bus center of mass and the wheels center, in the bus frame, useful to compute the moments of the forces, is $\mathbf{R}_B^{CM_1} = [-R_{CM_1} \ 0 \ 0]^T$, where $R_{CM_1} = 0.15 \text{ m}$. Finally, the moments of the forces

are:

$$\begin{bmatrix} M_B^x \\ M_B^y \\ M_B^z \end{bmatrix} = \mathbf{R}_B^{CM_1} \times \mathbf{F}_{W_1}^B = \begin{bmatrix} -R_{CM_1} \\ 0 \\ 0 \end{bmatrix} \times \begin{bmatrix} 0 \\ F_1^y \\ F_1^x \end{bmatrix} = \begin{bmatrix} 0 \\ R_{CM_1} F_1^x \\ -R_{CM_1} F_1^y \end{bmatrix} \quad (1.21)$$

Reaction Wheel 2

In a similar way, reaction wheel 2 disturbance moments, expressed in the wheel frame, are $\mathbf{M}_{W_2} = [M_2^x \ M_2^y \ 0]^T$. Therefore, their expression in the bus reference frame is:

$$\begin{bmatrix} M_B^x \\ M_B^y \\ M_B^z \end{bmatrix} = \mathbf{R}_{W_2}^B \mathbf{M}_{W_2} = \begin{bmatrix} 1 & 0 & 0 \\ 0 & 0 & -1 \\ 0 & 1 & 0 \end{bmatrix} \begin{bmatrix} M_2^x \\ M_2^y \\ 0 \end{bmatrix} = \begin{bmatrix} M_2^x \\ 0 \\ M_2^y \end{bmatrix} \quad (1.22)$$

The disturbance forces in the wheel frame are $\mathbf{F}_{W_2} = [F_2^x \ F_2^y \ 0]^T$. And their specific expression in the bus frame is:

$$\mathbf{F}_{W_2}^B = \begin{bmatrix} F_B^x \\ F_B^y \\ F_B^z \end{bmatrix} = \mathbf{R}_{W_2}^B \mathbf{F}_{W_2} = \begin{bmatrix} 1 & 0 & 0 \\ 0 & 0 & -1 \\ 0 & 1 & 0 \end{bmatrix} \begin{bmatrix} F_2^x \\ F_2^y \\ 0 \end{bmatrix} = \begin{bmatrix} F_2^x \\ 0 \\ F_2^y \end{bmatrix} \quad (1.23)$$

Furthermore, the distance between the bus center of mass and the wheels center, in the bus frame, useful to compute the moments of the forces, is $\mathbf{R}_B^{CM_2} = [0 \ -R_{CM_2} \ 0]^T$, where $R_{CM_2} = 0.05 \text{ m}$. Finally, the moments of the forces are:

$$\begin{bmatrix} M_B^x \\ M_B^y \\ M_B^z \end{bmatrix} = \mathbf{R}_B^{CM_2} \times \mathbf{F}_{W_2}^B = \begin{bmatrix} 0 \\ -R_{CM_2} \\ 0 \end{bmatrix} \times \begin{bmatrix} 0 \\ F_2^x \\ F_2^y \end{bmatrix} = \begin{bmatrix} -R_{CM_2} F_2^y \\ 0 \\ R_{CM_2} F_2^x \end{bmatrix} \quad (1.24)$$

Reaction Wheel 3

Finally, the same procedure is repeated for wheel 3. Then, its disturbance moments, in the wheel frame, are $\mathbf{M}_{W_3} = [M_x^3 \ M_y^3 \ 0]^T$. And their expression in the bus frame is:

$$\begin{bmatrix} M_B^x \\ M_B^y \\ M_B^z \end{bmatrix} = \mathbf{R}_{W_3}^B \mathbf{M}_{W_3} = \begin{bmatrix} 1 & 0 & 0 \\ 0 & 1 & 0 \\ 0 & 0 & 1 \end{bmatrix} \begin{bmatrix} M_3^x \\ M_3^y \\ 0 \end{bmatrix} = \begin{bmatrix} M_3^x \\ M_3^y \\ 0 \end{bmatrix} \quad (1.25)$$

Instead, the disturbance forces in the wheel frame are $\mathbf{F}_{W_3} = [F_3^x \ F_3^y \ 0]^T$ and their specific expression in the bus frame is:

$$\mathbf{F}_{W_3}^B = \begin{bmatrix} F_B^x \\ F_B^y \\ F_B^z \end{bmatrix} = \mathbf{R}_{W_3}^B \mathbf{F}_{W_3} = \begin{bmatrix} 1 & 0 & 0 \\ 0 & 1 & 0 \\ 0 & 0 & 1 \end{bmatrix} \begin{bmatrix} F_3^x \\ F_3^y \\ 0 \end{bmatrix} = \begin{bmatrix} F_3^x \\ F_3^y \\ 0 \end{bmatrix} \quad (1.26)$$

Moreover, the distance between the bus center of mass and the wheels center, in the bus frame, useful to compute the moments of the forces, is $\mathbf{R}_B^{CM_3} = [0 \ 0 \ R_{CM_3}]^T$, where $R_{CM_3} = 0.05 \text{ m}$. Finally, the moments of the forces are:

$$\begin{bmatrix} M_B^x \\ M_B^y \\ M_B^z \end{bmatrix} = \mathbf{R}_B^{CM_3} \times \mathbf{F}_{W_3}^B = \begin{bmatrix} 0 \\ 0 \\ R_{CM_3} \end{bmatrix} \times \begin{bmatrix} F_3^x \\ F_3^y \\ 0 \end{bmatrix} = \begin{bmatrix} -R_{CM_3} F_3^y \\ R_{CM_3} F_3^x \\ 0 \end{bmatrix} \quad (1.27)$$

So, the total disturbance moments acting on the satellite, expressed in the bus reference frame, can be defined by summing all the contributions coming from the three wheels, related to the pure moments and the forces moments, as shown by (1.28).

$$\begin{bmatrix} M_B^x \\ M_B^y \\ M_B^z \end{bmatrix} = \begin{bmatrix} M_2^x + M_3^x - R_{CM_2} F_2^y - R_{CM_3} F_3^y \\ M_1^y + M_3^y + R_{CM_1} F_1^x + R_{CM_3} F_3^x \\ M_1^x + M_2^y - R_{CM_1} F_1^y + R_{CM_2} F_2^x \end{bmatrix} \quad (1.28)$$

Chapter 2

The attitude control problem

In this chapter, the general aspects of the control system used to manage the satellite attitude will be analysed. First of all, it is crucial to define all the objectives of the attitude control, in order to understand what the control system is supposed to do. Then, the general structure of the overall system must be defined. In particular, it is necessary to deeply characterize every single subsystem through its function and constitutive equations. In particular, it will be given the full description of the satellite model (from now on called plant) and the actuator one (an electric motor used to drive the flywheel). Instead, only a general characterization of the reference generator, the control input system and the controller will be provided in this chapter, since their structure changes according to the type of control strategy that is adopted. However, about the reference generator, even though its structure is subject to the above-mentioned variations, there is a specific part that does not change. This one, as it will be shown, comes from the general activity that the whole control system must perform and it is related to the orbital motion of the satellite and its goal i.e. pointing the target star. The full analysis of these subsystem will be performed in the chapter 3 and 4. Finally, it will be shown how the control system can be implemented in the two simulations environments analysed in this work of thesis: MATLAB/Simulink and the company's software EICASLAB.

2.1 Main goals of the attitude control

The objectives definition of a control system is a fundamental step that must be carefully carried out. Indeed, it has to be clear what the overall system should do, in order to be able implementing the correct structure of each subsystem that composes the whole control environment.

For the situation under analysis, the main objective is to manage the pointing action of the satellite telescope towards a specific target star. Indeed, as mentioned in the previous chapter, a CubeSat is often equipped with a telescope used to perform a photometric analysis of the desired star. Through a correct photometric evaluation, it is possible to study the stellar activities or transiting exoplanets or other astrophysical phenomena. In this work of thesis, the following scenario has been considered:

- a $3U$ CubeSat with three orthogonal reaction wheels, as previously shown by figure 1.14.
- a circular Low Earth Orbit (LEO) with 0° of inclination and altitude of 600 Km .
- a target star in the same plane of the orbit, as it will be analysed, and about $4,22\text{ ly}$ (*light years*) distant from the satellite orbit.

For the attitude control, it is important to consider two main reference frames: the inertial frame fixed in the orbit center (which coincides also with Earth center) and the body frame fixed in the satellite center of mass. The first one has the z -axis orthogonal to the plane of the orbit and exiting from it. The remaining axes, that complete the right-hand frame, lay on the orbital plane. Instead, the satellite frame is initially considered with all the three axes parallel to the fixed frame. It must be pointed out that the orientation representation of the cubic-shaped satellite is done through the relative position of its frame with respect to the inertial one. In particular, as it will be mentioned later, the attitude representation is done by considering the three angles of the Tait-Bryan convention.

Now, if only the orbital motion effects are considered (i.e. without activating the controller), the following situation occurs: the satellite in the Earth orbit

is characterized by a translational motion of its CoM and a rotational one about an axis passing through it. For the case under analysis, the z-axis of two reference frames are parallel and it is considered a rotation about this axis. This means that the satellite reference frame continuously changes its orientation with respect to the inertial frame, by performing a rotation about the z-axis. The detailed analysis of the complete scenario will be considered in the following sections.

Therefore, according to a specific reference input, which takes into account the orbital motion of the satellite around the Earth, the controller must be able to change the spacecraft orientation such that the telescope points the target star in the best way possible i.e. by ensuring a theoretically zero error between the actual position and the desired one.

2.2 A general control scheme and its subsystems

A general representation of the attitude control scheme is given by figure 2.1. It is possible to identify 7 subsystems related by direct and feedback connections. It is worth highlighting that there are two feedback paths, both ending in the *control inputs* block and starting respectively from the *plant* and the *actuators* block. As it will be analysed later, the output signal of the *plant* enters the *control inputs* block and it is properly elaborated with the signals coming from the *reference generator* block, to produce the specific output of the *control inputs* subsystem. Instead, the actuators signal will only transit through the *control inputs* block and go to the *sampler* one.

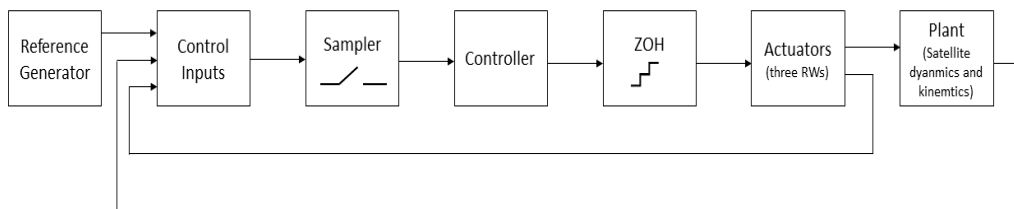


Figure 2.1: General attitude control scheme

So, the 7 subsystems are:

- **Plant:** it is one of the core subsystems of the overall scheme, since it defines the element that must be controlled i.e. the cubic-shaped satellite. Its description is split in two part: the dynamics and the kinematics. The first one is represented by the relation between torques coming from the actuators and the derivative of the satellite angular velocity (and so its integral i.e. the angular speed). The second one defines the link between the angular speed and the specific representation of the satellite attitude. In this work of thesis, the quaternion one has been used.
- **Actuators:** they are the subsystems responsible for the application of the specific control action to the plant. In the following scenario, they are defined by a set of three reaction wheels that, as mentioned in chapter 1, are essentially composed by flywheels driven by electric motors, which provides torques of suitable values to control the spacecraft attitude. In this thesis, the description of these subsystems is given by the constitutive equations of a DC motor. Moreover, as it will be shown later, a simple but fundamental control must be considered in order to obtain a suitable torque-command scheme and to neglect the motors dynamics.
- **ZOH:** it is the acronym of Zero Order Holder and it, basically, plays the role of a digital to analog converter (DAC). It must be highlighted that, in this thesis project, it has been considered only a discrete controller and not a proper digital one. This means that the effects coming from the quantization operation are neglected and only the discrete time properties have been considered. So, the ZOH implements an holding action on the samples coming from the controller (i.e. it keeps constant the value of a sample for the duration of the sampling period) in order to build a continuous-time signal starting from a discrete one. Therefore, it is a crucial interface between the discrete time world (the controller) and the continuous time one (actuators and plant).
- **Controller:** it is the other core part of the overall system because it

is responsible for the control command generation, necessary to obtain the desired satellite attitude. Basically, it receives specific signals, as shown in figure 2.1, and makes some computations to generate the control output. As mentioned before, a discrete-time controller has been considered which is able to produce suitable values of control torque at specific time instants, spaced by the sampling period (control samples). Its structure is strongly related to the control strategy. For this reason, the specific implementation of the controller will be given directly in the dedicated chapters.

- **Sampler:** this subsystem is the complementary one of the ZOH. Indeed, it characterizes an analog to digital converter (DAC). As mentioned before, since the quantization procedure is neglected, the only operation to be analysed is the sampling one. Therefore, this system is responsible for providing the proper control inputs to the controller block at equally spaced time instants (samples). The temporal distance between them is the sampling period.
- **Control inputs block:** this block is responsible for the generation of the control inputs required by the controller to produce the suitable control action (the command torques). The control inputs derive from some elaborations of the reference signals and the ones coming from the plant (feedback path). Also in this case, the implementation of this block is linked to the specific controller structure. So, its detailed analysis will be provided in the proper chapters.
- **Reference generator:** this is the other key subsystem of the control scheme. Indeed, it plays a fundamental role because the signal that must be tracked (the desired satellite attitude) is produced by this system. For the application under analysis, the reference signals are the Tait-Bryan angles (Cardan angles) related to the wanted orientation and, as mentioned at the beginning of this chapter, the objective is to point the satellite telescope towards the target star. However, these reference angles are not directly injected in the control inputs block, but they are subject to some elaborations. The kind of computations

that must be done on the angles is strictly related to the specific control strategy. Therefore, in the chapter 3 and 4, it will be also given the complete specific implementation of this block.

Plant

The plant is the main subsystem of the overall control scheme because it represents the object the has to be controlled. In particular, it is applied a control action such that the orientation of the satellite is properly modified. Indeed, the goal is to point the telescope towards the target star so that a precise photometric analysis can be performed. In order to understand how the attitude can be changed, it is crucial to deeply study the equations that characterize this system. The plant structure can be divided in two main parts: the first one deals with the dynamics and the second one describes the kinematics. Figure 2.2 represents, once again, the physical structure of the plant, with its three actuators, that has been considered in this work of thesis. Therefore, the overall system is given by a $3U$ cubic-shaped satellite bus with three identical orthogonal reaction wheels attached to it. As already mentioned in chapter 1, this kind of structure differ from the one of figure 1.6, about the RWs positions, and it has been considered to make the analysis simpler.

Satellite dynamics

The satellite dynamics is described by the well-known *Euler's moments equation* which must consider not only the satellite body but also the contribution coming from the three reaction wheels. Therefore, as mentioned by [8], the angular momentum variation of the complete system, expressed in the inertial reference frame, can be computed as:

$$\mathbf{M}_I^{ext} = \dot{\mathbf{H}}_I = \dot{\mathbf{H}}_I^{(sc)} + \dot{\mathbf{H}}_I^{(w)} \quad \text{where} \quad \dot{\mathbf{H}}_I^{(w)} = \sum_{i=1}^3 \dot{\mathbf{H}}_I^{(w_i)} \quad (2.1)$$

As already mentioned in section 1.2.1, the subscript I defines that the specific quantity is evaluated in the inertial reference frame, the superscript (sc) is linked to the spacecraft total angular momentum variation, (w_i) is

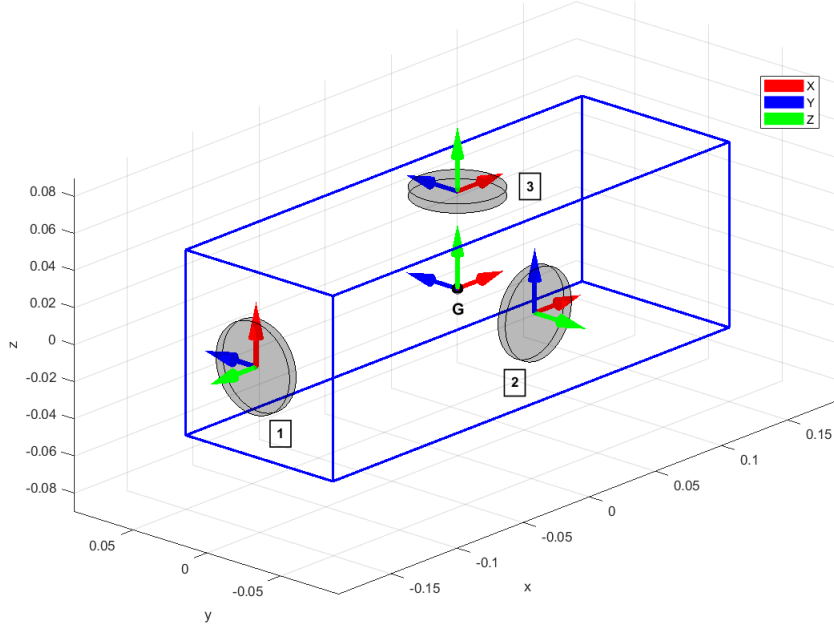


Figure 2.2: Representation of 3U CubeSat with 3 reaction wheels

related to the i -th wheel angular momentum variation and \mathbf{M}^{ext} describes the external torque applied to the overall system (both environmental and on-board torque disturbances and other control actions different from the reaction wheels ones). It is really important to highlight that, as discussed in [8], $\mathbf{H}_I^{(sc)}$ defines the total angular momentum of all the rigid body i.e. the spacecraft body plus the reaction wheels masses concentrated at their center of mass. Instead, $\mathbf{H}_I^{(w_i)}$ represents the net angular momentum of the i -th reaction wheel about its center of mass. Moreover, $\mathbf{H}_I^{(sc)}$ is referred to the overall system center of mass (spacecraft/satellite body+wheel). Now, it is crucial to highlight that, for the following analysis, the angular momenta will be always expressed in the vehicle frame (the one placed in G, as shown by figure 2.2). So, from now on the following quantities are considered $\mathbf{H}_B^{(sc)}$, $\mathbf{H}_B^{(w)}$ and \mathbf{M}_B^{ext} which are simply projections of $\mathbf{H}_I^{(sc)}$, $\mathbf{H}_I^{(w)}$ and \mathbf{M}_I^{ext} in the vehicle fixed frame.

Since all the angular momenta are expressed in the vehicle frame, which is

non-inertial, the relation given by (2.1) modifies in the following way:

$$\mathbf{M}_B^{ext} = [\dot{\mathbf{H}}_B^{(sc)} + \boldsymbol{\omega} \times \mathbf{H}_B^{(sc)}] + [\dot{\mathbf{H}}_B^{(w)} + \boldsymbol{\omega} \times \mathbf{H}_B^{(w)}] \quad (2.2)$$

where

$$\mathbf{H}_B^{(sc)} = \mathbf{J}^{(sc)} \boldsymbol{\omega} \quad \text{and} \quad \dot{\mathbf{H}}_B^{(sc)} = \mathbf{J}^{(sc)} \dot{\boldsymbol{\omega}} \quad (2.3)$$

$$\mathbf{H}_B^{(w)} = \sum_{i=1}^3 \mathbf{H}_B^{(w_i)} = \sum_{i=1}^3 \mathbf{J}^{(w_i)} \boldsymbol{\omega}^{(i)} \quad \text{and} \quad \dot{\mathbf{H}}_B^{(w)} = \sum_{i=1}^3 \dot{\mathbf{H}}_B^{(w_i)} = \sum_{i=1}^3 \mathbf{J}^{(w_i)} \dot{\boldsymbol{\omega}}^{(i)} \quad (2.4)$$

Now, it is important to analyse the meaning of the following quantities:

- $\boldsymbol{\omega} = [\omega_x \ \omega_y \ \omega_z]^T$ and $\dot{\boldsymbol{\omega}} = [\dot{\omega}_x \ \dot{\omega}_y \ \dot{\omega}_z]^T$ are the satellite angular speed and its derivative expressed in the satellite frame.
- $\boldsymbol{\omega}^{(i)}$ and $\dot{\boldsymbol{\omega}}^{(i)}$ are the angular speed and its derivatives of the i -th reaction wheels, always expressed in the satellite fixed frame. In particular, they can be written as $\boldsymbol{\omega}^{(i)} = \boldsymbol{\omega} + \boldsymbol{\Omega}^{(i)}$ and $\dot{\boldsymbol{\omega}}^{(i)} = \dot{\boldsymbol{\omega}} + \dot{\boldsymbol{\Omega}}^{(i)}$ where $\boldsymbol{\Omega}^{(i)}$ is the relative angular speed of the i -th wheel with respect to the spacecraft. E.g. $\boldsymbol{\omega}^{(1)} = [\omega_x \ \omega_y \ \omega_z]^T + [\omega_{rel}^{(1)} \ 0 \ 0]^T = [\omega_x + \omega_{rel}^{(1)} \ \omega_y \ \omega_z]^T$ and $\dot{\boldsymbol{\omega}}^{(1)} = [\dot{\omega}_x \ \dot{\omega}_y \ \dot{\omega}_z]^T + [\dot{\omega}_{rel}^{(1)} \ 0 \ 0]^T = [\dot{\omega}_x + \dot{\omega}_{rel}^{(1)} \ \dot{\omega}_y \ \dot{\omega}_z]^T$.
- $\mathbf{J}^{(sc)}$ is the inertia matrix, evaluated with respect to the center of mass of the whole system, of the satellite bus plus the three wheels masses concentrated at their center of mass. However, in this work of thesis, it has been neglected the contribution of three wheels masses (because in general it is not so relevant). Therefore, the satellite bus center of mass coincides with the overall system CoM (point G in figure 2.2). Then, for the inertia matrix computation, it has been simply considered an homogeneous rectangular cuboid, as in figure 2.2, where the center of mass coincides with the geometrical center. About the body frame, its origin is placed in the CoM and it is coincident with the principal axes of inertia. Therefore, the matrix can be written as:

$$\mathbf{J}^{(sc)} = \begin{bmatrix} J_x & 0 & 0 \\ 0 & J_y & 0 \\ 0 & 0 & J_z \end{bmatrix} = \begin{bmatrix} \frac{m}{12} (h_s^2 + w_s^2) & 0 & 0 \\ 0 & \frac{m}{12} (h_s^2 + d_s^2) & 0 \\ 0 & 0 & \frac{m}{12} (w_s^2 + d_s^2) \end{bmatrix} \quad (2.5)$$

where the mass m is equal to 5 Kg , the height $h_s = 10\text{ cm} = 0.1\text{ m}$, the width $w_s = 10\text{ cm} = 0.1\text{ m}$ and the depth $d_s = 30\text{ cm} = 0.3\text{ m}$.

- $\mathbf{J}^{(w_i)}$ is the i -th reaction wheel inertia matrix, evaluated in its center of mass and expressed in the vehicle fixed frame. As shown by figure 2.2, the z -axis (rotation axis) of each RW is aligned with the vehicle frame axes and the other RWs frame axes are parallel to the remaining satellite axes. So, at first, the inertia matrix of each wheel is expressed in its own reference frame (wheel frame) and then, through suitable rotation matrix, is evaluated in the vehicle frame. In the wheels frames (which are aligned with their principal axes), the inertia matrices are expressed by:

$$\mathbf{J}_W^{(w_1)} = \mathbf{J}_W^{(w_2)} = \mathbf{J}_W^{(w_3)} = \begin{bmatrix} \beta & 0 & 0 \\ 0 & \beta & 0 \\ 0 & 0 & J_{RW} \end{bmatrix} \quad (2.6)$$

Then, since the rotation matrices of the three wheels frame with respect to the satellite one are:

$$\mathbf{R}_{W_1}^B = \begin{bmatrix} \cos(\alpha) & 0 & \sin(\alpha) \\ 0 & 1 & 0 \\ -\sin(\alpha) & 0 & \cos(\alpha) \end{bmatrix} \stackrel{\alpha = -\frac{\pi}{2}}{=} \begin{bmatrix} 0 & 0 & -1 \\ 0 & 1 & 0 \\ 1 & 0 & 0 \end{bmatrix} \quad (2.7)$$

$$\mathbf{R}_{W_2}^B = \begin{bmatrix} 1 & 0 & 0 \\ 0 & \cos(\alpha) & -\sin(\alpha) \\ 0 & \sin(\alpha) & \cos(\alpha) \end{bmatrix} \stackrel{\alpha = \frac{\pi}{2}}{=} \begin{bmatrix} 1 & 0 & 0 \\ 0 & 0 & -1 \\ 0 & 1 & 0 \end{bmatrix} \quad (2.8)$$

$$\mathbf{R}_{W_3}^B = \mathbf{I} = \begin{bmatrix} 1 & 0 & 0 \\ 0 & 1 & 0 \\ 0 & 0 & 1 \end{bmatrix} \quad (2.9)$$

the wheels inertia matrices in the satellite frame are:

$$\mathbf{J}_B^{(w_1)} = \mathbf{R}_{W_1}^B \mathbf{J}_W^{(w_1)} (\mathbf{R}_{W_1}^B)^T = \begin{bmatrix} J_{RW} & 0 & 0 \\ 0 & \beta & 0 \\ 0 & 0 & \beta \end{bmatrix} \quad (2.10)$$

$$\mathbf{J}_B^{(w_2)} = \mathbf{R}_{W_2}^B \mathbf{J}_W^{(w_2)} (\mathbf{R}_{W_2}^B)^T = \begin{bmatrix} \beta & 0 & 0 \\ 0 & J_{RW} & 0 \\ 0 & 0 & \beta \end{bmatrix} \quad (2.11)$$

$$\mathbf{J}_B^{(w_3)} = \mathbf{R}_{W_3}^B \mathbf{J}_W^{(w_3)} (\mathbf{R}_{W_3}^B)^T = \begin{bmatrix} \beta & 0 & 0 \\ 0 & \beta & 0 \\ 0 & 0 & J_{RW} \end{bmatrix} \quad (2.12)$$

In this work of thesis, the contribution coming from the inertia components about the wheels axes that do not have a relative motion with respect to the satellite i.e. β is neglected (due to the non-relevant contribution in the equation (2.2)). Therefore, the only component that has been considered is the one related to the relative rotation i.e. J_{RW} . In this way, it is possible to build a single diagonal matrix which involves all the inertia contributions of the three wheels:

$$\mathbf{J}^{(w)} = \begin{bmatrix} J_{RW} & 0 & 0 \\ 0 & J_{RW} & 0 \\ 0 & 0 & J_{RW} \end{bmatrix} \quad (2.13)$$

Therefore, it is possible to write (2.4) as follows:

$$\mathbf{H}_B^{(w)} = \sum_{i=1}^3 \mathbf{H}_B^{(w_i)} = \mathbf{J}^{(w)} \boldsymbol{\omega}^{(w)} \quad \text{and} \quad \dot{\mathbf{H}}_B^{(w)} = \sum_{i=1}^3 \dot{\mathbf{H}}_B^{(w_i)} = \mathbf{J}^{(w)} \dot{\boldsymbol{\omega}}^{(w)} \quad (2.14)$$

where $\boldsymbol{\omega}^{(w)} = [\omega_x + \omega_{rel}^{(1)} \quad \omega_y + \omega_{rel}^{(2)} \quad \omega_z + \omega_{rel}^{(3)}]^T$.

Now, if there are not any kind of external disturbances and only the control action coming from the three reaction wheels is considered, $\mathbf{M}^{ext} = 0$ and the angular momentum conservation holds. Indeed, in this case, $\dot{\mathbf{H}}_I = \dot{\mathbf{H}}_I^{(sc)} + \dot{\mathbf{H}}_I^{(w)} = 0 \Rightarrow \mathbf{H}_I^{(sc)} + \mathbf{H}_I^{(w)} = \text{const}$. Therefore, by considering all the above information, it is possible to rewrite the equation (2.2) in the following way:

$$\dot{\boldsymbol{\omega}} = \mathbf{J}^{(sc)-1} (-\boldsymbol{\omega} \times (\mathbf{J}^{(sc)} \boldsymbol{\omega} + \mathbf{H}_B^{(w)}) + \boldsymbol{\tau}) \quad (2.15)$$

Equation (2.15) describes the dynamics of the satellite (plant). It is important to make some comments about (2.15). The term $\mathbf{H}_B^{(w)}$ is the same of (2.14) and $\boldsymbol{\tau}$ defines the control torque coming from the reaction wheels, expressed as $\boldsymbol{\tau} = -\dot{\mathbf{H}}_B^{(w)}$.

Now, the reaction wheels are put in rotation by the electric motors through the application of a suitable torque that, for each wheel, can be obtained by using the Euler's equation, as mentioned by [8]. It is important to remind that all the angular momenta are expressed in the vehicle frame, so, the Euler's equation for the i -th wheel is:

$$\mathbf{M}_B^{(i)} = \dot{\mathbf{H}}_B^{(i)} + \boldsymbol{\omega} \times \mathbf{H}_B^{(i)} \quad (2.16)$$

As it will be shown in the following example, since the rotation axis of each wheel is aligned with the vehicle frame axes, the motor torque for each wheel is described only by the vectorial component of (2.16) in correspondence of the proper satellite frame axis i.e. the specific component of $\dot{\mathbf{H}}_B^{(i)}$. The other term that appears in (2.16) is simply a gyroscopic effect, already shown by equation (2.2). The wheel 1 situation is taken as example. As shown by figure 2.2, the wheel 1 has the rotation axis aligned with the x-axis of the satellite frame. So:

$$\mathbf{M}_B^{(1)} = \begin{bmatrix} M \\ 0 \\ 0 \end{bmatrix} \quad \dot{\mathbf{H}}_B^{(1)} = \begin{bmatrix} J_{RW} & 0 & 0 \\ 0 & 0 & 0 \\ 0 & 0 & 0 \end{bmatrix} \begin{bmatrix} \dot{\omega}_x + \dot{\omega}_{rel}^{(1)} \\ \dot{\omega}_y \\ \dot{\omega}_z \end{bmatrix} \quad (2.17)$$

$$\boldsymbol{\omega} \times \mathbf{H}_B^{(1)} = \begin{bmatrix} \omega_x \\ \omega_y \\ \omega_z \end{bmatrix} \times \begin{bmatrix} J_{RW} & 0 & 0 \\ 0 & 0 & 0 \\ 0 & 0 & 0 \end{bmatrix} \begin{bmatrix} \omega_x + \omega_{rel}^{(1)} \\ \omega_y \\ \omega_z \end{bmatrix} \quad (2.18)$$

therefore

$$\begin{bmatrix} M \\ 0 \\ 0 \end{bmatrix} = \begin{bmatrix} J_{RW}(\dot{\omega}_x + \dot{\omega}_{rel}^{(1)}) \\ 0 \\ 0 \end{bmatrix} + \begin{bmatrix} 0 \\ J_{RW} \omega_z (\omega_x + \omega_{rel}^{(1)}) \\ -J_{RW} \omega_y (\omega_x + \omega_{rel}^{(1)}) \end{bmatrix} \quad (2.19)$$

Equation (2.19) shows that the motor torque applied to the flywheel, expressed in the satellite frame, is $M = J_{RW}(\dot{\omega}_x + \dot{\omega}_{rel}^{(1)})$ which is the first component of $\dot{\mathbf{H}}_B^{(1)}$ and also the first component of $\dot{\mathbf{H}}_B^{(w)}$ in the equation (2.14).

A similar analysis can be done for the other wheels.

So, it has been shown that the torque applied by the reaction wheels to the satellite is the same but opposite to the one produced by the electric motor. Therefore, it is possible to write for the wheel 1 $\tau_x = -M = -J_{RW}(\dot{\omega}_x + \dot{\omega}_{rel}^{(1)})$

where τ_x is the first component of the previous quantity $\boldsymbol{\tau}$. The same reasoning must be done for wheel 2 and 3.

Finally, it is important to notice that in presence of external disturbances, both environmental and on-board, the quantity $\boldsymbol{\tau}$ of equation (2.15) must include the disturbance contribution. In this work of thesis, the only disturbances that have been analysed are the ones coming from the reaction wheels, described in section 1.2.3, which are considered on-board disturbances. Therefore, the expression (1.28) must be added to the control torque coming from the reaction wheel such that $\boldsymbol{\tau} = \boldsymbol{\tau}_c + \mathbf{M}_B^{dist} = -\dot{\mathbf{H}}_B^{(w)} + \mathbf{M}_B^{dist}$. Moreover, it is important to clarify that for the analysis of the overall vehicle dynamics and wheels disturbances the following situation has been considered: all the reaction wheels rotate with respect to their CoM and the principal axis of inertia, even though in section 1.2.3 it has been stated that the disturbances are given by the shift of the CoM with respect to the axis of rotation and the tilt of the principal axis with respect to it. Then, to represent the effect of these two situations, the torque contributions given by (1.28) are added to equation (2.15), as previously mentioned.

Kinematics

The satellite kinematics deals with the relation between the angular speed $\boldsymbol{\omega}$ and specific quantities used to represent the attitude of the spacecraft. In this thesis, it has been chosen the quaternions approach to represent the vehicle orientation. Indeed, they do not introduce the singularity problem when the integration procedure is performed to obtain the entities that describe the attitude. It is important to highlight that, as will be shown later, the quaternions description is strictly related to the Tait-Bryant angles, which give a clearer representation of the satellite orientation.

So, as mentioned at the beginning of this chapter, the satellite attitude and so the kinematics are studied by considering two reference frames. The first one is inertial and fixed in the center of the satellite orbit. The second frame is non-inertial and fixed in the CoM of the satellite (point G of figure 2.2). The orientation of the satellite frame is expressed with respect to the inertial one by considering a set of three angles. As mentioned before, in this

thesis, the Tait-Bryan convention is used. It considers three angles known as ϕ , θ , ψ and states that the satellite orientation is given by considering three consecutive rotations in the following way: each elementary rotation must be done about x, y and z axis of the inertial fixed frame. Where the angle ϕ describes the rotation about the x-axis, θ about the y-axis and ψ about the z-axis. This means that the rotation matrix used to represent the overall rotation (given by the composition of the elementary rotations) is defined by pre-multiplying the matrix of the x-axis rotation with the y-axis one and, in turns, this must be pre-multiplied by the z-axis matrix.

However, this is not the only interpretation of the Tait-Bryan convention. Indeed, it is possible to consider the *extrinsic* interpretation, which is the above-mentioned one, and the *intrinsic* interpretation. This one states that the satellite orientation can be defined by considering a first rotation of ψ about the z-axis of the inertial frame. Then, the second rotation must be performed about the new y-axis of the mobile frame (i.e the satellite frame). The related angle is θ . Finally, the third rotation must be done about the new x-axis of the mobile frame and the angle that describes this motion is ϕ . So, as it is possible to see, the first rotation is done with respect to the inertial frame and the others are done about the satellite body frame as it changes its orientation. This is the interpretation that has been considered in this work of thesis since it the most suitable to understand the vibrational motion of the satellite telescope due to the reaction wheels disturbances.

Now, the first step is to define the constitutive equations of the satellite kinematics. As mentioned before, the quaternion approach is used such that the following relation can be written:

$$\dot{\mathbf{q}} = \frac{1}{2} \boldsymbol{\Omega} \mathbf{q} \quad (2.20)$$

where $\mathbf{q} = [q_0 \ q_1 \ q_2 \ q_3] = [q_0 \ \mathbf{q}]$ and $\dot{\mathbf{q}}$ are respectively the quaternion related to the specific attitude configuration and its derivative. It can be noticed that the generic quaternion \mathbf{q} is composed by a scalar part q_0 and a vectorial

one $\mathbf{q} = [q_1 \ q_2 \ q_3]$. Instead, $\mathbf{\Omega}$ is the angular speed matrix defined as:

$$\mathbf{\Omega} = \begin{bmatrix} 0 & -\omega_x & -\omega_y & -\omega_z \\ \omega_x & 0 & \omega_z & -\omega_y \\ \omega_y & -\omega_z & 0 & \omega_x \\ \omega_z & \omega_y & -\omega_x & 0 \end{bmatrix} \quad (2.21)$$

It is quite interesting to notice that the kinematics analysis exploits the values of the angular speed $\boldsymbol{\omega}$, coming from satellite dynamics part and in particular from the integration procedure of equation (2.15), to define the quaternion derivative $\dot{\mathbf{q}}$ and through an integration the attitude quaternion \mathbf{q} .

The second step is to figure out the relation between the attitude quaternion and the Tait-Bryan angles. To do so, it is fundamental to define the transformation/rotation matrix \mathbf{T} , that is another way to represent the relative orientation of the satellite frame with respect to the inertial one. This matrix is also called DCM (Direction Cosine Matrix) and it can be written with respect to the generic quaternion \mathbf{q} as follows:

$$\mathbf{T} = \begin{bmatrix} q_0^2 + q_1^2 - q_2^2 - q_3^2 & 2(q_1q_2 - q_0q_3) & 2(q_1q_3 + q_0q_2) \\ 2(q_1q_2 + q_0q_3) & q_0^2 - q_1^2 + q_2^2 - q_3^2 & 2(q_2q_3 - q_0q_1) \\ 2(q_1q_3 - q_0q_2) & 2(q_2q_3 + q_0q_1) & q_0^2 - q_1^2 - q_2^2 + q_3^2 \end{bmatrix} \quad (2.22)$$

Once the DCM is known, the Tait-Bryan angles ϕ, θ, ψ can be computed as:

$$\phi = \text{atan2}(T_{32}, T_{33}) \quad (2.23)$$

$$\theta = \text{atan2}(-T_{31}, \sin(\phi)T_{32} + \cos(\phi)T_{33}) \quad (2.24)$$

$$\psi = \text{atan2}(-\cos(\phi)T_{12} + \sin(\phi)T_{13}, \cos(\phi)T_{22} - \sin(\phi)T_{23}) \quad (2.25)$$

Actuators

The actuator is the device used to apply the specific control law to the plant. It is an interface between the controller and system to be controlled, able to convert the signal coming from the control device into a suitable one for the plant. For the attitude control analysed in this thesis, the actuator is a reaction wheel which is basically a flywheel driven by an electric motor. In

general, the electric motor is a DC-Brushless but, in this thesis, a DC motor has been considered to simplify the whole analysis. Moreover, it is important to remind that, in order to completely control the satellite attitude, at least three reaction wheels must be used. In the following part, at first, it will be considered the case of a satellite with one reaction wheel and, then, it will be given a generalization with three RWs. Now, let's imagine to have the satellite in figure 2.2 but with only one wheel. For example, the wheel 3 i.e. the one aligned with the satellite z-axis. With only one wheel, it is possible to have just a *planar motion* which means that the only allowed rotation takes place in the plane x-y of the satellite frame. In this situation, the dynamics equation (2.15) can be simplified by considering that the gyroscopic term is null. So, the equation related to the only axis about which the rotation takes place can be written as:

$$\dot{\omega}_z = \frac{1}{J_z} \tau_z \quad (2.26)$$

or equivalently:

$$\dot{\omega}_s = \frac{1}{J_{sc}} M_{sc} \quad (2.27)$$

Instead, about the reaction wheel, its dynamics equation has been analysed in the previous section (from equation (2.16) to (2.19)) and it is strictly related to DC motor equations as follows:

$$\begin{cases} V = R_M I + E \\ E = K_V \omega_{rel} \\ M = K_M I \\ \dot{\omega}_W = \frac{1}{J_{RW}} M \end{cases} \quad (2.28)$$

The block scheme representing equations (2.27) and (2.28) is shown by figure, as mentioned in [14]. Some comments about figure 2.3 are necessary to better understand the meaning of the quantities involved in the scheme.

V and R_M are the command voltage and motor resistance. Instead, K_M and K_V are respectively the torque constant, which links the armature current I_M and the produced torque M , and the speed constant that relates the relative speed of the motor with respect to the spacecraft and the back electromotive force E (indeed, the satellite is considered the stator of the DC motor and it

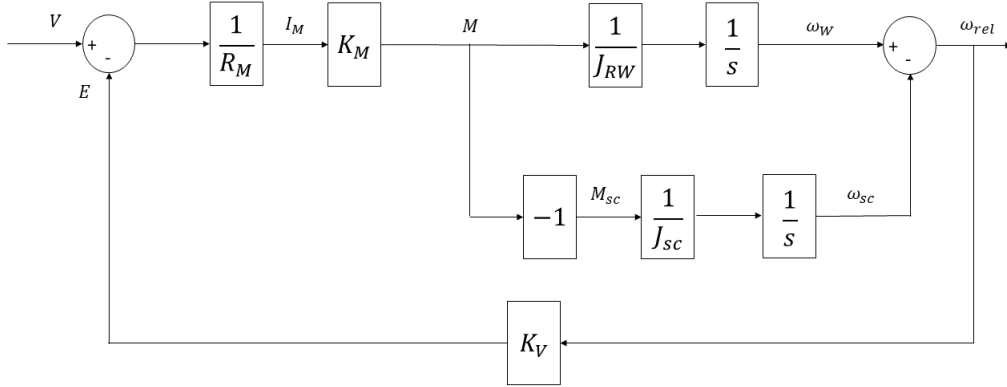


Figure 2.3: Block scheme of satellite plus one reaction wheel

moves. Moreover, the rotor/flywheel moves with respect to the satellite). It is important to notice that if the MSK (Meter Second Kilogram) measurement units are used, it is possible to consider $K_M = K_V = K$. Then, J_{RW} is the inertia of the flywheel about the axis where the rotation takes place (which is the same of (2.6)) and J_{sc} is the inertia of the satellite always related to the only axis along which it can rotate. As it is possible to see from figure 2.3 and deeply analysed in the previous section, ω_W is the reaction wheel speed intended as the sum of the satellite speed plus the relative motion between them i.e. $\omega_W = \omega_{sc} + \omega_{rel}$. For this reason, it is important to compute the difference $\omega_W - \omega_{sc}$ to get the relative speed used to determine the back electromotive force. Finally, it can be noticed that, as seen in the previous section, the torque applied to the satellite M_{sc} is equal and opposite to the one applied by the motor to the flywheel. This is the reason why there is a minus sign that relates the torque M and M_{sc} .

Now, the scheme in figure 2.3 has to be modified in order to build a torque command structure instead of a voltage command one, as mentioned by [14]. This new scheme is shown by figure 2.4 and it involves some new blocks with respect to the previous structure. At first, T_c is the torque command that comes from the controller (in particular from the ZOH) and it is converted in a current command. Then, there is a current limitation to produce the torque limitation (M_{max}) that characterizes all the reaction wheels. A summing node between the current command and the actual motor current produces

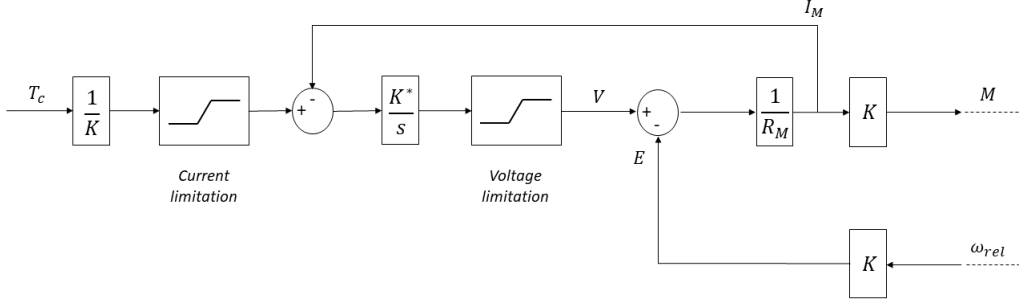


Figure 2.4: Satellite plus one reaction wheel with torque command

a specific signal for the controller $\frac{K^*}{s}$. This is an integral controller with gain K^* , which is fundamental to build a relation between the torque command and the actual motor torque such that the motor dynamics can be neglected. The controller output is the voltage that must be applied to the motor. However, it is evident the presence of a voltage limitation since there is a maximum value of voltage that can be applied to the motor. Then, the other blocks of the scheme are the same ones of the previous structure (figure 2.3). Now, it is important to show the transfer function that relates the torque command and actual motor torque. By considering figure 2.3 and 2.4, it is possible to write the following relation:

$$\frac{M(s)}{T_c(s)} = \frac{\frac{K^*}{R_M}}{s + \frac{K^*}{R_M}} = \frac{1}{1 + s \frac{R_M}{K^*}} \quad (2.29)$$

This transfer function is obtained by considering that $\frac{1}{J_{sc}} \ll \frac{1}{J_{RW}}$. Then, if the control gain K^* is chosen such that $K^* \gg \frac{K^2}{J_{RW}}$, the following relation holds $M \approx T_c$ and so all the motor dynamics can be neglected.

Now, a brief discussion on the motor parameters R_M and K must be done. The datasheet of a wheel similar to the one used in this thesis (i.e. MAI-200 by Adcole Maryland Aerospace) provides the values of the maximum voltage and the maximum torque. Then, to compute the values of the resistance R_M and constant K of the DC motor model, the following procedure has been applied. The mechanical characteristic of a DC motor is shown in figure 2.5. This characteristic moves parallel to itself when the applied voltage changes. So, at the maximum voltage is possible to evaluate the maximum torque M_{max} and the maximum relative speed ω_{max} . Figure 2.5 highlights



Figure 2.5: DC motor mechanical characteristic

this situation. Now, according to the first three motor equation of (2.28), the relation between the torque and the speed is given by:

$$M = K \frac{V}{R_M} - K^2 \frac{\omega_{rel}}{R_M} \quad (2.30)$$

therefore, the characteristic points M_{max} and ω_{max} are expressed as:

$$\begin{cases} M_{max} = K \frac{V_{max}}{R_M} \\ \omega_{max} = \frac{V_{max}}{K} \end{cases} \quad (2.31)$$

where the additional data ω_{max} is given by [10]. From (2.31), the desired quantities are determined as:

$$\begin{cases} K = \frac{V_{max}}{\omega_{max}} \\ R_M = K \frac{V_{max}}{M_{max}} = \frac{V_{max}^2}{\omega_{max} M_{max}} \end{cases} \quad (2.32)$$

Now, the previous analysis is extended to the three reaction wheels case. To do so, it is fundamental to consider that the gyroscopic term in the equation (2.15) is always compensated/cancelled by including it in the control signal. This means that the control torque can be written as $\tau_c = \tau_c' + (\omega \times (\mathbf{J}^{(sc)} \omega + \mathbf{H}_B^{(w)}))$ and equation (2.15) becomes

$$\dot{\omega} = \mathbf{J}^{(sc)-1} \tau_c' \quad (2.33)$$

Since the matrix $\mathbf{J}^{(sc)^{-1}}$ is diagonal, the results is a decoupled dynamics where each component of $\boldsymbol{\tau}'_c$ acts exclusively on the correspondent component of $\dot{\boldsymbol{\omega}}$. Moreover, from the equation (2.29), it has obtained the approximated equality between the torque command and the motor torque that, with the minus sign, acts on the satellite. So, as mentioned before, the motor dynamics can be neglected. This situation leads to represent the overall system of three reaction wheels and the satellite bus through an equivalent scheme composed by three structures like figures 2.3 and 2.4 where each of them describes the complete vehicle dynamics along the specific frame axis. It is clear that, in these three structure, the torque command T_c coincides with the proper component of the quantity $\boldsymbol{\tau}'_c$ and each inertia term $\frac{1}{J_{sc}}$ must be defined by the specific axis contribution (e.g. $\frac{1}{J_x}$). All this structure will be shown in detail in the chapter related to the MATLAB/Simulink implementation. Finally, it is important to highlight that all the analysis carried out in this section refers to a free-disturbance case. As it will be shown in the simulation implementation sections, to take into account the reaction wheel disturbances, it is simply necessary to add their contribution to the torque applied by reaction wheels to the satellite (i.e. M_{sc} in figure 2.3).

Reference generator

The reference generator is the subsystem responsible for producing the signals that must be tracked. However, the specific reference signals vary with the kind of control strategy. Anyway, there is a part of the reference computation procedure that is independent from the specific control approach and it is the determination of the reference angles related to the orientation that the satellite must follow. This orientation is defined through the relative attitude of the satellite frame with respect to the inertial one, fixed in the orbit, and it follows the Tait-Bryan convention.

Before analysing the reference computation procedure, it is fundamental to state that this kind of structure has been considered only from an academic point of view and only computer simulations have been performed. This means that it has been evaluated as an analog/continuous time system (as shown by figure 2.1), which not a good solution for a practical implemen-

tation due to its high complexity, as it will be shown in the following part. The best practical solution requires a micro-controller, so a digital/discrete time structure. The choice of this kind of implementation is compliant with the academic background about the digital control field. Therefore, in this thesis, the only important elements are the outputs provided by this block rather than the implementation type.

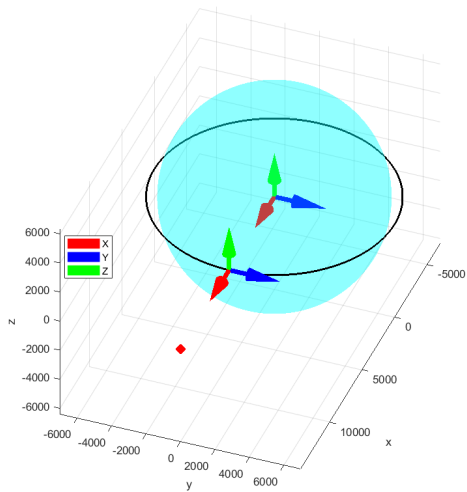
In order to understand how the references angles can be computed, the scenario represented by figures 2.6 and 2.7 has to be considered.

Figures 2.6 (a), (b), (c), (d) show in 3D and 2D how the satellite reference frame change its orientation during the orbital motion. Moreover, the red dot represents the target star.

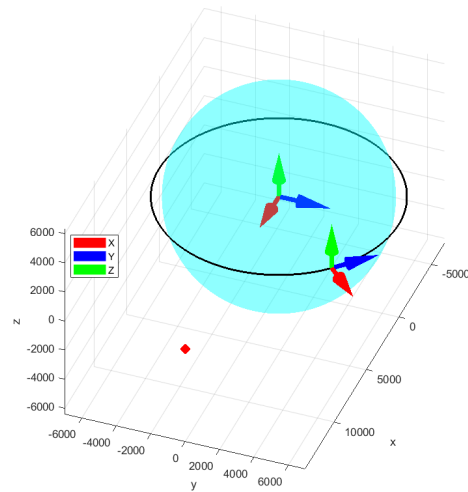
Now, it is crucial to say that the satellite telescope is considered coincident with the x-axis of the satellite frame and it passes through the central point of the focal plane. Therefore, the objective of the control is to point the x-axis towards the target star. Figure 2.7 shows the orientation that the satellite must have, in the same orbital point of figure 2.6 (b) and (d), in order to perform a perfect pointing action.

To compute the reference angle that must be tracked, the scenario in figure 2.8 has to be considered. The objective is to find the angle α . To do so, it is necessary to apply the *law of the cosines* and the *law of sines*. In particular, the first one is used to compute the quantity d_{sb} and the second one for α . Before analysing the computation procedure, the meaning of all the quantities involved in the scenario of figure 2.8 has to be cleared.

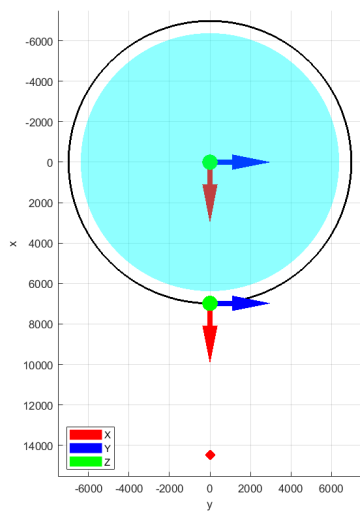
- \mathbf{R}_{or} : it represents the radius of the orbit, whose value is given by the sum between the mean Earth radius and the orbit altitude. So, $R_{or} = R_E + a = 6378 + 600 \text{ Km} = 6978 \text{ Km}$.
- \mathbf{d}_{so} : it defines the distance between the orbit and the target star. Its value is about $4.22 \text{ ly (light years)} = 4 \cdot 10^{13} \text{ Km}$.
- \mathbf{d}_{sb} : it characterizes the distance between the target star and the origin of the satellite reference frame (placed in its CoM). Its value is computed through the *law of cosines*.
- α : it is the angle between the segments $R_{or} + d_{so}$ and d_{sb} . As it is shown



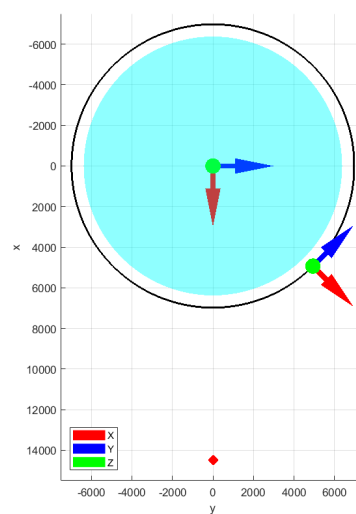
(a) 3D view-initial position



(b) 3D view-generic position

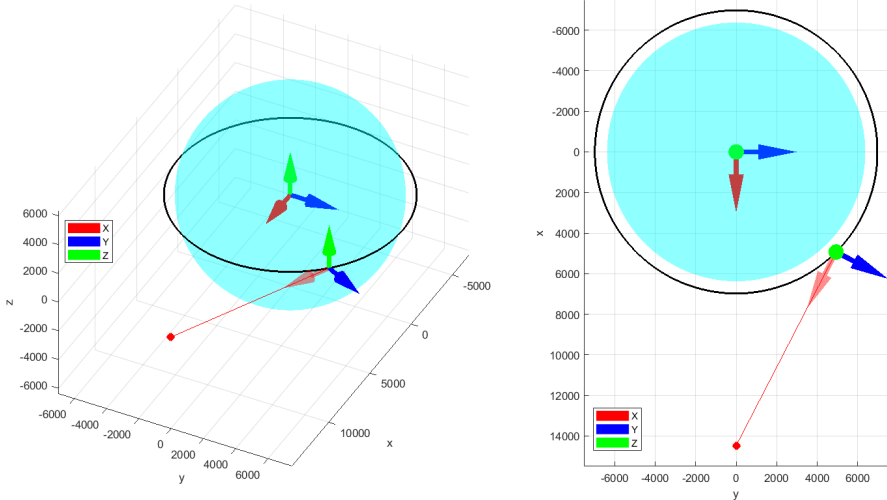


(c) 2D view-initial position



(d) 2D view-generic position

Figure 2.6: 3D and 2D view of the orbital motion scenario



(a) 3D view-pointing action

(b) 2D view-pointing action

Figure 2.7: Representantion of the pointing action

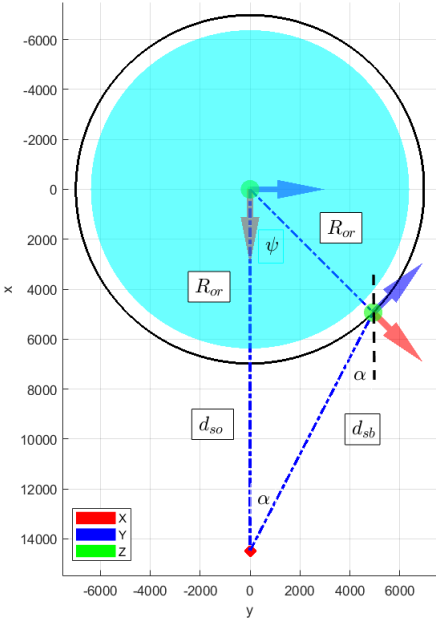


Figure 2.8: Schematic scenario for the α angle computation

by figure 2.8, it is also the angle between a line parallel to the x-axis of the inertial frame and the segment d_{sb} . This angle is computed by using the *law of sines*.

- ψ : it defines the angle between the segment that connects the origin of the inertial frame and the origin of the satellite frame (i.e. R_{or}) and the x-axis of the inertial frame. This angle is computed by considering the following situation: the satellite travels on an orbit whose radius is $R_{or} = 6978 \text{ Km}$. The velocity of the spacecraft CoM is given by $v = \sqrt{\frac{\mu}{R_{or}}}$ where $\mu = 0.3989 \cdot 10^{15} \frac{\text{m}^3}{\text{s}}$ is the *Earth gravitational parameter*. Since the following relation between the linear velocity and the angular one holds $v = \omega_{psi} R_{or}$, it is possible to compute the angular velocity as $\omega_{psi} = \omega_z = \frac{v}{R_{or}}$. Finally, the angle ψ is given by $\psi = \omega_{psi} t + \psi_0$ where ψ_0 is the initial angle, assumed equal to 0, as shown by figure 2.1 (c). It is worth noticing that ψ is the angle of the spacecraft frame with respect to the inertial frame and it varies along all the orbit.

As mentioned before, the *law of cosines* (2.34) and *the law of sines* (2.35) are used to determine the quantities d_{sb} and α .

$$d_{sb} = \sqrt{R_{or}^2 + (R_{or} + d_{so}^2 - 2R_{or}(R_{or} + d_{so})\cos\phi} \quad (2.34)$$

$$\frac{R_{or}}{\sin\alpha} = \frac{d_{sb}}{\sin\psi} \Rightarrow \sin\alpha = \frac{R_{or}}{d_{sb}}\sin\psi \Rightarrow \alpha = \text{asin}\left(\frac{R_{or}}{d_{sb}}\sin\psi\right) \quad (2.35)$$

Now, it is possible to define the reference angles that must be tracked by the control system. They are represented by ϕ_{ref} , θ_{ref} and ψ_{ref} and assume the following values:

$$\phi_{ref} = 0 \quad (2.36)$$

$$\theta_{ref} = 0 \quad (2.37)$$

$$\psi_{ref} = \begin{cases} -\alpha & 0 \leq \psi \leq \pi \\ \alpha & \pi < \psi < 2\pi \end{cases} \quad (2.38)$$

Some important comments must be made about (2.36), (2.37) and (2.38). ϕ_{ref} and θ_{ref} are set to 0 because, as mentioned before, the target star is

in the orbit plane and so the only angle that must be modified (due to the orbital motion) is ψ_{ref} . It is fundamental to highlight that these three angles are defined according to the Tait-Bryan convention, which can have two interpretations as mentioned in section 2.2 about the plant kinematics. Instead, the angle ψ_{ref} is set to $\pm\alpha$ since the orientation that the satellite must have is expressed with respect to the inertial frame and, as shown by figure, the rotation that has to be performed to point the x-axis towards the target star is a clockwise one of α (i.e. $\psi_{ref} = -\alpha$) in the first half of the orbit and a counter-clockwise one of α (i.e. $\psi_{ref} = \alpha$) in the second half of the orbit.

It is fundamental to highlight that once that the angle ψ belongs to the interval $(\frac{\pi}{2}, \frac{3}{2}\pi)$, the day-time phase of the orbital motion occurs. In this situation, the satellite attitude must be modified such that the solar panel point the Sun. However, as it can be notice from (2.38), the reference angles do not change. The reason behind this unmodified references is that if the solar panels of the satellite are placed such that the unit vectors normal to their surfaces are anti-parallel to the vehicle frame x-axis, the reference angles (2.36), (2.37) and (2.38) can be considered a good choice in terms of Sun-pointing to allow the accumulators charging operation.

Instead, when the angle ψ satisfies the relation $\frac{3}{2}\pi \leq \psi \leq \frac{5}{2}\pi$, the nigh-time phase begins. In this situation, the satellite orientation must be changed to guarantee the target star pointing.

Finally, it is also important to notice that when $\psi > \pi$ (2.34) and (2.35) must be modified by substituting $\cos \phi$ with $\cos(2\pi - \phi)$ and $\sin \phi$ with $\sin(2\pi - \phi)$.

2.3 MATLAB/Simulink implementation

MATLAB/Simulink is a software tool used to perform simulations of control systems. As it will be shown later, to build a simulation scheme, a set of specific blocks are used. In particular, for the structure analysed in this thesis, the main blocks are integrators, with specific initial conditions, and MATLAB function blocks which allow to implements the state equations of each subsystem. In this way, it has been possible to build a structure

that is able to provide the system outputs, through the integration of the differential state equations. Other blocks will be shown in the next figures and their functions will be explained during the specific analysis.

Plant

The Simulink scheme of the plant is shown by figure 2.9. It is immediately evident the two main parts that characterize this subsystem: *dynamics* and *kinematics*. As mentioned in section 2.2 and shown by figure 2.9, the dy-

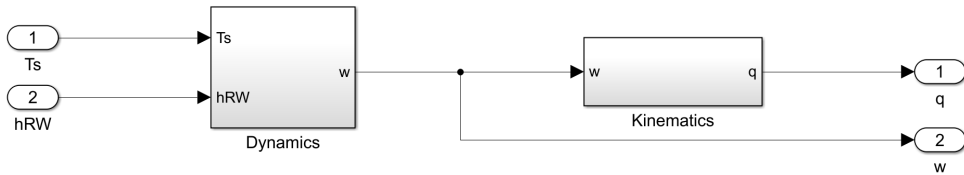


Figure 2.9: Simulink plant structure

namics block takes as inputs the satellite-applied torque T_s (control torque plus disturbances) and the contribution coming from the actuators h_{RW} and it produces as output the spacecraft angular speed w . A detailed implementation of this block is given by figure 2.10. The MATLAB function labelled

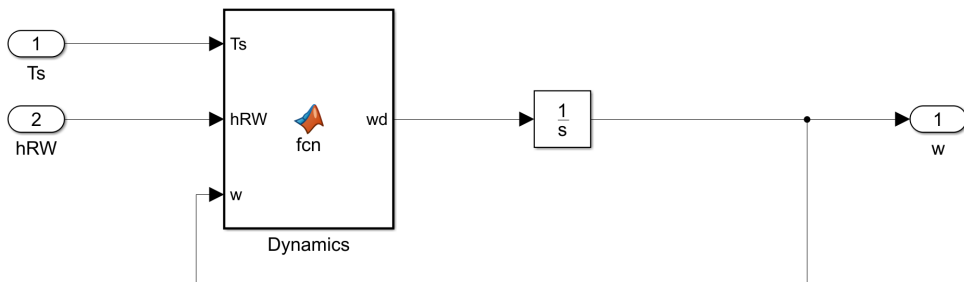


Figure 2.10: Plant dynamics block

as *Dynamics* is used to implement the equation (2.15). Then, the integrator block is responsible for the integration operation so that the angular speed w can be computed from its derivative w_d . This block contains the speed initial condition, describing the orbital angular motion of the satellite before the control action activation. Moreover, it is important to highlight that T_s

and h_{RW} of the Simulink scheme coincide respectively with $\boldsymbol{\tau}$ and $\mathbf{H}_B^{(w)}$ of (2.15).

Instead, the kinematics implementation is sketched in figure 2.11. Also in

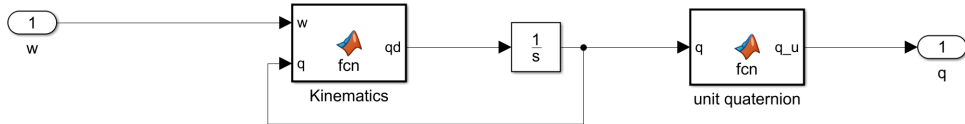


Figure 2.11: Plant kinematics

this case, there is a MATLAB function called *Kinematics* which is used to represent the relation between the quaternion derivative and angular speed, as shown by (2.20). Then, the integrator block, whose initial condition is $q_{init} = [1 \ 0 \ 0 \ 0]^T$ (i.e. no initial rotation with respect to the inertial frame, as mentioned in section 2.2 about the reference generation), is employed to compute the attitude quaternion q . Moreover, there is another block labelled as *unit quaternion* which is used to set the quaternion norm to 1. Actually, the quaternions describing rotations are already unit quaternion. However, due to computational error, their norm slightly differs from 1. For this reason, it is important to consider this block.

It is fundamental to highlight that, as it will be shown in chapters 3 and 4, the plant outputs q and w of figure 2.9 follow a feedback path towards the *control inputs* block. Finally, it must be pointed out that the attitude quaternion is injected in another block (not shown in figure 2.9) which extracts the Tait-Bryan angles from it. This operation is really important since allows to compute the pointing error, intended as difference between the reference angles and the actual ones.

Actuators

The complete Simulink scheme of the three reaction wheels is shown by figure 2.12. There are four main blocks and three of them represent the RWs used to apply the control torque to the satellite. Each of them takes as inputs the specific axial component of the control/command torque (e.g. the third block, which describes the reaction wheel aligned with the z-axis of the vehicle

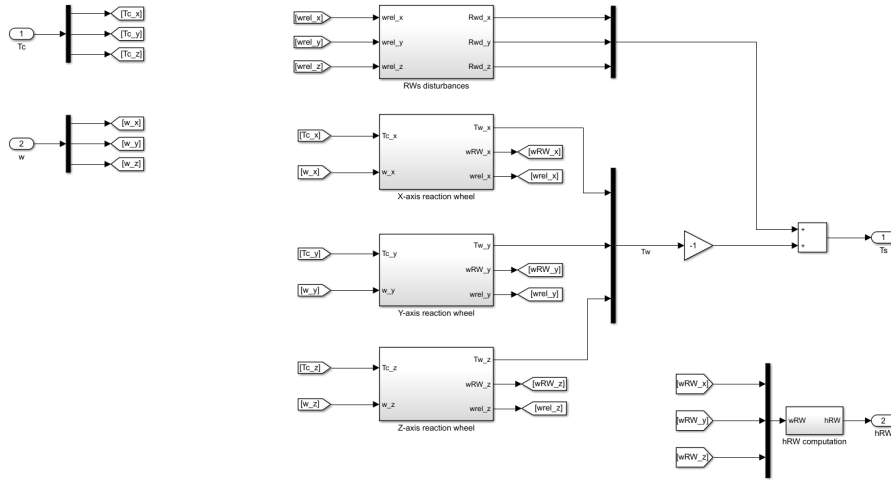


Figure 2.12: Actuators scheme

frame, receives the signal T_{cz}) and the axial component of the satellite speed (e.g. w_z). As outputs, the RWs block provide the specific wheel/motor torque T_w , the absolute wheel angular speed w_{RW} and the relative speed with respect to the satellite w_{rel} . All the motor torques are grouped through a *mux* block to create a vectorial structure and it is considered the opposite value (-1 block) to determine the torque that must be applied to the satellite, according to the analysis made in section 2.2. Moreover, the absolute angular speeds of the wheels are used to compute the angular momenta h_{RW} (block on the lower right angle of the figure 2.12) used in the satellite dynamics equation. Instead, the relative velocities are injected in the *RWs disturbances* block to compute all the disturbances produced by these actuators. By the way, the above-mentioned block is sketched in figure 2.13. The three blocks implement the disturbances acting on each axis of the vehicle frame, according to analysis made in section 1.2.3 and the relations (1.28). As it is possible to see, if a frame axis is considered (e.g. x-axis), the disturbance about it is given by the contributions coming from the wheels aligned with the other two axes (e.g. y-axis and z-axis). These disturbances are linked to the relative speeds of the wheels, as mentioned in section 1.2.3. This is the reason why each block of figure 2.13 has the quantity w_{rel} as input. Then, as shown by figure 2.12, the three disturbance contributions are grouped by using a *mux* and summed to

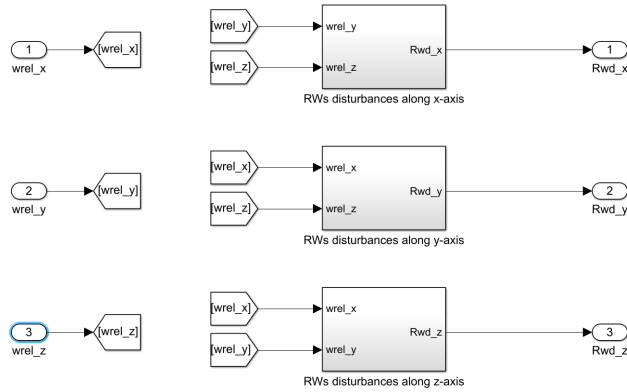


Figure 2.13: RWs implementation

the opposite of the wheel/ motor torque $-T_w$, in order to be applied to the plant.

Finally, the detailed structure of a reaction wheel is shown by figure 2.14 (as example it is considered the z-axis wheel). This is the same scheme

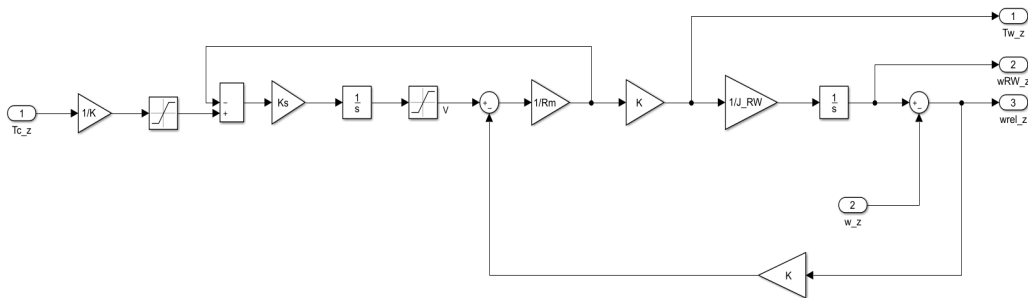


Figure 2.14: Structure of z-axis reaction wheel

analysed in the section 2.2 (figure 2.3 and 2.4). So, as mentioned before, the overall actuators structure is given by three block schemes as figure 2.14. The only difference is that, in the previous analysis, an equivalent scheme has been considered, characterized by the decoupled dynamics expression, due to the gyroscopic compensation, such that the terms $\frac{1}{J_{sc}}$ and the net control/command torques (i.e. without the compensation) could be directly considered. Instead, figure 2.14 shows the *real* implementation scheme. It must be highlighted that the two schemes are completely analogous.

Reference generator

Finally, the first part of the reference generator implementation is shown by figure 2.15. The MATLAB function contains the expressions of the *law of*

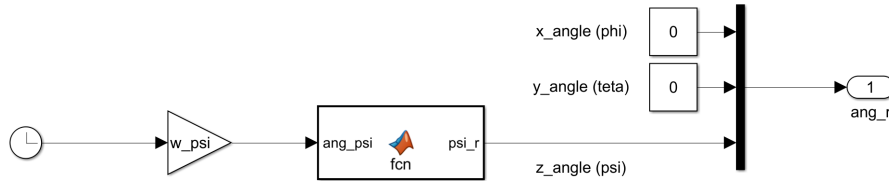


Figure 2.15: First part of the reference generator structure

sines and cosines used for computing the reference angle ψ_{ref} , as described by (2.34), (2.35) and (2.38). The input of the MATLAB function is simply the relation that determines the ψ angle due to the orbital motion, as described by $\psi = \omega_{psi} t + \psi_0$ where ψ_0 is the initial angle, assumed equal to 0. The angles ϕ and θ are set to 0, according to (2.37) and (2.38), and they complete the reference angles vector ang_r of figure 2.15.

2.4 EICASLAB implementation

EICASLAB is a software suite developed by EICAS Automazione S.p.A., the company where this work of thesis has been developed. It was born to allow a professional implementation of control systems to be used in different fields like the aerospace one. The main characteristic of this software is the C code-based implementation. Indeed, every subsystem of the control structure requires a specific development in C code. As it will be mentioned in the following chapters, this is a really useful approach since to build a controller for a real application, the C code of the control law is required. Indeed, this code must be loaded in a target board. Therefore, in this work of thesis, the usage of the EICASLAB suite has represented a step towards a possible real implementation. The following part will briefly analyse how the subsystems mentioned in this chapter have been built in EICASLAB.

Plant and Actuators

Figure 2.16 shows the EICASLAB block related to the plant, the actuators and the disturbances produced by the latter. Inside this block, there is the

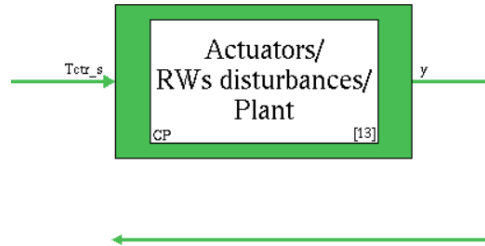


Figure 2.16: Plant, actuators and disturbances block

C code describing all the dynamics of the actuators (including the integral control used to define the torque command and to neglect the motors dynamics), the plant and the RWs disturbances. In particular, the C code is divided in three main functions called *Initialization*, *Execution* and *Output*. which are called by the solver to get the simulation results. In the *Initialization* function there are the initial values for the desired variables, like the states, and it is called once at the beginning of the simulation. The *Execution* function performs all the computations linked to the state equations. It must be highlighted that this function is used by the integration routine which is responsible for solving the specific differential equations. Finally, the *Output* function is used to define the output equations needed for the computation of all the block output variables. As shown by figure 2.16, the input is the control/command torque T_{ctr_s} . Instead, the output y contains the quaternion attitude q , the satellite angular speed ω and the actuators angular momenta which can be labelled as h_{RW} , as in the MATLAB/Simulink implementation. As shown by figure 2.16, the output follows a feedback path that ends in the *control inputs* block, as it will be deeply analysed in the following chapters. By exploring the C code of this block is possible to find the specific implementations of the state equations that characterize the actuators dynamics (according to (2.28) and the schemes of figures 2.3 and 2.4) and the plant dynamics (2.15) and kinematics (2.20). This C code is characterized by suit-

able functions that have been built for this work of thesis and grouped in a specific library. Moreover, the code lines for the disturbances description follow the analysis made in section 1.2.3 and the relation (1.28). Finally, it must be highlighted this simulation block produces also the Tait-Bryan angles (not shown in figure 2.16 but in the following chapters), that are injected in another block responsible for the computation of the difference between the reference angles and the actual ones.

Reference generator

The block shown by figure 2.17 represents the overall reference generator structure. In particular, inside it, there are the C code functions used to implement the first part of the reference generation, as mentioned in 2.2.3. Also in this case, there are the three main functions *Initialization*, *Execution* and *Output*. However, in this situation, it has been decided to use only the *Output* function, and leaving empty the other ones, since no initialization has been necessary and the *Execution* function could be included in the *Output* one because, from a logical point of view, the distinction between them could be neglected.

The code lines of this block mainly refer to the *law of sines and cosines*, which allow to determine the reference angle ψ_r , as shown by (2.34), (2.35) and (2.38). Moreover, it is possible to notice the two constant/step references ϕ_r and θ_r whose values are set to 0 according to (2.36) and (2.37). These reference variables are the inputs of the *reference generator* block since are useful to build the complete *reference angles* variable, labelled as ang_r . Finally, it is important to highlight that this block contains also the code lines related to the second part of the reference generation, which is specific for each kind of control strategy and it will be deeply analysed in the following chapters.

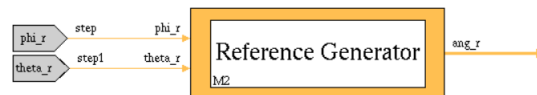


Figure 2.17: Reference generator block

Chapter 3

Benchmark control system

This chapter deals with a particular control approach used in many attitude modification procedures. Indeed, there are lots of papers, like [1] and [9] that exploit this control strategy or a similar one, characterized by small modifications/additions with respect to the one that has been considered in this work of thesis. As it will be shown in section 3.2, the controller considered in the benchmark control system is a non-linear PD one. Instead, the modified controller mentioned before, simply consider an additional feedforward term with respect to the basic PD structure. The first step, towards the analysis of the benchmark control system, will be the evaluation of that part of the reference generator which, as mentioned in chapter 2, changes according to specific control approach. Moreover, the structure of the *control inputs* subsystem will be considered since it is also subject to the specific control methodology.

The second step is the theoretical analysis of the PD controller structure, starting from the expression of the control signal. After that, the relation between the desired orientation angles and the actual ones will be shown, in the free-disturbance case. Then, the effect of the RWs disturbances on the actual attitude angles will be pointed out. This will be a crucial part of the chapter since it allows to understand how RWs disturbances can affect the pointing stability of the satellite telescope. Finally, it will be shown how the overall simulation scheme, and in particular the controller structure, has been built both in MATLAB/Simulink and EICASLAB.

3.1 Reference generator and control inputs: specific analysis

As mentioned before, the two subsystems known as *reference generator* and *control inputs* have a variable structure according to the control methodology. In this section, their specific structure will be analysed. Since in the previous chapter it has been pointed out that the plant kinematics is characterized by the quaternion description, the same approach has to be followed for these subsystem. This means that the reference signal and the control input must be quaternions. Moreover, as it will be shown later, there is another kinematic variable that is used to define the control action i.e. the satellite angular speed. Therefore, the *reference generator* and *control inputs* block will also produce specific signals related to the angular velocity

Reference generation

The reference generation procedure is characterized by two parts, as mentioned in chapter 2. The first one, that deals with the definition of the Tait-Bryan angles to be tracked, has been already analysed in the previous chapter. Now, it is fundamental to define the second part which is related to the implementation of the reference signals used to build the control variable. The starting point is the definition of the reference quaternion \mathbf{q}_{ref} coming from the Tait-Bryan angles $\phi_{\text{ref}}, \theta_{\text{ref}}, \psi_{\text{ref}}$, expressed by (2.36), (2.37) and (2.38). As stated in section 2.2, the Tait-Bryan convention defines the rotation matrix between the inertial fixed frame and the satellite mobile frame as a sequence of multiplications among the elementary rotations matrices. According the *extrinsic* interpretation, the rotation matrix about x-axis is pre-multiplied by the one related to the y-axis rotation and, in turn, pre-multiplied by the matrix linked to the z-axis rotation. It is important to remind that all the rotations are performed about the fixed frame axes. Equivalently, the *intrinsic* interpretation states that the rotation matrix about the z-axis must be post-multiplied by the one related to the y-axis rotation, which is post-multiplied by the x-axis matrix. In this case, the first rotation is about the reference frame z-axis and the others are performed

with respect to the mobile frame axes as it changes orientation.

In the same way, it is possible to define the complete quaternion that describes the general attitude, given by the sequence of three elementary rotations. Therefore, for the reference quaternion, the following relation holds:

$$\mathbf{q}_{\text{ref}} = \mathbf{q}_\psi \otimes \mathbf{q}_\theta \otimes \mathbf{q}_\phi \quad (3.1)$$

where

$$\begin{cases} \mathbf{q}_\psi = [\cos(\frac{\psi}{2}) & 0 & 0 & \sin(\frac{\psi}{2})]^T \\ \mathbf{q}_\theta = [\cos(\frac{\theta}{2}) & 0 & \sin(\frac{\theta}{2}) & 0]^T \\ \mathbf{q}_\phi = [\cos(\frac{\phi}{2}) & \sin(\frac{\phi}{2}) & 0 & 0]^T \end{cases} \quad (3.2)$$

are the quaternions describing the elementary rotations about x, y and z axis. It is important to highlight that \otimes defines the *quaternion product*. Once the attitude quaternion is built, another signal must be computed: the reference angular speed related to the specific time trend of the Tait-Bryan reference angles. To do so, it is used the following relation:

$$\boldsymbol{\omega}_{\text{ref}} = \begin{bmatrix} \omega_{x_{\text{ref}}} \\ \omega_{y_{\text{ref}}} \\ \omega_{z_{\text{ref}}} \end{bmatrix} = \begin{bmatrix} 1 & 0 & -\sin(\theta_{\text{ref}}) \\ 0 & \cos(\phi_{\text{ref}}) & \sin(\phi_{\text{ref}})\cos(\theta_{\text{ref}}) \\ 0 & -\sin(\phi_{\text{ref}}) & \cos(\phi_{\text{ref}})\cos(\theta_{\text{ref}}) \end{bmatrix} \begin{bmatrix} \dot{\phi}_{\text{ref}} \\ \dot{\theta}_{\text{ref}} \\ \dot{\psi}_{\text{ref}} \end{bmatrix} \quad (3.3)$$

It is important to point out that relation (3.3) is valid only for the Tait-Bryan convention and, as it is possible to notice, it requires the knowledge of the reference angles and their derivatives.

Control inputs

This subsystem is responsible for the generation of proper signals required by the controller to define the control action. In order to determine these signals, some computations must be done on the reference variables and the output ones. Indeed, the inputs of this subsystem are the reference quaternion \mathbf{q}_{ref} , the reference angular speed $\boldsymbol{\omega}_{\text{ref}}$, the actual attitude quaternion \mathbf{q} and the satellite angular speed $\boldsymbol{\omega}$. The last two characterize the feedback path starting from the plant.

The first computation is the difference between $\boldsymbol{\omega}_{\text{ref}}$ and $\boldsymbol{\omega}$ such that the angular speed error is defined as $\boldsymbol{\omega}_e = \boldsymbol{\omega}_{\text{ref}} - \boldsymbol{\omega}$.

The second computation deals with the reference and actual quaternions. However, instead of considering the difference between them, another approach is used, conceptually identical to the difference operation. For this reason a new quaternion is introduced, called *error quaternion* \mathbf{q}_e . As mentioned by [1], it is defined as the quaternion that starting from the actual attitude \mathbf{q} provides the desired orientation \mathbf{q}_{ref} , by considering an *extrinsic* rotation i.e. $\mathbf{q}_e \otimes \mathbf{q} = \mathbf{q}_{\text{ref}}$. From this definition, the following relation holds:

$$\mathbf{q}_e = \begin{bmatrix} q_{e0} \\ \mathbf{q}_e \end{bmatrix} = \mathbf{q}_{\text{ref}} \otimes \mathbf{q}^{-1} = \mathbf{q}_{\text{ref}} \otimes \mathbf{q}^* \quad (3.4)$$

where the inverse quaternion \mathbf{q}^{-1} coincides with the conjugate one \mathbf{q}^* , since the attitude is represented by the unit quaternion \mathbf{q} .

Finally, it is important to highlight that, as it will be shown in the following section and in the simulation schemes, the control variable requires other two signals: the actual satellite angular speed $\boldsymbol{\omega}$ and the reaction wheels angular momenta $\mathbf{H}_B^{(w)}$, as described by equation (2.14), which come from the feedback paths starting from the actuators and plant. Therefore, these signals can also be considered as part of the *control inputs* block, even though no modification is made to them, but they simply pass across the system and go to the *sampler*. Moreover, it is important to highlight that this system has been considered as an analog/continuous time structure since, as displayed by figure 2.1. From a practical point of view, its implementation is a little bit more complex than the one that can be developed with a digital/discrete system (micro-controller), due to the nature of the quaternion product. Anyway, an analog implementation is not so hard, since relation (3.4) involves basically summations, subtractions, products and signs inversions.

3.2 Benchmark controller general analysis

The benchmark control system for the satellite attitude modification is based on a non-linear PD (Proportional-Derivative) controller, also defined in this thesis *benchmark controller*. Figure 3.1 shows the overall control scheme. Before starting the study, it must be highlighted that all the analysis is made by considering the overall control scheme as a continuous-time structure. Then,

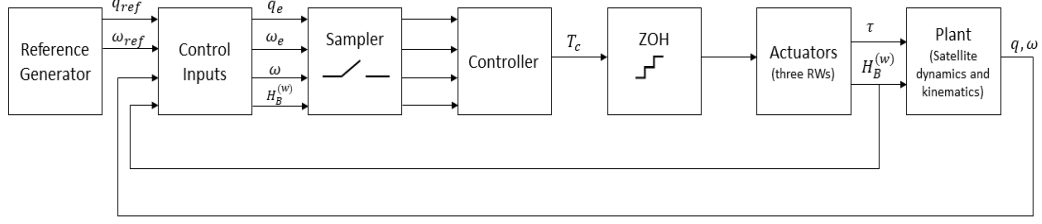


Figure 3.1: Complete control scheme

since the control strategy analysed in this thesis is based on a digital/discrete controller, some comments will be made in order to clarify the passage from a total continuous-time system to an hybrid structure (discrete controller plus actuators and plant that are continuous-time structures).

The expression of the control variable, which is the set of three torques that the RWs must apply to the satellite, is given by equation (3.5). This relation is mentioned by [1] and [9]. The latter shows a more explicit form that will be analysed later.

$$\boldsymbol{\tau}_c = \mathbf{J}^{(sc)} \mathbf{K}_P \mathbf{q}_e + \mathbf{J}^{(sc)} \mathbf{K}_D \boldsymbol{\omega}_e + \boldsymbol{\omega} \times (\mathbf{J}^{(sc)} \boldsymbol{\omega} + \mathbf{H}_B^{(w)}) = \boldsymbol{\tau}'_c + \boldsymbol{\omega} \times (\mathbf{J}^{(sc)} \boldsymbol{\omega} + \mathbf{H}_B^{(w)}) \quad (3.5)$$

where \mathbf{K}_P is the *proportional gain* matrix, \mathbf{q}_e is the vectorial part of the *error quaternion*, \mathbf{K}_D is the *differential gain* matrix, $\boldsymbol{\omega}_e$ is the *angular speed error* and $\boldsymbol{\omega} \times (\mathbf{J}^{(sc)} \boldsymbol{\omega} + \mathbf{H}_B^{(w)})$ is the term used for the *gyroscopic compensation*. As it is possible to see, the relation includes two linear terms given by $\mathbf{K}_P \mathbf{q}_e$ and $\mathbf{K}_D \boldsymbol{\omega}_e$ and one non-linear term i.e. $\boldsymbol{\omega} \times (\mathbf{J}^{(sc)} \boldsymbol{\omega} + \mathbf{H}_B^{(w)})$. The variable $\boldsymbol{\tau}'_c$ can be defined as the *net control torque*. The reason why this control structure is called PD will be explained later. It is fundamental to highlight that equation (3.5) defines the first element of the quantity $\boldsymbol{\tau}$ shown by figure 3.1. Indeed, as mentioned in section 2.2, the variable $\boldsymbol{\tau}$ of equation (2.15) can be expressed as $\boldsymbol{\tau} = \boldsymbol{\tau}_c + \mathbf{M}_B^{dist}$, where $\boldsymbol{\tau}_c$ is the control torque applied by the RWs to the satellite and \mathbf{M}_B^{dist} defines the RWs disturbances. The latter, for notation simplicity, will be written as \mathbf{M}^{dist} . Moreover, the relation among the control commands \mathbf{T}_c , the actual torques produced by the DC motors \mathbf{M} on the flywheels and the ones applied by the RWs to the satellite $\boldsymbol{\tau}_c$ has been deeply described in section 2.2.

The first step of the analysis focuses on some simplifications about all the quaternions used in the overall control scheme of figure 3.1. As mentioned by [1], the quaternion that describes the general orientation of a satellite can be approximated by the relation (3.6), if the well-known angles ϕ , θ and ψ assume small values.

$$\mathbf{q} = \begin{bmatrix} 1 \\ \frac{1}{2}\phi \\ \frac{1}{2}\theta \\ \frac{1}{2}\psi \end{bmatrix} \quad (3.6)$$

Now, let's recall the definition of error quaternion i.e. $\mathbf{q}_e = \mathbf{q}_{ref} \otimes \mathbf{q}^{-1} = \mathbf{q}_{ref} \otimes \mathbf{q}^*$. By exploiting the situation expressed by (3.6), if the quaternions \mathbf{q} and \mathbf{q}_{ref} are sufficiently close such that the error quaternion \mathbf{q}_e can describe a small rotation, the following relation holds:

$$\mathbf{q}_e = \begin{bmatrix} 1 \\ \frac{1}{2}(\phi_{ref} - \phi) \\ \frac{1}{2}(\theta_{ref} - \theta) \\ \frac{1}{2}(\psi_{ref} - \psi) \end{bmatrix} \quad (3.7)$$

This result can be proved by considering a nominal quaternion \mathbf{q}^0 around which \mathbf{q} and \mathbf{q}_{ref} are supposed to lay. This means that \mathbf{q} and \mathbf{q}_{ref} are sufficiently close to the nominal attitude \mathbf{q}^0 . This quaternion is considered a linearisation point for the kinematics equation (2.20). In this work of thesis, $\mathbf{q}^0 = [1 \ 0 \ 0 \ 0]^T$ which is the initial attitude condition, as mentioned in the previous chapter. According to the above-mentioned situation, \mathbf{q} and \mathbf{q}_{ref} can be written as:

$$\mathbf{q} = \begin{bmatrix} 1 \\ \frac{1}{2}\phi \\ \frac{1}{2}\theta \\ \frac{1}{2}\psi \end{bmatrix} \quad \mathbf{q}_{ref} = \begin{bmatrix} 1 \\ \frac{1}{2}\phi_{ref} \\ \frac{1}{2}\theta_{ref} \\ \frac{1}{2}\psi_{ref} \end{bmatrix} \quad (3.8)$$

Now, by performing the quaternion product $\mathbf{q}_{ref} \otimes \mathbf{q}^*$ and considering the first order approximation, it is obtained relation (3.7). An interesting observation, that will be used in the following analysis, must be made about relation (3.7). As pointed out by [1], from the vectorial parts of \mathbf{q}_e , it is possible to recover the angles by multiplying the expressions by 2. Therefore, from

the error quaternion can be recovered the differences between the reference angles and actual angles, that define the *error angles*. Now, by inserting the first relation of (3.8) in the kinematics equation (2.20) and considering the first order approximation, the following relation holds:

$$\begin{bmatrix} \dot{\phi} \\ \dot{\theta} \\ \dot{\psi} \end{bmatrix} = \begin{bmatrix} \omega_x \\ \omega_y \\ \omega_z \end{bmatrix} \quad (3.9)$$

Expression (3.9) defines the linearised kinematics equation, where, as mentioned before, \mathbf{q}^0 is the linearisation point. Finally, it is easy to see that this reasoning can be applied to the reference quaternion (and so to the reference angles) and the reference angular speeds such that:

$$\begin{bmatrix} \dot{\phi}_{ref} \\ \dot{\theta}_{ref} \\ \dot{\psi}_{ref} \end{bmatrix} = \begin{bmatrix} \omega_{x_{ref}} \\ \omega_{y_{ref}} \\ \omega_{z_{ref}} \end{bmatrix} \quad (3.10)$$

The second step of the analysis deals with the gyroscopic compensation term and the net control torque. As it can be easily seen, the gyroscopic compensation allows to remove the non-linearity of the dynamics equation (2.15), such that it can be rewritten as

$$\dot{\boldsymbol{\omega}} = \mathbf{J}^{(sc)^{-1}} (\boldsymbol{\tau}'_c + \mathbf{M}^{dist}) \quad (3.11)$$

Instead, according to the previous analysis about the linearised kinematics, the net control torque can be written as:

$$\boldsymbol{\tau}'_c = \mathbf{J}^{(sc)} \mathbf{K}'_P \begin{bmatrix} \phi_{ref} - \phi \\ \theta_{ref} - \theta \\ \psi_{ref} - \psi \end{bmatrix} + \mathbf{J}^{(sc)} \mathbf{K}_D \begin{bmatrix} \omega_{x_{ref}} - \omega_x \\ \omega_{y_{ref}} - \omega_y \\ \omega_{z_{ref}} - \omega_z \end{bmatrix} \quad (3.12)$$

where it must be considered that $\mathbf{K}_P = 2\mathbf{K}'_P$, in order to recover the error angles from the error quaternion. Now, by adding (3.12) into (3.11), considering that differentiation of (3.9) is given by $[\ddot{\phi} \ \ddot{\theta} \ \ddot{\psi}]^T = [\dot{\omega}_x \ \dot{\omega}_y \ \dot{\omega}_z]^T = \dot{\boldsymbol{\omega}}$ and taking into account (3.9)-(3.10), relation (3.13) is obtained.

$$\begin{bmatrix} \ddot{\phi} \\ \ddot{\theta} \\ \ddot{\psi} \end{bmatrix} = \mathbf{K}'_P \begin{bmatrix} \phi_{ref} - \phi \\ \theta_{ref} - \theta \\ \psi_{ref} - \psi \end{bmatrix} + \mathbf{K}_D \begin{bmatrix} \dot{\phi}_{ref} - \dot{\phi} \\ \dot{\theta}_{ref} - \dot{\theta} \\ \dot{\psi}_{ref} - \dot{\psi} \end{bmatrix} + \mathbf{J}^{(sc)^{-1}} \mathbf{M}^{dist} \quad (3.13)$$

So, as it is possible to notice, (3.12) and (3.13) are characterized by the proportionality relation with respect to the error angles and their differentiation. For this reason, this controller is called PD.

Starting from relation (3.13), it is possible to determine two useful vectorial transfer functions: the first one describes the time evolution of the actual attitude angles when the desired ones are considered as inputs of the system. The second one considers as inputs the RWs disturbances and highlights their influence on the actual attitude angles. Now, before computing the *tfs*, it is important to notice that if the matrix \mathbf{K}'_P and \mathbf{K}'_D are chosen to be diagonal, as shown by (3.14), it is obtained a decoupled structure where each input affect only the correspondent output. This situation is still valid for \mathbf{M}^{dist} , since $\mathbf{J}^{(sc)^{-1}}$ is a diagonal matrix.

$$\mathbf{K}'_P = \begin{bmatrix} k_{P\phi} & 0 & 0 \\ 0 & k_{P\theta} & 0 \\ 0 & 0 & k_{P\psi} \end{bmatrix} \quad \mathbf{K}'_D = \begin{bmatrix} k_{D\phi} & 0 & 0 \\ 0 & k_{D\theta} & 0 \\ 0 & 0 & k_{D\psi} \end{bmatrix} \quad (3.14)$$

So, let's consider the first vectorial transfer function which involves the reference angles and the actual ones. To do so, first of all the quantity $\mathbf{J}^{(sc)^{-1}}\mathbf{M}^{dist}$ is set to 0 and, then, it is performed a separation of the considered variables, such that the following relations can be written:

$$\begin{cases} \ddot{\phi} + k_{D\phi}\dot{\phi} + k_{P\phi}\phi = k_{D\phi}\dot{\phi}_{ref} + k_{P\phi}\phi_{ref} \\ \ddot{\theta} + k_{D\theta}\dot{\theta} + k_{P\theta}\theta = k_{D\theta}\dot{\theta}_{ref} + k_{P\theta}\theta_{ref} \\ \ddot{\psi} + k_{D\psi}\dot{\psi} + k_{P\psi}\psi = k_{D\psi}\dot{\psi}_{ref} + k_{P\psi}\psi_{ref} \end{cases} \quad (3.15)$$

By considering the Laplace transformation of (3.15), the following transfer functions can be considered:

$$\begin{cases} \frac{\phi(s)}{\phi_{ref}(s)} = \frac{k_{D\phi}s + k_{P\phi}}{s^2 + k_{D\phi}s + k_{P\phi}} \\ \frac{\theta(s)}{\theta_{ref}(s)} = \frac{k_{D\theta}s + k_{P\theta}}{s^2 + k_{D\theta}s + k_{P\theta}} \\ \frac{\psi(s)}{\psi_{ref}(s)} = \frac{k_{D\psi}s + k_{P\psi}}{s^2 + k_{D\psi}s + k_{P\psi}} \end{cases} \quad (3.16)$$

A mentioned by [9], it is possible to choose all the proportional coefficients as $k_P = \omega_n^2$ and the derivative ones like $k_D = 2\zeta\omega_n$, such that the denominators of (3.16) coincide with the one of the classical 2^{nd} order transfer function. Moreover, it can be noticed the presence of a zero at $s = -\frac{k_P}{k_D} = -\frac{\omega_n}{2\zeta}$. Anyway, it is fundamental to highlight that the DC-gain of all the transfer functions is equal to 1. All the effects related to this kind of transfer function will be analysed in chapter 5, which deals with the specific simulation results. Finally, it must be pointed out that, to determine (3.16), all the initial conditions about the angles (both reference and actual ones) and their derivatives are considered 0. Actually, there are some non-zero initial conditions i.e. the initial angular speeds, as mentioned in sections 2.2. However, these values are quite small and they can be considered zero.

Instead, the second vectorial transfer function describes the influence of the reaction wheel disturbances on the time evolution of the actual attitude angles. In this case, starting from equation (3.13), the reference angles $\phi_{ref}, \theta_{ref}, \psi_{ref}$ are set to 0. So, the following relations hold:

$$\begin{cases} \ddot{\phi} + k_{D\phi}\dot{\phi} + k_{P\phi}\phi = J_x^{-1}M_x^{dist} \\ \ddot{\theta} + k_{D\theta}\dot{\theta} + k_{P\theta}\theta = J_y^{-1}M_y^{dist} \\ \ddot{\psi} + k_{D\psi}\dot{\psi} + k_{P\psi}\psi = J_z^{-1}M_z^{dist} \end{cases} \quad (3.17)$$

By applying the Laplace transformation to (3.17), the following transfer functions can be written:

$$\begin{cases} \frac{\phi(s)}{M_x^{dist}(s)} = \frac{J_x^{-1}}{s^2 + k_{D\phi}s + k_{P\phi}} \\ \frac{\theta(s)}{M_y^{dist}(s)} = \frac{J_y^{-1}}{s^2 + k_{D\theta}s + k_{P\theta}} \\ \frac{\psi(s)}{M_z^{dist}(s)} = \frac{J_z^{-1}}{s^2 + k_{D\psi}s + k_{P\psi}} \end{cases} \quad (3.18)$$

The coefficients k_P and k_D are always set to ω_n^2 and $2\zeta\omega_n$. In this case, the DC-gain is expressed by $\frac{J^{-1}}{k_P}$. This relation is really important since it will allow to explain all the system behaviours experienced in the simulations (chapter 5). Finally, the comment made for the initial conditions of (3.16) is

still valid for (3.18).

Now, it is important to clarify a particular aspect of the control system shown by figure 3.1. It is evident that the overall scheme is hybrid, which means that includes both continuous-time subsystems and discrete-time ones. Their interfaces are managed by the *sampler* and *ZOH*. As mentioned before, all the previous analysis is based on a full continuous-time structure. However, the controller is defined by a static relation which means that there are only suitable gains that multiply specific variables. So, the discretization of the control law (3.5) does not modify the specific relation. However, when a discrete controller is obtained by a continuous one, the dynamics of the *ZOH* must be included in the *plant+actuator* structure. Since in this work of thesis the above-mentioned situation has been neglected (only because the thesis aims to perform an initial study of the whole attitude control problem with RWs and their influence), the sampling time has been chosen smaller than the one coming from the specific selection rules. In this way, the input signal to the *actuators* block (coming from the *ZOH*) is more similar to the one that can be obtained with a full continuous-time control scheme (where there is not a *ZOH*) and so the *ZOH* dynamics can be, more or less, considered negligible.

3.3 MATLAB/Simulink implementation

Figure 3.2 shows the complete simulation scheme developed in MATLAB-Simulink. As it is possible to see, there are some extra block with respect to scheme of figure 3.1. Indeed, the conversion from quaternions to Tait-Bryan angles is performed by the *q-ang conversion* block. Then, the output of the latter is injected in the summing node so that the difference between the reference quantities ang_r and the actual ones ang is computed. The result of this operation produces the signal labelled as ang_e^{rad} , which defines the error angles expressed in radians. Since the analysis of the pointing stability is made by considering all the angles expressed in arcseconds, the *rad to as* block is responsible for this transformation.

The following part will focus one the detailed implementations of the *reference generator*, *control inputs* and *controller* block.

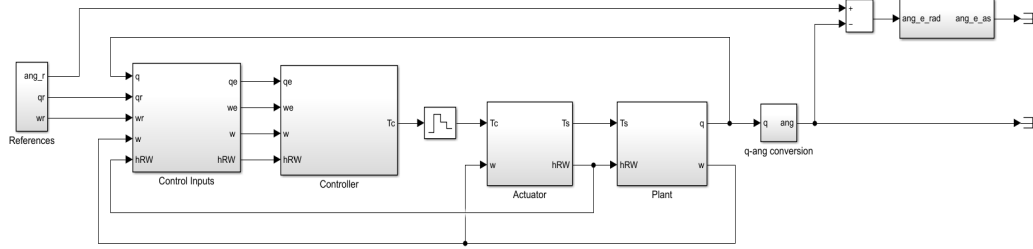


Figure 3.2: Complete Simulink scheme

Reference generator

As mentioned in section 3.1, the reference generation changes its structure according to the control strategy. Figure 3.3 shows the complete Simulink implementation of this block. The first part of the reference generation pro-

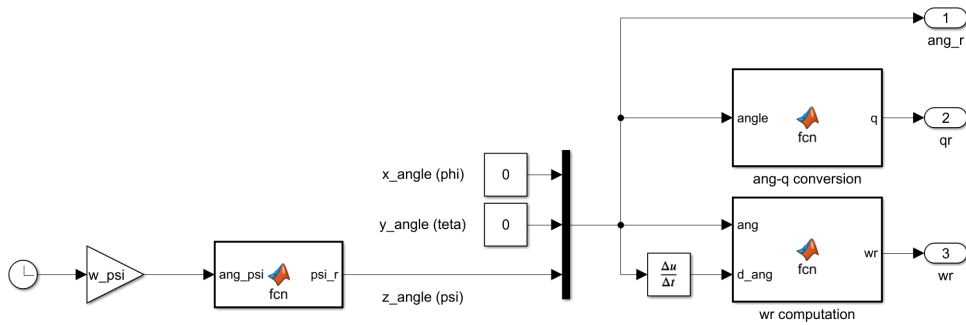


Figure 3.3: Complete reference generator structure

cedure has been deeply analysed in section 2.3. So, once the reference angles are known, two fundamental operations must be done to fully define all the necessary reference signals. The first one deals with the angles transformation into quaternion and it is performed by the MATLAB function labelled as *ang-q conversion*. It basically implements relation (3.1). Instead, the second operation is the reference angular speed computation. It is managed by the MATLAB function *wr computation* of figure 3.3, which implements relation (3.3). As already mentioned in section 2.2, this operation requires the knowledge of the reference angles and their derivatives. For this reason, there is a *derivative* block before the above-mentioned MATLAB function.

Control Inputs

The *control inputs* block, responsible for the generation of the signals that are used to compute the control action, is sketched in figure 3.4. Two main

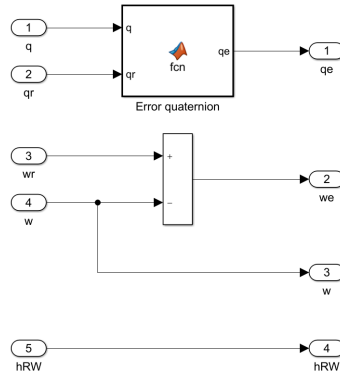


Figure 3.4: Control inputs block

operations are performed by this block: the error quaternion computation $\mathbf{q}_{ref} \otimes \mathbf{q}^*$, according to relation (3.4), and the angular speed error definition $\boldsymbol{\omega}_e = \boldsymbol{\omega}_{ref} - \boldsymbol{\omega}$. The first one has been implemented through a MATLAB function and the second one by using a summing block. Finally, as mentioned in section 3.1, signals $\boldsymbol{\omega}$ and h_{RW} (which is equivalent to $\mathbf{H}_B^{(w)}$ of equation (3.5)), of figure 3.4, are the other two outputs of this subsystem and exit it without being subject to any modification. They will be used by the *controller* block to compute the gyroscopic compensation term. Finally, about the *sampler* implementation, it is important to notice that the solver performs operation at discrete time instants, both when major and minor steps are considered. In particular, only the final results at major steps are considered as outputs. So, since the controller is simply composed by static elements i.e. gain, the only operation that must be performed is the construction of a continuous time variable from a discrete one with the specific sampling time. The sampling operation is automatically considered when the specific sample is computed and then kept constant for all the sampling interval.

Controller

The control action/law given by (3.5) is simply implemented through a MATLAB function, as shown by figure 3.5. So, all the signals coming from the *control inputs* block are injected in the MATLAB function which produces the control/torque command T_c . This is a vectorial discrete signal and it must be subject to the *ZOH* operations, before entering the *actuator* block of figure 3.2. It is important to mention that variables $\mathbf{J}^{(sc)}$, \mathbf{K}_P and \mathbf{K}_D of equation (3.5) are defined inside the MATLAB function.

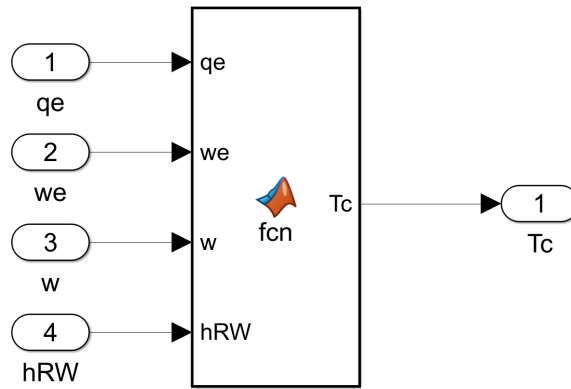


Figure 3.5: Control inputs block

3.4 EICASLAB implementation

The whole control scheme developed in EICASLAB is shown by figure 3.6. Some important comments are necessary to clarify the differences between this scheme and the Simulink one of figure 3.2. First of all, it can be noticed

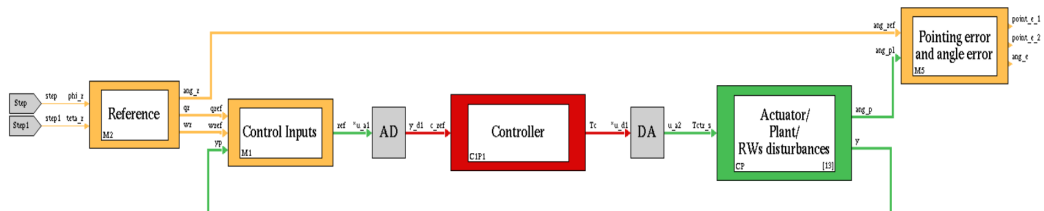


Figure 3.6: Overall control scheme

the *AD* and *DA* blocks. Indeed, since this software suite is used to build professional control systems, it is not possible to substitute them with a simple sampler and a zero order holder. However, since the analysis performed in this thesis neglects the contribution coming from the quantization process, it has been implemented the best possible approximation. Therefore, it has been chosen the smallest resolution of this two subsystem, in order to mitigate the quantization effects. It is important to highlight that resolution value is constrained by the specific values interval of the quantities to be converted and by the available number of bits. Since the two converters can manage at most integer variables of 32 bits, this value represents the maximum number of available bits. Moreover, to know in advance the interval of values assumed by the variables, some Simulink simulation have been used. The other difference is about the on-line computation of the RMS pointing error, in a specific time interval of observation. Indeed, in Simulink scheme does not appear this implementation because there has been the possibility to compute it off-line by using MATLAB. In EICASLAB this operation is performed by the block labelled as *pointing error and angle error* which is also responsible for the computation of the difference between the reference angles and the actual ones.

Reference generator

Figure 3.7 shows the *reference generator* block structure. As already mentioned in section 2.4, the subsystem behaviour is described by a set of C code lines. The first part of the reference generation has been already discussed

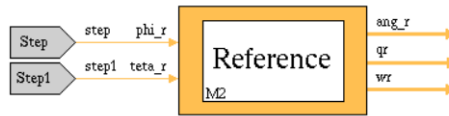


Figure 3.7: Reference generator block

in the above-mentioned section. The second one is mainly an extension of the previous part since it includes the computation of the following quantities: reference quaternion q_r , reference angular speed w_r and reference angles

ang_r . As shown by figure 3.7, they are the outputs of this subsystem. The C code of the reference generation second part is always implemented in the *Output* function, as already mentioned in section 2.4, and it is defined by some specific functions which are used to build equations (3.1) and (3.3), including the differentiation of the reference angles. These ones are the step inputs ϕ_r , θ_r , set to 0, and the internal reference angle ψ_r which is computed according to the procedure explained in section 2.2 and 2.4.

Control inputs

The EICASLAB implementation of the *control inputs* system is sketched in figure 3.8. It receives the signals q_{ref} , w_{ref} from the *reference generator* and y_p from the *plant* and produces the variable ref , which contains all the quantities used to compute the control command. In particular, y_p is defined by the actual quaternion \mathbf{q} , the angular speed $\boldsymbol{\omega}$ and the wheels angular momenta $\mathbf{H}_B^{(w)}$. Instead, ref contains the error quaternion \mathbf{q}_e , the angular speed error $\boldsymbol{\omega}_e$, the angular speed $\boldsymbol{\omega}$ and the wheels angular momenta $\mathbf{H}_B^{(w)}$. Also in this block, only the *Output* function has been used to develop the C code of relation (3.4) and the angular speed error, for the same reasons mentioned in section 2.4 about the *reference generator*. Finally, it is important to highlight *sampler* implementation is simply performed by considering the specific simulation settings. Indeed, the *Control Inputs* block is solved for discrete time instants spaced by the simulation step that is taken equal to the sampling time.

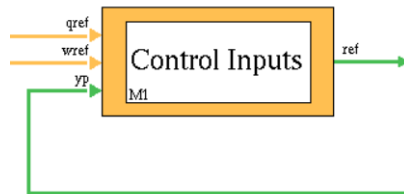


Figure 3.8: EICASLAB control inputs block

Controller

Finally, the controller structure is depicted by figure 3.9. The reference signals c_{ref} come from the *AD* block which, in turn, are produced by the *control inputs* subsystem. Since these signals are subject to the *analog to digital* conversion, they are represented in C by 32 bits integer variables, as mentioned before. The C code implementation of the controller exploits only the *Output* function and it is basically divided in three parts: the pre-processing section, the main computation one and the post-processing procedure. The first one is used to get real numbers from the integer ones. Basically, it is performed the *DA* operation in order to work with the *actual* values of the variables and not with the converted ones. So, specific code lines are written to implement this conversion. It is interesting to notice that the quantities coming from the pre-processing procedure are defined by the C variable type *double*. Once these computations are done, the core part of the controller block is considered. Indeed, specific functions are used to develop relation (3.5) which defines the control command.

Then, the post-processing phase is used to transform the real numbers that characterize the control variable in the required integer representation, since the output T_c must be represented by 32 bit integer variables to be sent to the *DA* block of figure 3.6. Therefore, a set of code lines are used to perform this *AD* operation. Finally, it is important to highlight that the controller C code has been developed by taking into account a memory usage optimization procedure which tends to avoid any kind of memory waste. This operation is very useful for a potential future real implementation.



Figure 3.9: Controller structure

Chapter 4

New approach for the control system

The core part of this thesis aims to study a new kind of approach to control the satellite attitude with RWs. So, the main objective is to understand if this new methodology is as valid as the one seen in the previous chapter by considering both the free-disturbances case and its behaviour in presence of RWs disturbances. As it will be clarified later, this control strategy can be split in two parts: the first one is known as *feedback linearisation* and its purpose is to create some linear relations starting from non-linear ones. In particular, it will be considered the *input-output linearisation*. The second part deals with the *real* control action and two different controllers will be analysed: a linear one based on the *pole placement* approach and a non-linear controller which exploits the *sliding mode* theory.

The chapter will start with the analysis of the feedback linearisation control strategy. So, it will be considered a theoretical part about the main aspects of this strategy and how it has been applied to the situation analysed by this work of thesis. In particular, it will be given the equations that define the relation between the attitude Cardan angles and the specific input signals (both references and disturbances).

Once the first control structure is defined, it is possible to choose the *real* control action responsible for managing the system dynamics. Indeed, it will be shown two kinds of controllers both from a generic theoretical point of

view and from the specific application one. As mentioned before, these two methodologies are the *pole placement* and the *sliding mode*. Also in these cases, it will be analysed the above-mentioned input-output relations.

Then, the discussion will focus on the analysis of the specific reference generation since, as mentioned many times in the previous chapters, it varies its structure according to the selected control approach. So, it will be defined all the reference signals that are used to compute the specific control action. Moreover, it will be evaluated the structure of the *Control Inputs* subsystem, since it is also subject to the specific type of control system. Finally, the simulations schemes developed in MATLAB/Simulink and EICASLAB will be deeply analysed.

4.1 Feedback linearisation approach

This section aims to provide some basic notions about the feedback linearisation (FL) control strategy and how it has been applied to the system analysed in this thesis. It is important to say that all the theoretical background about this control methodology comes from [6].

The first part of this chapter deals with the generic notions about feedback linearisation, in particular for SISO (Single Input-Single Output) systems. Then, the extension to MIMO (Multi Input-Multi Output) system will be deeply analysed, since the system under analysis is a MIMO one. Anyway, the theory about SISO systems is really important because, as it will be mentioned later, the MIMO system described in this thesis can be split in three SISO structures.

The feedback linearisation approach is, in general, really used because it allows to transform non-linear relations into linear ones. So, the systems subject to this procedure move from non-linear to linear. The main goal of feedback linearisation is to determine a specific control input able to cancel the non-linearities of the system under analysis. In this way, an exact linearisation is performed and not an approximated one. This is the key characteristic of the feedback linearisation methodology. As mentioned by [6], the feedback linearisation theory is strongly related to the *Lie derivative* concept. Without going into detail about this aspect, it is simply sufficient

to say that given two functions $f(x) : \mathbb{R}^n \rightarrow \mathbb{R}^n$ and, $h(x) : \mathbb{R}^n \rightarrow \mathbb{R}$ with continuous partial derivatives of any desired order, the Lie derivative of h with respect to f is a scalar function expressed as:

$$L_f h = \nabla h f \in \mathbb{R} \text{ where } \nabla h = \frac{\partial h}{\partial x} = \left[\frac{\partial h}{\partial x_1} \quad \frac{\partial h}{\partial x_2} \quad \dots \quad \frac{\partial h}{\partial x_n} \right] \in \mathbb{R}^n \quad (4.1)$$

If a SISO system, described by $\dot{x} = f(x, u)$ and $y = h(x)$, is considered, the following illustrative relations hold:

$$\begin{cases} \dot{y} = \nabla \dot{x} = L_f h \\ \ddot{y} = \nabla(L_f h)\dot{x} = L_f^2 h \end{cases} \quad (4.2)$$

Before going into detail with the feedback linearisation theory, it must be pointed out that this approach is characterized by two possible implementations: the *input-state linearisation* and the *input-output linearisation*. In this work of thesis, the second structure has been considered.

SISO system case

Let's consider a generic non-linear SISO system represented by the following *affine* form:

$$\begin{cases} \dot{x} = f(x) + g(x)u \\ y = h(x) \end{cases} \quad (4.3)$$

where $x \in \mathbb{R}^n$, $y \in \mathbb{R}$ and $u \in \mathbb{R}$ define respectively the state, the output and the input. Now, the key element of the feedback linearisation procedure is the following one, as mentioned by [6]: differentiating persistently the output y until the input variable u appears. Then, define u in order to remove the non-linearities. Therefore, by exploiting and extending the first relation of (4.3), it is possible to write the following expression:

$$\dot{y} = \nabla h(x)\dot{x} = \nabla h(x)(f(x) + g(x)u) = L_f h(x) + L_g h(x)u \quad (4.4)$$

So, if the Lie derivatives of h with respect to g is different from zero in some region $\Lambda \in \mathbb{R}^n$ (NB: $x \in \Lambda$), the input variable can be written as follows:

$$u = \frac{1}{L_g h(x)}(v - L_f h(x)) \quad (4.5)$$

By applying this input, the system described by (4.3) becomes a linear one, characterized by equation (4.5).

$$\dot{y} = v \quad (4.6)$$

where the variable v is a suitable control signal able to define a specific dynamic for the output y . Equation (4.6) shows that the system output is given by the integration of the control command v . Now, it must be pointed out that if $L_g h(x)$ is always null, it is necessary to perform another differentiation of the output.

$$\ddot{y} = L_f^2 h(x) + L_g(L_f h(x))u \quad (4.7)$$

Now, the following relations hold if the quantity $L_g(L_f h(x))$ is not null in some region Λ' :

$$u = \frac{1}{L_g(L_f h(x))}(v - L_f^2 h(x)) \quad (4.8)$$

$$\ddot{y} = v \quad (4.9)$$

In this case, the application of the input u (4.8) leads to establish a double integration relation between the output y and the suitable control input v . All this steps must be repeated if the quantity at the denominator of the input u is always zero.

So, the general case can be expressed by (4.10) and (4.11).

$$u = \frac{1}{L_g(L_f^{\gamma-1} h(x))}(v - L_f^\gamma h(x)) \quad (4.10)$$

$$y^{(\gamma)} = v \quad (4.11)$$

where $\gamma \leq n$ is the differentiation order. Also in this case, (4.10) holds in some region Λ'' where $L_g(L_f^{\gamma-1} h(x)) \neq 0$.

The feedback linearisation procedure is characterized by a coordinates transformation. As it will be mentioned later, it is possible to consider new state variables known as *external state* μ and *internal state* ξ . Therefore, suitable differential equations are, in general, considered, related to the external dynamics and the internal ones.

Let's start by considering the following state equation which involves only the external state μ :

$$\begin{cases} \dot{\mu} = A\mu + Bv \\ y = \mu_1 \end{cases} \quad (4.12)$$

where

$$A = \begin{bmatrix} 0 & 1 & 0 & 0 & \dots & 0 \\ 0 & 0 & 1 & 0 & \dots & 0 \\ \dots & \dots & \dots & \dots & \dots & \dots \\ \dots & \dots & \dots & \dots & \dots & \dots \\ 0 & 0 & \dots & \dots & 0 & 1 \\ 0 & 0 & \dots & \dots & 0 & 0 \end{bmatrix} \quad B = \begin{bmatrix} 0 \\ 0 \\ \dots \\ \dots \\ 0 \\ 1 \end{bmatrix} \quad \mu = \begin{bmatrix} \mu_1 \\ \mu_2 \\ \dots \\ \dots \\ \dots \\ \mu_\gamma \end{bmatrix} = \begin{bmatrix} y \\ \dot{y} \\ \ddot{y} \\ \dots \\ \dots \\ y^{(\gamma-1)} \end{bmatrix} \quad (4.13)$$

Relation (4.12) describes the so-called *external dynamics* and it is known as *companion form*. Now, there exists a more complete structure to represent the above-mentioned variables transformation induced by the feedback linearisation process. It is called *normal form* and it takes into account both the external dynamics and the internal one, as shown by (4.14).

$$\begin{cases} \dot{\mu} = \begin{bmatrix} \mu_2 \\ \dots \\ \dots \\ \mu_\gamma \\ a(\mu, \xi) + b(\mu, \xi)u \end{bmatrix} \\ \dot{\xi} = w(\mu, \xi) \\ y = \mu_1 \end{cases} \quad (4.14)$$

where $\mu \in \mathbb{R}^\gamma$ and $\xi \in \mathbb{R}^{n-\gamma}$ represent respectively the external state, as mentioned before, and the internal one. The complete set of new state variables (μ, ξ) is called *normal state*. It is easily to understand that the second differential equation of (4.14) characterizes the internal dynamics, which do not depend on the system input. Finally, it is interesting to notice that functions a and b of (4.14) are defined as $a(\mu, \xi) = a(x) = L_f^\gamma h(x)$ and $b(\mu, \xi) = b(x) = L_g(L_f^{\gamma-1} h(x))$.

MIMO systems case

Now, let's generalize the previous analysis to the MIMO systems case, as shown by [6]. Suppose to have a system described by (4.3) where, in this case, $x \in \mathbb{R}^n$, $u \in \mathbb{R}^{n_u}$ and $y \in \mathbb{R}^{n_y}$. So, more than one input and output are considered. The input-output linearisation follows the same steps shown for the SISO systems case. Therefore, it is necessary to differentiate each output y_i until at least one input appears. Once the differentiation procedure is completed, the following relation holds:

$$\begin{bmatrix} y_1^{(\gamma_1)} \\ y_2^{(\gamma_2)} \\ \dots \\ y_{n_y}^{(\gamma_{n_y})} \end{bmatrix} = \alpha(x) + \beta(x)u \quad (4.15)$$

where

$$\alpha(x) = \begin{bmatrix} L_f^{\gamma_1} h_1(x) \\ L_f^{\gamma_2} h_2(x) \\ \dots \\ L_f^{\gamma_{n_y}} h_{n_y}(x) \end{bmatrix} \quad \text{and} \quad \beta(x) = \begin{bmatrix} L_g(L_f^{\gamma_1-1} h_1(x)) \\ L_g(L_f^{\gamma_2-1} h_2(x)) \\ \dots \\ L_g(L_f^{\gamma_{n_y}-1} h_{n_y}(x)) \end{bmatrix} \quad (4.16)$$

It is important to highlight that for each output, a relative degree γ_i and a specific region $\Lambda_i \in \mathbb{R}^n$ is considered. Moreover, a general region $\Lambda \in \mathbb{R}^n$ is defined as $\Lambda = \bigcap_i \Lambda_i$. Now, if matrix β is invertible on Λ , the input u assumes this form:

$$u = \beta^{-1}(x) \begin{bmatrix} v_1 - L_f^{\gamma_1} h_1(x) \\ v_2 - L_f^{\gamma_2} h_2(x) \\ \dots \\ v_{n_y} - L_f^{\gamma_{n_y}} h_{n_y}(x) \end{bmatrix} \quad (4.17)$$

With (4.16), it is possible to get n_y linear relations like:

$$y_i^{(\gamma_i)} = v_i \quad (4.18)$$

Equation (4.18) shows that the output y_i is affected only by the corresponding input v_i , which means that a decoupled system is obtained. Finally, it must be pointed out that the sum of all the relative degrees γ_i defines the total

relative degree γ . As it will be mentioned later, γ defines the number of external states μ and the difference $n - \gamma$ characterizes the number of internal states ξ .

Input-output feedback linearisation for attitude control

This section deals with the application of the previous concepts about MIMO systems to the attitude control analysed by this work of thesis. Indeed, the equations that govern the satellite dynamics and kinematics show that the system under analysis is a MIMO one. Therefore, the starting point is equations (2.15) and (2.20), displayed below.

$$\begin{cases} \dot{\boldsymbol{\omega}} = \mathbf{J}^{(sc)^{-1}} (-\boldsymbol{\omega} \times (\mathbf{J}^{(sc)} \boldsymbol{\omega} + \mathbf{H}_B^{(w)}) + \boldsymbol{\tau}) \\ \dot{\mathbf{q}} = \frac{1}{2} \boldsymbol{\Omega} \mathbf{q} \end{cases} \quad (4.19)$$

If no disturbance acts on the system, it is possible to write $\boldsymbol{\tau} = \boldsymbol{\tau}_c = \boldsymbol{\tau}'_c + \boldsymbol{\omega} \times (\mathbf{J}^{(sc)} \boldsymbol{\omega} + \mathbf{H}_B^{(w)})$. By inserting this relation into (4.19), the following structure is obtained:

$$\begin{cases} \dot{\boldsymbol{\omega}} = \mathbf{J}^{(sc)^{-1}} \boldsymbol{\tau}'_c \\ \dot{\mathbf{q}} = \frac{1}{2} \boldsymbol{\Omega} \mathbf{q} \end{cases} \quad (4.20)$$

or in the extended form:

$$\begin{cases} \dot{\omega}_x = J_x^{-1} \tau'_{c_x} \\ \dot{\omega}_y = J_y^{-1} \tau'_{c_y} \\ \dot{\omega}_z = J_z^{-1} \tau'_{c_z} \\ \dot{q}_0 = -\frac{1}{2} (\omega_x q_1 + \omega_y q_2 + \omega_z q_3) \\ \dot{q}_1 = \frac{1}{2} (\omega_x q_0 + \omega_z q_2 - \omega_y q_3) \\ \dot{q}_2 = \frac{1}{2} (\omega_y q_0 - \omega_z q_1 + \omega_x q_3) \\ \dot{q}_3 = \frac{1}{2} (\omega_z q_0 + \omega_y q_1 - \omega_x q_2) \end{cases} \quad (4.21)$$

Now, in order to be compliant with (4.3) for MIMO systems, the following situation occurs:

$$f(x) = \begin{bmatrix} 0 \\ 0 \\ 0 \\ -\frac{1}{2}(\omega_x q_1 + \omega_y q_2 + \omega_z q_3) \\ \frac{1}{2}(\omega_x q_0 + \omega_z q_2 - \omega_y q_3) \\ \frac{1}{2}(\omega_y q_0 - \omega_z q_1 + \omega_x q_3) \\ \frac{1}{2}(\omega_z q_0 + \omega_y q_1 - \omega_x q_2) \end{bmatrix} \quad g(x) = \begin{bmatrix} J_x^{-1} & 0 & 0 \\ 0 & J_y^{-1} & 0 \\ 0 & 0 & J_z^{-1} \\ 0 & 0 & 0 \\ 0 & 0 & 0 \\ 0 & 0 & 0 \\ 0 & 0 & 0 \end{bmatrix} \quad h(x) = \begin{bmatrix} q_1 \\ q_2 \\ q_3 \end{bmatrix} \quad (4.22)$$

$$x = \begin{bmatrix} \omega_x \\ \omega_y \\ \omega_z \\ q_0 \\ q_1 \\ q_2 \\ q_3 \end{bmatrix} = \begin{bmatrix} \boldsymbol{\omega} \\ \mathbf{q} \end{bmatrix} \quad u = \boldsymbol{\tau}'_c = \begin{bmatrix} u_1 \\ u_2 \\ u_3 \end{bmatrix} = \begin{bmatrix} \tau'_{c_x} \\ \tau'_{c_y} \\ \tau'_{c_z} \end{bmatrix} \quad (4.23)$$

From (4.24), it is clear that the system output is defined by the vector $y = [y_1 \ y_2 \ y_3]^T = [q_1 \ q_2 \ q_3]^T$, which coincides with the quaternion vectorial part \mathbf{q} . The next step is to start differentiating each output until an input appears.

Output 1

$$y_1 = q_1 \quad \text{and} \quad \dot{y}_1 = \dot{q}_1 = \frac{1}{2}(\omega_x q_0 + \omega_z q_2 - \omega_y q_3) \quad (4.24)$$

Since in both relations of (4.22) there is not an input, it is necessary to differentiate again.

$$\ddot{y}_1 = \ddot{q}_1 = \frac{1}{2}(q_0 \dot{\omega}_x + \omega_x \dot{q}_0) + \frac{1}{2}(q_2 \dot{\omega}_z + \omega_z \dot{q}_2) - \frac{1}{2}(q_3 \dot{\omega}_y + \omega_y \dot{q}_3) \quad (4.25)$$

By substituting (4.21) into (4.24), the following expression can be written:

$$\ddot{y}_1 = -\frac{1}{4}q_1(\omega_x^2 + \omega_y^2 + \omega_z^2) + \frac{1}{2}J_x^{-1}q_0 u_1 - \frac{1}{2}J_y^{-1}q_3 u_2 + \frac{1}{2}J_z^{-1}q_2 u_3 \quad (4.26)$$

The differentiation procedure must be stopped since (4.26) contains at least one input. So, the relative degree is $\gamma_1 = 2$.

Output 2

$$y_2 = q_2 \quad \text{and} \quad \dot{y}_2 = \dot{q}_2 = \frac{1}{2}(\omega_y q_0 - \omega_z q_1 - \omega_x q_3) \quad (4.27)$$

Also in this case, another differentiation is required

$$\ddot{y}_2 = \ddot{q}_2 = \frac{1}{2}(q_0 \dot{\omega}_y + \omega_y \dot{q}_0) - \frac{1}{2}(q_1 \dot{\omega}_z + \omega_z \dot{q}_1) + \frac{1}{2}(q_3 \dot{\omega}_x + \omega_x \dot{q}_3) \quad (4.28)$$

By substituting (4.21) into (4.28), the result is:

$$\ddot{y}_2 = -\frac{1}{4}q_2(\omega_x^2 + \omega_y^2 + \omega_z^2) + \frac{1}{2}J_x^{-1}q_3u_1 + \frac{1}{2}J_y^{-1}q_0u_2 - \frac{1}{2}J_z^{-1}q_1u_3 \quad (4.29)$$

Relation (4.29) contains at least one input. So, the relative degree is $\gamma_2 = 2$.

Output 3

$$y_3 = q_3 \quad \text{and} \quad \dot{y}_3 = \dot{q}_3 = \frac{1}{2}(\omega_z q_0 + \omega_y q_1 - \omega_x q_2) \quad (4.30)$$

It is evident that another differentiation must be performed.

$$\ddot{y}_3 = \ddot{q}_3 = \frac{1}{2}(q_0 \dot{\omega}_z + \omega_z \dot{q}_0) + \frac{1}{2}(q_1 \dot{\omega}_y + \omega_y \dot{q}_1) - \frac{1}{2}(q_2 \dot{\omega}_x + \omega_x \dot{q}_2) \quad (4.31)$$

By putting (4.21) into (4.31), the following relation holds:

$$\ddot{y}_3 = -\frac{1}{4}q_3(\omega_x^2 + \omega_y^2 + \omega_z^2) - \frac{1}{2}J_x^{-1}q_2u_1 + \frac{1}{2}J_y^{-1}q_1u_2 - \frac{1}{2}J_z^{-1}q_0u_3 \quad (4.32)$$

Some inputs are involved in relation (4.32). Therefore, the relative degree is $\gamma_3 = 2$.

All these results allow to build the structure expressed by (4.15).

$$\begin{bmatrix} \ddot{y}_1 \\ \ddot{y}_2 \\ \ddot{y}_3 \end{bmatrix} = \underbrace{\begin{bmatrix} -\frac{1}{4}q_1(\omega_x^2 + \omega_y^2 + \omega_z^2) \\ -\frac{1}{4}q_2(\omega_x^2 + \omega_y^2 + \omega_z^2) \\ -\frac{1}{4}q_3(\omega_x^2 + \omega_y^2 + \omega_z^2) \end{bmatrix}}_{\alpha(x)} + \underbrace{\begin{bmatrix} \frac{1}{2}J_x^{-1}q_0 & -\frac{1}{2}J_y^{-1}q_3 & \frac{1}{2}J_z^{-1}q_2 \\ \frac{1}{2}J_x^{-1}q_3 & \frac{1}{2}J_y^{-1}q_0 & -\frac{1}{2}J_z^{-1}q_1 \\ -\frac{1}{2}J_x^{-1}q_2 & \frac{1}{2}J_y^{-1}q_1 & -\frac{1}{2}J_z^{-1}q_0 \end{bmatrix}}_{\beta(x)} \begin{bmatrix} u_1 \\ u_2 \\ u_3 \end{bmatrix} \quad (4.33)$$

Therefore, the vectorial input u , used to perform the input-output linearisation, is given by (4.34), according to (4.17).

$$u = \beta^{-1}(x)(v - \alpha(x)) \quad (4.34)$$

where $v = [v_1 \ v_2 \ v_3]^T$ is the control input used to define the specific dynamics for the system outputs. Indeed, the final relations, coming from the feedback linearisation procedure, are:

$$\begin{cases} \ddot{y}_1 = v_1 \\ \ddot{y}_2 = v_2 \\ \ddot{y}_3 = v_3 \end{cases} \quad (4.35)$$

Finally, it must be highlighted that, for simplicity, the global region Λ , where the matrix $B(x)$ is invertible, has not been theoretically determined. However, through simulations, it has been checked if the intervals of values inside which the system states move are such that the matrix invertibility is possible.

Now, the new state equation, describing the external dynamics, is built by considering the extension of (4.12) to MIMO systems.

$$\begin{cases} \dot{\mu} = A\mu + Bv \\ y = C\mu \end{cases} \quad (4.36)$$

where

$$A = \begin{bmatrix} 0 & 1 & 0 & 0 & 0 & 0 \\ 0 & 0 & 0 & 0 & 0 & 0 \\ 0 & 0 & 0 & 1 & 0 & 0 \\ 0 & 0 & 0 & 0 & 0 & 0 \\ 0 & 0 & 0 & 0 & 0 & 1 \\ 0 & 0 & 0 & 0 & 0 & 0 \end{bmatrix} \quad B = \begin{bmatrix} 0 & 0 & 0 \\ 1 & 0 & 0 \\ 0 & 0 & 0 \\ 0 & 1 & 0 \\ 0 & 0 & 0 \\ 0 & 0 & 1 \end{bmatrix} \quad C = \begin{bmatrix} 1 & 0 & 0 & 0 & 0 & 0 \\ 0 & 0 & 1 & 0 & 0 & 0 \\ 0 & 0 & 0 & 0 & 1 & 0 \end{bmatrix} \quad (4.37)$$

$$\mu = \begin{bmatrix} \mu_1 \\ \mu_2 \\ \mu_3 \\ \mu_4 \\ \mu_5 \\ \mu_6 \end{bmatrix} = \begin{bmatrix} \mu_1^1 \\ \mu_2^1 \\ \mu_1^2 \\ \mu_2^2 \\ \mu_1^3 \\ \mu_2^3 \end{bmatrix} = \begin{bmatrix} y_1 \\ \dot{y}_1 \\ y_2 \\ \dot{y}_2 \\ y_3 \\ \dot{y}_3 \end{bmatrix} = \begin{bmatrix} q_1 \\ \dot{q}_1 \\ q_2 \\ \dot{q}_2 \\ q_3 \\ \dot{q}_3 \end{bmatrix} \quad v = \begin{bmatrix} v_1 \\ v_2 \\ v_3 \end{bmatrix} \quad (4.38)$$

From (4.37) and (4.38), it is easy to notice that, for the external dynamics, the MIMO system (4.36) is composed by three decoupled SISO subsystems,

which can be defined by their own companion form, as shown by (4.39). Indeed, this result is compliant with the decoupling effect of matrix $\beta(x)$.

$$\left\{ \begin{array}{l} \dot{\mu}^1 = A^1 \mu^1 + B^1 v_1 \\ y_1 = C^1 \mu^1 \\ \\ \dot{\mu}^2 = A^2 \mu^2 + B^1 v_2 \\ y_2 = C^2 \mu^2 \\ \\ \dot{\mu}^3 = A^3 \mu^3 + B^1 v_3 \\ y_3 = C^3 \mu^3 \end{array} \right. \quad (4.39)$$

where

$$A^1 = A^2 = A^3 = \begin{bmatrix} 0 & 1 \\ 0 & 0 \end{bmatrix} \quad B^1 = B^2 = B^3 = \begin{bmatrix} 0 \\ 1 \end{bmatrix} \quad C^1 = C^2 = C^3 = \begin{bmatrix} 1 & 0 \end{bmatrix} \quad (4.40)$$

$$\left\{ \begin{array}{l} \mu^1 = \begin{bmatrix} \mu_1^1 \\ \mu_2^1 \end{bmatrix} = \begin{bmatrix} y_1 \\ \dot{y}_1 \end{bmatrix} = \begin{bmatrix} q_1 \\ \dot{q}_1 \end{bmatrix} \\ \\ \mu^2 = \begin{bmatrix} \mu_1^2 \\ \mu_2^2 \end{bmatrix} = \begin{bmatrix} y_2 \\ \dot{y}_2 \end{bmatrix} = \begin{bmatrix} q_2 \\ \dot{q}_2 \end{bmatrix} \\ \\ \mu^3 = \begin{bmatrix} \mu_1^3 \\ \mu_2^3 \end{bmatrix} = \begin{bmatrix} y_3 \\ \dot{y}_3 \end{bmatrix} = \begin{bmatrix} q_3 \\ \dot{q}_3 \end{bmatrix} \end{array} \right. \quad (4.41)$$

Moreover, it is important to highlight that, in this thesis, only the external dynamics (and so the companion form are) have been analysed. The internal dynamic and its characteristics have been evaluated directly in the simulation environment, as it will be mentioned later. Therefore, the normal form has been neglected. Anyway, it is important to notice that since the total relative degree γ is equal to 6, the number of external states μ is 6 and the number of internal states ξ is 1.

Another important step in the feedback linearisation procedure is the so-called *state transformation*. Therefore, the following equations put in evidence the link between each external state μ_i and the *classical* system states x .

$$\begin{cases} \mu_1 = \mu_1^1 = q_1 \\ \mu_2 = \mu_2^1 = \dot{q}_1 = \frac{1}{2}(\omega_x q_0 + \omega_z q_2 - \omega_y q_3) \\ \mu_3 = \mu_1^2 = q_2 \\ \mu_4 = \mu_2^2 = \dot{q}_2 = \frac{1}{2}(\omega_y q_0 - \omega_z q_1 + \omega_x q_3) \\ \mu_5 = \mu_1^3 = q_3 \\ \mu_6 = \mu_2^3 = \dot{q}_3 = \frac{1}{2}(\omega_z q_0 + \omega_y q_1 - \omega_x q_2) \end{cases} \quad (4.42)$$

These transformations are fundamental since they allow to compute the external states, necessary for the control variable (v) implementation.

Before analysing the effects of RWs disturbances on the satellite attitude, when it is controlled through a feedback linearisation method, it is worth noticing the following situation. Expression (4.35) shows the linear relations between the chosen output $y_1 = q_1$, $y_2 = q_2$ and $y_3 = q_3$ and the corresponding control commands v_1 , v_2 and v_3 . By recalling equation (3.6), which approximates the generic attitude quaternion as $\mathbf{q} = [q_0 \ q_1 \ q_2 \ q_3]^T = [1 \ \frac{1}{2}\phi \ \frac{1}{2}\theta \ \frac{1}{2}\psi]^T$, if small angles are considered, (4.35) can be rewritten as:

$$\begin{cases} \ddot{q}_1 = \frac{1}{2}\ddot{\phi} = v_1 \Rightarrow \ddot{\phi} = 2v_1 \\ \ddot{q}_2 = \frac{1}{2}\ddot{\theta} = v_2 \Rightarrow \ddot{\theta} = 2v_2 \\ \ddot{q}_3 = \frac{1}{2}\ddot{\psi} = v_3 \Rightarrow \ddot{\psi} = 2v_3 \end{cases} \quad (4.43)$$

So, (4.43) defines the link between the control inputs and the Cardan angles. Now, let's analyse the effect of RWs disturbances on the input-output feedback linearisation. The starting point is relation (4.19). Indeed, by considering some disturbances acting on the system, it is possible to write $\boldsymbol{\tau} = \boldsymbol{\tau}_c + \mathbf{M}^{dist} = \boldsymbol{\tau}'_c + \boldsymbol{\omega} \times (\mathbf{J}^{(sc)}\boldsymbol{\omega} + \mathbf{H}_B^{(w)}) + \mathbf{M}^{dist}$ and (4.19) becomes (4.41).

$$\begin{cases} \dot{\boldsymbol{\omega}} = \mathbf{J}^{(sc)-1} (\boldsymbol{\tau}'_c + \mathbf{M}^{dist}) \\ \dot{\mathbf{q}} = \frac{1}{2} \boldsymbol{\Omega} \mathbf{q} \end{cases} \quad (4.44)$$

or equivalently

$$\begin{cases} \dot{\omega}_x = J_x^{-1}(\tau'_{c_x} + M_x^{dist}) \\ \dot{\omega}_y = J_y^{-1}(\tau'_{c_y} + M_y^{dist}) \\ \dot{\omega}_z = J_z^{-1}(\tau'_{c_z} + M_z^{dist}) \\ \dot{q}_0 = -\frac{1}{2}(\omega_x q_1 + \omega_y q_2 + \omega_z q_3) \\ \dot{q}_1 = \frac{1}{2}(\omega_x q_0 + \omega_z q_2 - \omega_y q_3) \\ \dot{q}_2 = \frac{1}{2}(\omega_y q_0 - \omega_z q_1 + \omega_x q_3) \\ \dot{q}_3 = \frac{1}{2}(\omega_z q_0 + \omega_y q_1 - \omega_x q_2) \end{cases} \quad (4.45)$$

From now on, $\tau'_c = u$ as before and $\mathbf{M}^{dist} = d$.

By recalling equations (4.25), (4.28), (4.31) and substituting (4.45), the following relations hold:

$$\begin{aligned} \ddot{y}_1 = & \underbrace{\left(-\frac{1}{4}q_1(\omega_x^2 + \omega_y^2 + \omega_z^2) + \frac{1}{2}J_x^{-1}q_0u_1 - \frac{1}{2}J_y^{-1}q_3u_2 + \frac{1}{2}J_z^{-1}q_2u_3 \right)}_{v_1} + \\ & + \left(\frac{1}{2}J_x^{-1}q_0d_1 - \frac{1}{2}J_y^{-1}q_3d_2 + \frac{1}{2}J_z^{-1}q_2d_3 \right) \end{aligned} \quad (4.46)$$

$$\begin{aligned} \ddot{y}_2 = & \underbrace{\left(-\frac{1}{4}q_2(\omega_x^2 + \omega_y^2 + \omega_z^2) + \frac{1}{2}J_x^{-1}q_3u_1 + \frac{1}{2}J_y^{-1}q_0u_2 - \frac{1}{2}J_z^{-1}q_1u_3 \right)}_{v_2} + \\ & + \left(\frac{1}{2}J_x^{-1}q_3d_1 + \frac{1}{2}J_y^{-1}q_0d_2 - \frac{1}{2}J_z^{-1}q_1d_3 \right) \end{aligned} \quad (4.47)$$

$$\begin{aligned} \ddot{y}_3 = & \underbrace{\left(-\frac{1}{4}q_3(\omega_x^2 + \omega_y^2 + \omega_z^2) - \frac{1}{2}J_x^{-1}q_2u_1 + \frac{1}{2}J_y^{-1}q_1u_2 + \frac{1}{2}J_z^{-1}q_0u_3 \right)}_{v_3} + \\ & + \left(-\frac{1}{2}J_x^{-1}q_2d_1 + \frac{1}{2}J_y^{-1}q_1d_2 + \frac{1}{2}J_z^{-1}q_0d_3 \right) \end{aligned} \quad (4.48)$$

therefore

$$\begin{cases} \ddot{y}_1 = \ddot{q}_1 = v_1 + \left(\frac{1}{2}J_x^{-1}q_0d_1 - \frac{1}{2}J_y^{-1}q_3d_2 + \frac{1}{2}J_z^{-1}q_2d_3 \right) \\ \ddot{y}_2 = \ddot{q}_2 = v_2 + \left(\frac{1}{2}J_x^{-1}q_3d_1 + \frac{1}{2}J_y^{-1}q_0d_2 - \frac{1}{2}J_z^{-1}q_1d_3 \right) \\ \ddot{y}_3 = \ddot{q}_3 = v_3 + \left(-\frac{1}{2}J_x^{-1}q_2d_1 + \frac{1}{2}J_y^{-1}q_1d_2 + \frac{1}{2}J_z^{-1}q_0d_3 \right) \end{cases} \quad (4.49)$$

By recalling (4.38), which shows the relations between a quaternion component and an external state, and writing q_0 as function of the external states i.e. $q_0 = \sqrt{1 - (\mu_1^1)^2 - (\mu_1^2)^2 - (\mu_1^3)^2}$, the following non-linear companion form can be written.

$$\begin{cases} \dot{\mu}_1^1 = \mu_2^1 \\ \dot{\mu}_2^1 = v_1 + \frac{1}{2}(\sqrt{1 - (\mu_1^1)^2 - (\mu_1^2)^2 - (\mu_1^3)^2}J_x^{-1}d_1 - \mu_1^3J_y^{-1}d_2 + \mu_1^2J_z^{-1}d_3) \\ \dot{\mu}_1^2 = \mu_2^2 \\ \dot{\mu}_2^2 = v_2 + \frac{1}{2}(\mu_1^3J_x^{-1}d_1 + \sqrt{1 - (\mu_1^1)^2 - (\mu_1^2)^2 - (\mu_1^3)^2}J_y^{-1}d_2 - \mu_1^1J_z^{-1}d_3) \\ \dot{\mu}_1^3 = \mu_2^3 \\ \dot{\mu}_2^3 = v_3 + \frac{1}{2}(-\mu_1^2J_x^{-1}d_1 + \mu_1^1J_y^{-1}d_2 + \sqrt{1 - (\mu_1^1)^2 - (\mu_1^2)^2 - (\mu_1^3)^2}J_z^{-1}d_3) \\ y = [\mu_1^1 \ \mu_1^2 \ \mu_1^3]^T \end{cases} \quad (4.50)$$

Relation (4.5) shows that two inputs are now acting on the external dynamics: the control input v and the disturbance d .

Finally, also in this case, the approximation given by (3.6) can be exploited to write the following relations:

$$\begin{cases} \ddot{\phi} = 2v_1 + J_x^{-1}d_1 - \psi J_y^{-1}d_2 + \theta J_z^{-1}d_3 \\ \ddot{\theta} = 2v_2 + \psi J_x^{-1}d_1 + J_y^{-1}d_2 - \phi J_z^{-1}d_3 \\ \ddot{\psi} = 2v_3 - \theta J_x^{-1}d_1 + \phi J_y^{-1}d_2 + J_z^{-1}d_3 \end{cases} \quad (4.51)$$

It is crucial to remind that (4.51) is valid if small angles ϕ, θ and ψ are considered. Now, by using the first order approximation i.e. the products

between the system variables ϕ, θ, ψ and d_1, d_2, d_3 are considered negligible, the following relations hold:

$$\begin{cases} \ddot{\phi} = 2v_1 + J_x^{-1}d_1 \\ \ddot{\theta} = 2v_2 + J_y^{-2}d_2 \\ \ddot{\psi} = 2v_3 + J_z^{-1}d_3 \end{cases} \quad (4.52)$$

The expressions given by (4.52) highlight how the two system inputs influence the time trend of the Cardan angles. In the following sections, it will be deeply analysed these relations, by considering the reference signals instead of the control inputs. To do so, the techniques used to implement the control command v must be analysed.

4.2 Linear controller: pole placement design

The feedback linearisation approach is able to build linear relations between the outputs and specific control inputs, which are user-defined. Therefore, in order to impose a particular dynamic to the system under analysis, a suitable controller must be added in series with the feedback linearisation structure. In this section, a linear controller, based on the pole placement approach, will be analysed. The complete control scheme and the detail of the controller structure are given by figures 4.1 and 4.2. Before analysing the design phases

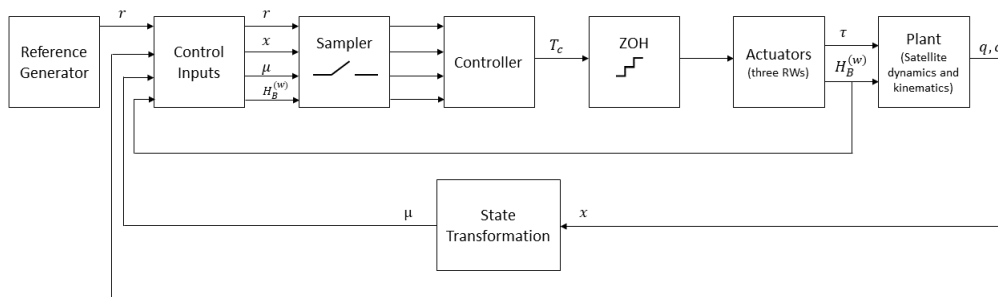


Figure 4.1: Complete control structure

of the linear controller, an important comment must be made about the structures of figures 4.1, 4.2 and the input-output linearisation, discussed in the

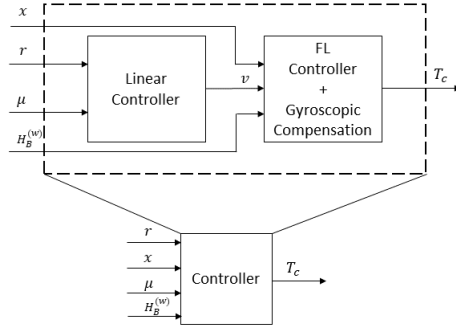


Figure 4.2: Detail of the controller block

previous section. The feedback linearisation approach previously developed, is based on the assumption that all the control scheme is a continuous time structure. However, as shown by figure 4.1, a hybrid system is considered which means that there exist an interaction between the discrete time controller and the continuous time plant (with the actuator). This interaction is managed by two interfaces i.e. *sampler* and *ZOH*, as mentioned in chapter 3. So, in order to mitigate undesired effects coming from the discrepancy between the actual situation and the theoretical one, it has been considered a sufficiently small sampling time. Indeed, in general, the dynamics of the ZOH should be considered in the controller design. However, for simplicity, this situation has been neglected and a suitably small sampling period has been considered to reduce the effect of this approximation, as mentioned before. This consideration is also valid for the linear controller since it is a discrete time system too and, as it will be shown later, it has been treated as a continuous time structure.

Now, all the necessary steps to build the linear controller must be analysed. The starting point is the companion forms of each SISO subsystems, given by (4.39). For each of them, the following control law is designed:

$$v_i = -K_c^i \mu^i + N^i r_i \quad (4.53)$$

Relation (4.53) describes a *static state feedback* control law, where K_c^i is a suitable matrix such that the closed loop system has the eigenvalues placed in specific positions, N^i is a gain used to make the system DC-gain unitary and r_i is the reference signal, which is described by a quaternion component.

Therefore, the closed loop state equation is:

$$\begin{cases} \dot{\mu}^i = (A^i - B^i K_c^i) \mu^i + B^i N^i r_i \\ y_i = C^i \mu^i \end{cases} \quad (4.54)$$

It is important to highlight that the existence of matrix K_c^i is subject to the controllability condition. In particular, it can be shown that K_c^i is a 1×2 matrix, which can be written as $K_c^i = [k_1^i \ k_2^i]$. So, by fixing the eigenvalues/poles as $\lambda_{1/2} = -\zeta\omega_n \pm \omega_n \sqrt{1 - \zeta^2}$ the control gains k_1^i, k_2^i can be easily determined. Now, after some computations, it is possible to compute the close loop transfer functions between the i -th output and reference input as $G_0(s) = \frac{Y_i(s)}{R_i(s)} = C^i (sI - (A^i - B^i K_c^i)^{-1} B^i N^i)$. Therefore, since the DC-gain is defined as $\lim_{s \rightarrow 0} G_0(s)$ and the objective is to force it to 1, the gain N^i is determined by $N^i = (C^i (B^i K_c^i - A^i)^{-1} B^i)^{-1}$.

By recalling expression (4.35), which shows the main relations obtained after the input-output linearisation, and applying the control law (4.53), the following relation can be written:

$$\ddot{y}_i = v_i = -K_c^i \mu^i + N^i r_i = -k_2^i \dot{y}_i - k_1^i y_i + N^i r_i \quad (4.55)$$

or equivalently

$$\ddot{y}_i + k_2^i \dot{y}_i + k_1^i y_i = N^i r_i \quad (4.56)$$

By exploiting the Laplace transformation, (4.57) holds:

$$\frac{Y_i(s)}{R_i(s)} = \frac{N^i}{s^2 + k_2^i s + k_1^i} \quad (4.57)$$

This is the same close loop transfer function considered in the previous analysis. It can be shown that $N^i = k_1^i = \omega_n^2$ and $k_2^i = 2\zeta\omega_n$, according to the pole placement procedure and the objective of a unitary DC-gain. It is important to remind that y_i and r_i are described by a quaternion component. So, by considering the well-known approximation between the quaternion component and the Cardan angle (relation (3.6)), the transfer function given by (4.57) describes also the link between the actual angle and the reference

one. Therefore, the following relations can be considered:

$$\left\{ \begin{array}{l} \frac{\Phi(s)}{\Phi_r(s)} = \frac{N^1}{s^2 + k_2^1 s + k_1^1} \\ \frac{\Theta(s)}{\Theta_r(s)} = \frac{N^2}{s^2 + k_2^2 s + k_1^2} \\ \frac{\Psi(s)}{\Psi_r(s)} = \frac{N^3}{s^2 + k_2^3 s + k_1^3} \end{array} \right. \quad (4.58)$$

At first, the controller parameters of each SISO subsystem can be chosen as $k_1^1 = k_1^2 = k_1^3$, $k_2^1 = k_2^2 = k_2^3$ and $N^1 = N^2 = N^3$. It is important to highlight that all these relations characterize the free-disturbances case. Moreover, as already mentioned in the previous section, the internal dynamic equation has been neglected, for simplicity. However, it has a strong influence on the output tracking. Indeed, if the internal dynamics is asymptotically stable, the output is able to track the desired reference as $t \rightarrow \infty$. If this situation is not satisfied, the output will never reach the desired value. In this thesis, the influence of the internal dynamics on the overall system has been studied through simulations.

Now, the impact of the reaction wheels disturbances on the system outputs can be evaluated. To do so, expression (4.52) must be recalled and modified as follows:

$$\left\{ \begin{array}{l} \ddot{\phi} + k_2^1 \dot{\phi} + k_1^1 \phi = J_x^{-1} d_1 \\ \ddot{\theta} + k_2^2 \dot{\theta} + k_1^2 \theta = J_x^{-1} d_2 \\ \ddot{\psi} + k_2^3 \dot{\psi} + k_1^3 \psi = J_x^{-1} d_3 \end{array} \right. \quad (4.59)$$

By using the Laplace transformation, (4.60) holds.

$$\left\{ \begin{array}{l} \frac{\Phi(s)}{D_1(s)} = \frac{J_x^{-1}}{s^2 + k_2^1 s + k_1^1} \\ \frac{\Theta(s)}{D_2(s)} = \frac{J_y^{-1}}{s^2 + k_2^2 s + k_1^2} \\ \frac{\Psi(s)}{D_3(s)} = \frac{J_z^{-1}}{s^2 + k_2^3 s + k_1^3} \end{array} \right. \quad (4.60)$$

It is easy to notice that, to build (4.59), the well-known relation (3.6) has been used and the reference signals have been set to 0.

Some final comments must be done. First of all, the transfer functions given by (4.58) and (4.60) are computed by considering all the variables initial conditions null. However, as already mentioned in chapter 3, there are some non-zero initial conditions, which can be considered negligible. Furthermore, it is interesting to notice that relations (4.58) and (4.60) are similar to (3.16) and (3.18). So, it has been found out that the, with a linear controller, the feedback linearisation approach provides quite similar results to the classical PD controller, when small Cardan angles are considered. Finally, it must be highlighted that the control system behaviour analysed in this chapter will be deeply evaluated in chapter 5, where different simulations will be studied.

4.3 Non-linear controller: sliding mode design

The current section deals with another kind of controller to be put always in series with the feedback linearisation structure. The main difference with the previous one is the non-linearity that characterizes this new controller. The design methodology is known as *sliding mode*. At first, a theoretical introduction about the sliding mode approach applied to SISO systems will be given. Then, the extension to MIMO systems will be considered. As already mentioned, since the feedback linearisation controller produces the previously mentioned decoupling, the MIMO systems can be treated as three SISO subsystems. After that, it will show the application of this control approach to the attitude control of the small satellite. In particular, at first it will be shown the relation between the output and the reference signal in the disturbances-free case. Then, the influence of the reaction wheels on the control system will be analysed. Finally, it is important to highlight that the theory background about the sliding mode control, that will be analysed in the following part, is taken from [7].

Sliding mode for SISO systems

Let's consider a non-linear SISO system given by (4.3) and its companion form described by (4.12) and (4.13). The objective of a control system is to make the output y track the reference signal r . The sliding mode approach is based on the design of the so-called *sliding surface*, which is defined as:

$$S(t) = \{x \in \mathbb{R}^n : s(x, t) = 0\} \quad \text{where} \quad s(x, t) = \tilde{y}^{(\gamma-1)} + k_\gamma \tilde{y}^{(\gamma-2)} + \dots + k_2 \tilde{y} \quad (4.61)$$

Function $s(x, t)$ is such that $s : \mathbb{R}^{n+1} \rightarrow \mathbb{R}$. Moreover, relation (4.61) introduces some quantities whose meaning must be explained. At first, \tilde{y} is called *tracking error* and it is defined as $\tilde{y} = r - y$. Then, γ is the well-know relative degree that characterizes the input-output linearisation. Instead, $\tilde{y}^{(\gamma-i)}$ is the $(\gamma - i)$ -th derivative of the tracking error \tilde{y} . Finally, the coefficients k_i are selected such that the roots of the polynomial given by (4.62) have negative real part.

$$P(\lambda) = \lambda^{\gamma-1} + k_\gamma \lambda^{\gamma-2} + \dots + k_2 \quad (4.62)$$

$P(\lambda)$ is a fundamental element of the sliding mode theory. Indeed, if the system trajectory (i.e. the set of points in the state space describing the system state evolution) is constrained to the sliding surface, the tracking error \tilde{y} will tend to zero according to the roots of the polynomial. In order to prove the above-mentioned property, it is simply necessary to compute the Laplace transformation of the equation $s(x, t) = 0$, which leads to $P(s)\tilde{Y}(s) - P_0(s) = 0 \Rightarrow \tilde{Y}(s) = \frac{P_0(s)}{P(s)}$. $P(s)$ is the polynomial given by (4.62) expressed in the Laplace variable s and $P_0(s)$ is the polynomial that takes into account the initial conditions. So, as it is possible to see, the tracking error \tilde{y} follows a time trend based on the roots of $P(\lambda)$. However, this result is based on the assumption that the trajectory is on the sliding surface and it does not move from that. Indeed, it is possible to have the following scenarios: 1) the trajectory is on the surface at a certain time instant but it does not remain there for successive instants; 2) the trajectory is completely outside the sliding surface. Since the objective is to constrain the trajectory to the surface for every time instant, it is fundamental to build a specific control law to achieve the desired goal. With this control law, the surface can be defined as *invariant* and *attractive*. An invariant surface is such that if the

trajectory is on it, it will remain there. Instead, the surface is attractive if it is able to force on it a trajectory that lies outside. Now, let's analysed the contribution of these definition to the control law structure.

Consider to have a trajectory that lies on the sliding surface at a certain time instant t_0 . According to (4.61), the system state at t_0 is an element of $S(t)$ and $s(x(t_0), t_0) = 0$. To make the surface invariant, it is necessary to have $\dot{s} = 0$. So, the differentiation of (4.61) is considered and relation (4.14) from the feedback linearisation procedure must be recalled. The latter states that the γ -th derivative of the output can be written as $y^{(\gamma)} = a(x) + b(x)u$. Therefore:

$$\dot{s} = 0 \Rightarrow \tilde{y}^{(\gamma)} + k_\gamma \tilde{y}^{(\gamma-1)} + \dots + k_2 \dot{\tilde{y}} = 0 \quad (4.63)$$

which leads to (4.64), by substituting $\tilde{y}^{(\gamma)} = r^{(\gamma)} - y^{(\gamma)} = r^{(\gamma)} - a(x) - b(x)u$.

$$r^{(\gamma)} - a(x) - b(x)u + k_\gamma \tilde{y}^{(\gamma-1)} + \dots + k_2 \dot{\tilde{y}} = 0 \quad (4.64)$$

The control input expression can be obtained from (4.64), in the following way:

$$u = \frac{1}{b(x)} \left(r^{(\gamma)} - a(x) + k_\gamma \tilde{y}^{(\gamma-1)} + \dots + k_2 \dot{\tilde{y}} \right) \quad (4.65)$$

Once that the invariance property has been analysed, it is fundamental to characterize the attractiveness of the surface. The surface $S(t)$ is considered attractive if $s(x, t) \dot{s}(x, t) < 0 \forall x, t$. So, suppose that, at a time instant t_0 , the trajectory is considered outside the sliding surface. To make it attractive is simply necessary to add a specific term to (4.65), as follows:

$$u = \frac{1}{b(x)} \left(r^{(\gamma)} - a(x) + k_\gamma \tilde{y}^{(\gamma-1)} + \dots + k_2 \dot{\tilde{y}} + k_1 \text{sign}(s(x, t)) \right) \quad (4.66)$$

The derivative of $s(x, t)$ is expressed by:

$$\dot{s}(x, t) = r^{(\gamma)} - a(x) - b(x)u + k_\gamma \tilde{y}^{(\gamma-1)} + \dots + k_2 \dot{\tilde{y}} = -k_1 \text{sign}(s(x, t)) \quad (4.67)$$

Then, it can be noticed that $\dot{s} = -k_1 < 0$ when $s(x, t) > 0$, so $s(x, t) \dot{s}(x, t) < 0$. Instead, $\dot{s} = k_1 > 0$ when $s(x, t) < 0$, therefore $s(x, t) \dot{s}(x, t) < 0$. In both the cases, the above-mentioned property is satisfied i.e $s(x, t) \dot{s}(x, t) < 0$. So, the surface is attractive and, in particular, the trajectory (starting from the initial condition at t_0) moves on the surface in finite time, as clearly stated by

[7]. It is important to highlight that the additional term $sign(s(x, t))$ could lead to the so-called *chattering* which is defined by high frequency oscillations of the trajectory around the surface. For this reason, it is in general replaced by a *sigmoid* function like $\sigma(\eta s(x, t)) = \tanh(\eta s(x, t))$.

Now, it is quite easy to see that relation (4.66) can also be written as:

$$u = \frac{1}{b(x)}(v - a(x)) = \frac{1}{L_g(L_f^{\gamma-1} h(x))}(v - L_f^\gamma h(x)) \quad (4.68)$$

which is the well-know equation characterizing the input-output linearisation. Therefore, relation (4.69) defines the control input that modifies the system dynamics.

$$v = r^{(\gamma)} + k_\gamma \tilde{\mu}_\gamma + \dots + k_2 \tilde{\mu}_2 + k_1 \sigma(\eta s(x, t)) \quad (4.69)$$

The generic variable $\tilde{\mu}_i$ is defined as $\tilde{\mu}_i = \mu_{r_i} - \mu_i = r^{(i-1)} - y^{(i-1)} = \tilde{y}^{(i-1)}$. It can be noticed that the reference variable and its derivatives have been renamed as μ_{r_i} . Relation (4.69) is characterized by the non-linear term $k_1 \sigma(\eta s(x, t))$ which increases the controller robustness, as it will be shown in the simulation results. All the parameters that appear in the control law are properly chosen to obtain the desired performance, as it will be analysed in chapter 5. In particular, it must be highlighted that the close loop system dynamic, near the sliding surface, is imposed by the coefficients $k_2, k_3, \dots, k_\gamma$ which define the roots of $P(\lambda)$. Finally, as it is possible to see, relation (4.69) involves the external state μ , already defined in the feedback linearisation section. About the internal state/dynamic, it must be highlighted that it is fundamental for the tracking properties. Indeed, it must be asymptotically stable to achieve the desired tracking. This situation has been considered also for the linear controller of the previous section.

Sliding mode for MIMO systems: attitude control application

The characterization of the sliding mode approach for MIMO systems is, now, directly given by considering its application to the attitude control of the small satellite analysed in this thesis. The starting point is relations (4.15) and (4.16), proposed once again below, which describe the result of

the feedback linearisation procedure.

$$\begin{bmatrix} y_1^{(\gamma_1)} \\ y_2^{(\gamma_2)} \\ \dots \\ y_{n_y}^{(\gamma_{n_y})} \end{bmatrix} = \alpha(x) + \beta(x)u \quad (4.70)$$

where

$$\alpha(x) = \begin{bmatrix} L_f^{\gamma_1} h_1(x) \\ L_f^{\gamma_2} h_2(x) \\ \dots \\ L_f^{\gamma_{n_y}} h_{n_y}(x) \end{bmatrix} \quad \text{and} \quad \beta(x) = \begin{bmatrix} L_g(L_f^{\gamma_1-1} h_1(x)) \\ L_g(L_f^{\gamma_2-1} h_2(x)) \\ \dots \\ L_g(L_f^{\gamma_{n_y}-1} h_{n_y}(x)) \end{bmatrix} \quad (4.71)$$

Now, from the input-output linearisation, input u is expressed by:

$$u = \beta^{-1}(x)(v - \alpha(x)) \quad (4.72)$$

which leads to the well-known decoupling, expressed as:

$$y_i^{(\gamma_i)} = v_i \quad (4.73)$$

In order to keep this decoupling, the sliding surface surface is defined as follows:

$$S(t) = \{x \in \mathbb{R}^n : s(x, t) = \begin{bmatrix} s_1(x, t) \\ s_2(x, t) \\ \dots \\ s_{n_y}(x, t) \end{bmatrix} = 0\} \quad (4.74)$$

where

$$\begin{bmatrix} s_1(x, t) \\ s_2(x, t) \\ \dots \\ s_{n_y}(x, t) \end{bmatrix} = \begin{bmatrix} \tilde{y}_1^{(\gamma_1-1)} + k_{\gamma_1} \tilde{y}_1^{(\gamma_1-2)} + \dots + k_2 \tilde{y}_1 \\ \tilde{y}_2^{(\gamma_2-1)} + k_{\gamma_2} \tilde{y}_2^{(\gamma_2-2)} + \dots + k_2 \tilde{y}_2 \\ \dots \\ \tilde{y}_{n_y}^{(\gamma_{n_y}-1)} + k_{\gamma_{n_y}} \tilde{y}_{n_y}^{(\gamma_{n_y}-2)} + \dots + k_2 \tilde{y}_{n_y} \end{bmatrix} \quad (4.75)$$

Basically, this formulation consider a MIMO system as n_y SISO subsystems, each of them characterized by a function $s_i(x, t)$, which involves specific coefficients k_i , the i -th tracking error $\tilde{y}_i = r_i - y_i$ and its derivatives until the order $\gamma_i - 1$. As already mentioned in the feedback linearisation section, γ_i

is the relative degree associated with the i -th output y_i .

So, for each SISO subsystem, the corresponding control input v_i can be written as:

$$v_i = r_i^{(\gamma_i)} + k_{\gamma_i} \tilde{y}_i^{(\gamma_i-1)} + \dots + k_2 \tilde{y}_i + k_1 \sigma(\eta_i s_i(x, t)) \quad (4.76)$$

Now, the application to the system under analysis is considered. At first, relation (4.39) must be recalled, which defines the companion form of the overall MIMO system expressed as the composition of three SISO subsystems. In this case, the number of input is $n_y = 3$ and all the relative degrees are $\gamma_i = 2$. Since the external state characterizing each SISO subsystem is expressed by μ^i , as shown by (4.41), it is possible to consider $\mu_r^i = [\mu_{r_1}^i \ \mu_{r_2}^i]^T = [r_i \ \dot{r}_i]^T$. Then, the following relation holds: $\tilde{\mu}^i = [\tilde{\mu}_1^i \ \tilde{\mu}_2^i]^T = [\tilde{y}_i \ \dot{\tilde{y}}_i]^T$. Therefore, functions $s_i(x, t)$ and control commands v_i can be rewritten as:

$$\begin{bmatrix} s_1(x, t) \\ s_2(x, t) \\ s_3(x, t) \end{bmatrix} = \begin{bmatrix} \dot{\tilde{y}}_1 + k_2 \tilde{y}_1 \\ \dot{\tilde{y}}_2 + k_2 \tilde{y}_2 \\ \dot{\tilde{y}}_3 + k_2 \tilde{y}_3 \end{bmatrix} = \begin{bmatrix} \tilde{\mu}_2^1 + k_2 \tilde{\mu}_1^1 \\ \tilde{\mu}_2^2 + k_2 \tilde{\mu}_1^2 \\ \tilde{\mu}_2^3 + k_2 \tilde{\mu}_1^3 \end{bmatrix} \quad (4.77)$$

$$\begin{cases} v_1 = \ddot{r}_1 + k_2 \tilde{\mu}_1^1 + k_1 \sigma(\eta_1 s_1(x, t)) \\ v_2 = \ddot{r}_2 + k_2 \tilde{\mu}_1^2 + k_1 \sigma(\eta_2 s_2(x, t)) \\ v_3 = \ddot{r}_3 + k_2 \tilde{\mu}_1^3 + k_1 \sigma(\eta_3 s_3(x, t)) \end{cases} \quad (4.78)$$

In this case (4.73) becomes (4.79), as already analysed in the feedback linearisation section.

$$\begin{cases} \ddot{y}_1 = v_1 \\ \ddot{y}_2 = v_2 \\ \ddot{y}_3 = v_3 \end{cases} \quad (4.79)$$

By substituting (4.78) in (4.79), the following relations hold, in the free-disturbance case:

$$\begin{cases} \ddot{y}_1 = \ddot{r}_1 + k_2 \tilde{\mu}_1^1 + k_1 \sigma(\eta_1 s_1(x, t)) \\ \ddot{y}_2 = \ddot{r}_2 + k_2 \tilde{\mu}_1^2 + k_1 \sigma(\eta_2 s_2(x, t)) \\ \ddot{y}_3 = \ddot{r}_3 + k_2 \tilde{\mu}_1^3 + k_1 \sigma(\eta_3 s_3(x, t)) \end{cases} \quad (4.80)$$

It is important to remind that each output represents the specific component of the actual attitude quaternion and so, the reference signals are quaternion

components too. Moreover, it is possible to recall the approximation between quaternion and Cardan angles, given by (3.6), and substitute the quaternion component with the half of the correspondent angle. Indeed, the above mentioned relation states that $[q_1 \ q_2 \ q_3]^T = [\frac{\phi}{2} \ \frac{\theta}{2} \ \frac{\psi}{2}]^T$. The same can be done for the reference quaternion and angles. Due to the non-linearity introduced by the control action, the time evolution of each output, when the reference signals are applied, has been studied through specific simulations.

Instead, when reaction wheels disturbances act on the system, relation (4.80) can be modified by taking into account relation (4.50). Therefore:

$$\begin{aligned} \ddot{y}_1 &= \ddot{r}_1 + k_2 \tilde{\mu}_1^1 + k_1 \sigma(\eta_1 s_1(x, t)) + \\ &+ \frac{1}{2} (\sqrt{1 - (\mu_1^1)^2 - (\mu_1^2)^2 - (\mu_1^3)^2} J_x^{-1} d_1 - \mu_1^3 J_y^{-1} d_2 + \mu_1^2 J_z^{-1} d_3) = \quad (4.81) \\ &= \ddot{r}_1 + k_2 \tilde{\mu}_1^1 + k_1 \sigma(\eta_1 s_1(x, t)) + \frac{1}{2} J_x^{-1} d_1 \end{aligned}$$

$$\begin{aligned} \ddot{y}_2 &= \ddot{r}_2 + k_2 \tilde{\mu}_1^2 + k_1 \sigma(\eta_2 s_2(x, t)) + \\ &+ \frac{1}{2} (\mu_1^3 J_x^{-1} d_1 + \sqrt{1 - (\mu_1^1)^2 - (\mu_1^2)^2 - (\mu_1^3)^2} J_y^{-1} d_2 - \mu_1^1 J_z^{-1} d_3) = \quad (4.82) \\ &= \ddot{r}_2 + k_2 \tilde{\mu}_1^2 + k_1 \sigma(\eta_2 s_2(x, t)) + \frac{1}{2} J_y^{-1} d_2 \end{aligned}$$

$$\begin{aligned} \ddot{y}_3 &= \ddot{r}_3 + k_2 \tilde{\mu}_1^3 + k_1 \sigma(\eta_3 s_3(x, t)) + \\ &+ \frac{1}{2} (-\mu_1^2 J_x^{-1} d_1 + \mu_1^1 J_y^{-1} d_2 + \sqrt{1 - (\mu_1^1)^2 - (\mu_1^2)^2 - (\mu_1^3)^2} J_z^{-1} d_3) = \quad (4.83) \\ &= \ddot{r}_3 + k_2 \tilde{\mu}_1^3 + k_1 \sigma(\eta_3 s_3(x, t)) + \frac{1}{2} J_z^{-1} d_3 \end{aligned}$$

It is important to notice that the last equality of (4.81), (4.82) and (4.83) comes from the small approximation, where the first quaternion component q_0 (the term described by the square root) can be considered equal to 1 (cf (3.6)), and from a first order approximation (the product between variables i.e. disturbances and external state, that is the quaternion component, can be considered negligible). As it is possible to notice, relations (4.81), (4.82) and (4.83) are quite complex and introduce non-linearities, even after the above-mentioned approximations. This is due to the sigmoidal contribution coming from the sliding mode control command. Therefore, the time trend of the outputs, when both the reference signals and the disturbances act on the system, has been evaluated directly through simulations.

Figures 4.3 and 4.4 depict the overall control structure and the detail of the controller block. Both of them show new variables with respect to the previous analysis i.e. r^{γ_i} , μ_r and $\tilde{\mu}$. They are simply the composition of the previous mentioned quantities $r_i^{\gamma_i}$, μ_r^i and $\tilde{\mu}^i$, in the following way: $r^{\gamma_i} = [\ddot{r}_1 \ \ddot{r}_2 \ \ddot{r}_2]^T$, $\mu_r = [\mu_r^1 \ \mu_r^2 \ \mu_r^3]^T$ and $\tilde{\mu} = [\tilde{\mu}^1 \ \tilde{\mu}^2 \ \tilde{\mu}^3]^T$. As mentioned in the linear controller section, it must be highlighted that all the control system structure has been considered as a continuous time one, from a pure theoretical point of view. Indeed, the feedback linearisation approach, devel-

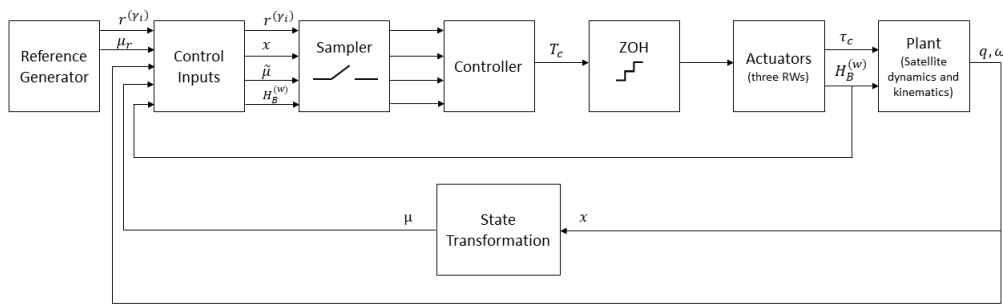


Figure 4.3: Complete control structure

oped in the specific section, is based on the assumption that all the control scheme is a continuous time structure. Therefore, the sliding mode controller (which is placed in series with the FL block, as shown by figure 4.4) is also considered as a continuous time system, according to the previous theoretical analysis. However, as shown by figure 4.3, the practical implementation

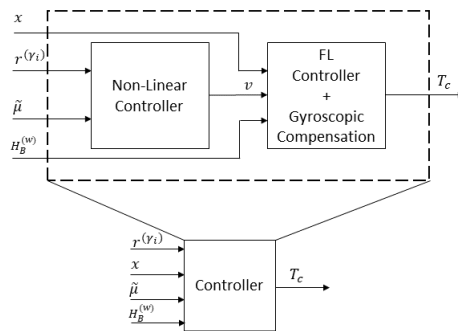


Figure 4.4: Detail of the controller block

of the overall control scheme is defined by a hybrid system, which means

that there exist an interaction between the discrete time controller and the continuous time plant (with the actuator), suitably managed by the *sampler* and *ZOH* blocks. So, in order to mitigate undesired effects coming from this discrepancy between the actual situation and the theoretical one, it has been considered a sufficiently small sampling time. Actually, the dynamic of the *ZOH* should be considered in the controller design. However, for simplicity, this situation has been neglected and a suitably small sampling period has been considered to reduce the effect of this approximation, as mentioned before. Then, it must be highlighted that the internal dynamic formulation has been neglected, for simplicity, and its effect on the output tracking has been directly evaluated through simulations.

4.4 Reference generator and control inputs: specific analysis

This section aims to briefly describe how the reference signals and the control inputs are generated, both for the pole placement approach and the sliding mode method. It must be highlighted that the first part of the reference generation has been already analysed in section 2.2 and it deals with the computation of the reference Cardan angles. Therefore, according to the specific control methodology, the second part must be discussed.

Pole placement approach

The pole placement methodology is based on a static state feedback control law, as shown by (4.53). So, according to this relation, it is necessary to compute only the reference quaternion and, then, consider for each control command v_i the specific quaternion component q_{ref_i} that describes the reference signal r_i . To do so, a conversion from the reference Cardan angles ϕ_{ref} , θ_{ref} , ψ_{ref} , to the reference quaternion must be performed, according to relations (3.1) and (3.2). They, basically, compute the quaternion products among the three elementary quaternions that can be associated with each reference angle. The result is the total reference quaternion $\mathbf{q}_{ref} = [q_{ref_0} \ q_{ref_1} \ q_{ref_2} \ q_{ref_3}]^T$. Therefore, the signal r shown by figures 4.1

and 4.2 is represented as $r = [r_1 \ r_2 \ r_3]^T = [q_{ref_1} \ q_{ref_2} \ q_{ref_3}]^T$. Instead, the *Control Inputs* subsystem of figure 4.1, in this case, does not perform any operation on its inputs since, to build the control action, it is not necessary any manipulation of these variables.

Sliding mode method

This control philosophy requires a more complex structure for the reference generator block, with respect to the pole placement approach. Indeed, as displayed by figure 4.3, this block provides as outputs $r^{(\gamma_i)}$ and μ_r , which can be expressed, according to the analysis of section 4.3, as:

$$r^{(\gamma_i)} = \begin{bmatrix} \ddot{r}_1 \\ \ddot{r}_2 \\ \ddot{r}_3 \end{bmatrix} = \begin{bmatrix} \ddot{q}_{ref_1} \\ \ddot{q}_{ref_2} \\ \ddot{q}_{ref_3} \end{bmatrix} \quad (4.84)$$

$$\mu_r = \begin{bmatrix} \mu_r^1 \\ \mu_r^2 \\ \mu_r^3 \end{bmatrix} = \begin{bmatrix} \mu_{1_r}^1 \\ \mu_{2_r}^1 \\ \mu_{1_r}^2 \\ \mu_{2_r}^2 \\ \mu_{1_r}^3 \\ \mu_{2_r}^3 \end{bmatrix} = \begin{bmatrix} q_{ref_1} \\ \dot{q}_{ref_1} \\ q_{ref_2} \\ \dot{q}_{ref_2} \\ q_{ref_3} \\ \dot{q}_{ref_3} \end{bmatrix} \quad (4.85)$$

So, these relations show that the reference quaternion vectorial part and its derivative are necessary. This means that, once the reference Cardan angles are computed, the usual angle-quaternion conversion is performed. Then, the vectorial part of the resulting quaternion is extracted and the differentiation of each component is performed. In particular, it is necessary a double differentiation.

Instead, the *Control Inputs* block of figure 4.3 is responsible for the computation of $\tilde{\mu}$, which represents the difference between the μ_r and μ . Therefore,

the following structure is considered:

$$\tilde{\mu} = \begin{bmatrix} \mu_r^1 - \mu^1 \\ \mu_r^2 - \mu^2 \\ \mu_r^3 - \mu^3 \end{bmatrix} = \begin{bmatrix} \mu_{1_r}^1 - \mu_1^1 \\ \mu_{2_r}^1 - \mu_2^1 \\ \mu_{1_r}^2 - \mu_1^2 \\ \mu_{2_r}^2 - \mu_2^2 \\ \mu_{1_r}^3 - \mu_1^3 \\ \mu_{2_r}^3 - \mu_2^3 \end{bmatrix} = \begin{bmatrix} q_{ref1} - q_1 \\ \dot{q}_{ref1} - \dot{q}_1 \\ q_{ref2} - q_2 \\ \dot{q}_{ref2} - \dot{q}_2 \\ q_{ref3} - q_3 \\ \dot{q}_{ref3} - \dot{q}_3 \end{bmatrix} \quad (4.86)$$

Finally, it must be pointed out that all the other inputs of the above-mentioned block are not subject to any manipulation, as shown by figure 4.3.

4.5 MATLAB/Simulink implementation

This section aims to show how the overall control schemes, previously analysed, have been developed in MATLAB/Simulink. Before starting the specific analysis for both the control approaches, the common element between them must be described i.e. the feedback linearisation controller plus the gyroscopic compensation. Figure 4.5 shows its structure. The system im-

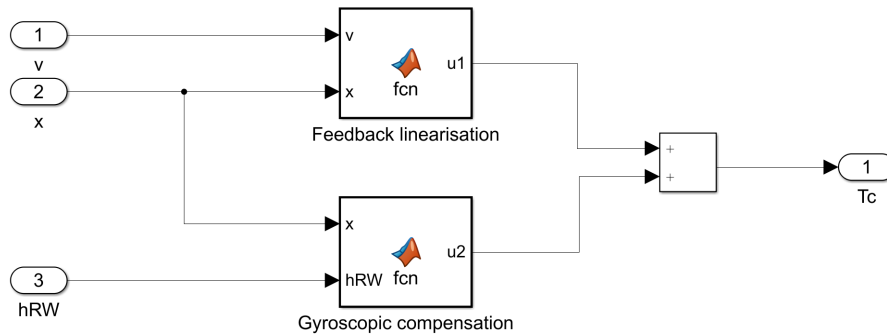


Figure 4.5: Structure of the FL controller with the gyroscopic compensation

plementation is characterized by two MATLAB functions. The first one is used to implement the control input coming from the input-output linearisation, according to relation (4.33) and (4.34). The second one implements the gyroscopic compensation, that removes the non-linearity from the satellite

dynamic equation (2.15). Then, both the outputs of the MATLAB functions are summed to get the vectorial torque command T_c . All this structure is compliant with the theoretical analysis of section 4.1. In the following part, the specific control structures with their subsystems will be analysed.

Pole placement design

The overall control scheme for the pole placement approach is depicted by figure 4.6. As it is possible to see, this figure introduces some new blocks with respect to figure 4.1. In particular, it can be noticed the *output*, the *q-ang conversion* and *rad to as* blocks. The first one is simply used to describe the $h(x)$ function of the MIMO system, which is responsible for the output definition. It is important to remind that the output y is the key element of the input-output linearisation procedure. Instead, the second block is responsible for the computation of the Cardan angles, given the specific attitude quaternion. Finally, the third block is used to convert the *error angles* (given by the differences between reference and actual angles) expressed in radians into arcseconds, since the pointing stability of the telescope is evaluated in this way.

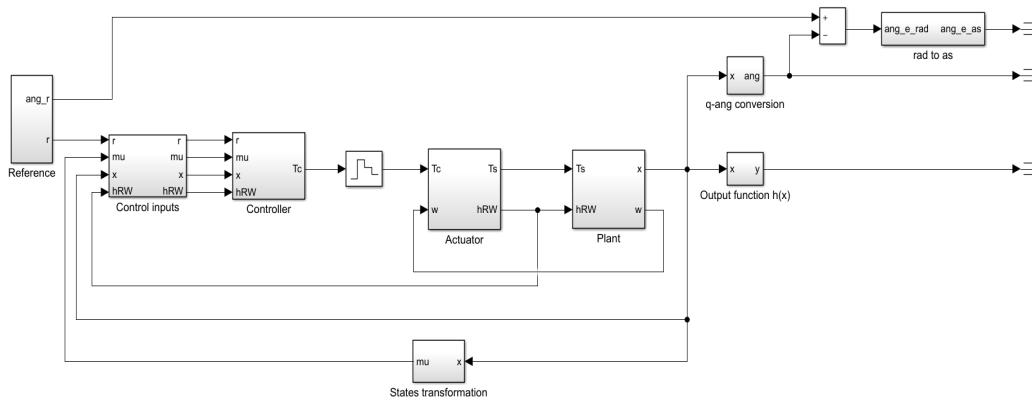


Figure 4.6: Pole placement method complete control structure

Reference generator

The following figure shows the Simulink implementation of the reference generation procedure, described in section 4.4. From figure 4.7, it is clear that the

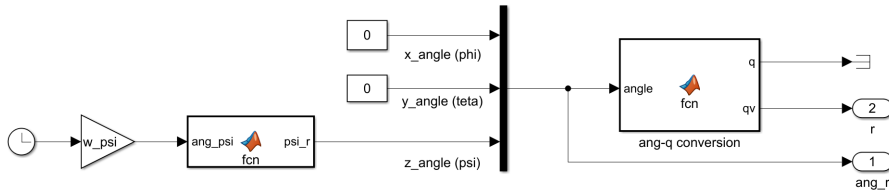


Figure 4.7: Reference generator block

reference signal r coincides with the vectorial part of the quaternion coming from a simple conversion described by (3.1) and (3.2), as mentioned in section 4.4. This computation is carried out by the MATLAB function labelled as *ang-q conversion*. Moreover, figure 4.7 shows that one of its outputs is the reference angles variable ang_r , which is fundamental for the computation of the error angles. Finally, before analysing the controller implementation, it must be pointed out that the *Control Inputs* block implementation will not be shown since it does not perform any variables manipulation, according to the analysis made in section 4.4.

Controller

This section deals with the development of the core structure of the whole control scheme. Figure 4.8 (a) depicts the complete controller structure, made by two contributions: the *feedback linearisation* block, already analysed at the beginning of section 4.4, and the *linear controller* block. Instead, figure 4.8 (b) displays the specific implementation of the pole placement controller. The latter is characterized by the state feedback control law given by (4.53), expressed in a compact way. Indeed, all the three reference signals (quaternion components), included in the vectorial variable r , are multiplied by the same gain N , which is compliant with the analysis of section 4.2 ($N^1 = N^2 = N^3 = N$). Instead, a suitable matrix, labelled as K_m , is used to perform all the multiplications between the external state μ and the control matrices K_c^i , mentioned by (4.53) and (4.54). According to the notations of

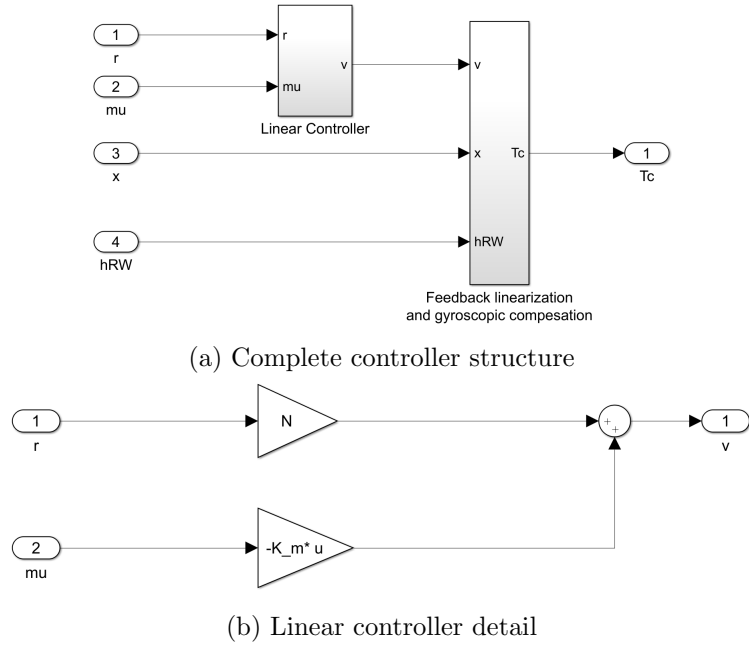


Figure 4.8: Pole placement plus FL controller

section 4.2, matrix K_m can be written as:

$$K_m = \begin{bmatrix} K_c^1 & 0_{1 \times 2} & 0_{1 \times 2} \\ 0_{1 \times 2} & K_c^2 & 0_{1 \times 2} \\ 0_{1 \times 2} & 0_{1 \times 2} & K_c^3 \end{bmatrix} = \begin{bmatrix} k_1^1 & k_2^1 & 0 & 0 & 0 & 0 \\ 0 & 0 & k_1^2 & k_2^2 & 0 & 0 \\ 0 & 0 & 0 & 0 & k_1^3 & k_2^3 \end{bmatrix} \quad (4.87)$$

and variable μ follows the formulation given by (4.38). In this way, it has been possible to implement equation (4.53) for each SISO subsystem, by summing the outputs from the *gain* blocks of figure 4.8 (b). The result is the vectorial control variable $v = [v_1 \ v_2 \ v_3]$.

Sliding mode method

Figure 4.9 shows the overall control scheme used when a sliding mode approach is considered. The major part of the scheme is equal to the one proposed by figure 4.6, about the pole placement approach. The only differences refer to the *Reference Generator*, *Control Inputs* and *Controller* blocks. Therefore, the specific blocks for the sliding mode design are directly analysed.

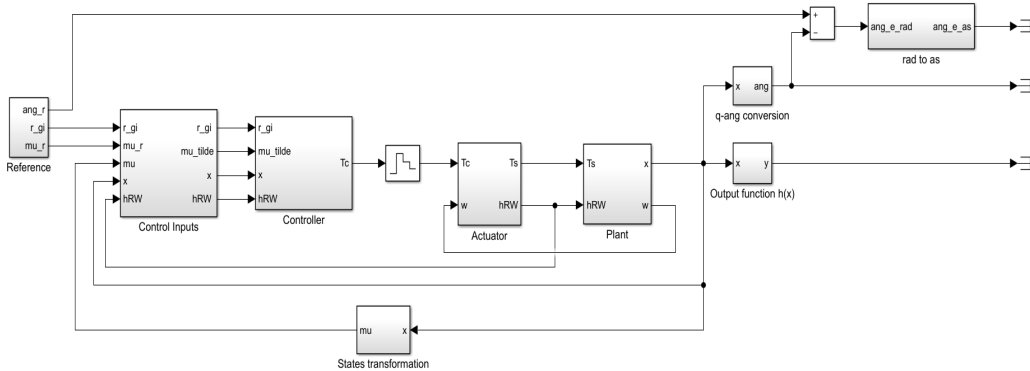


Figure 4.9: Sliding mode approach complete control structure

Reference generator

The reference generation implementation, for the sliding mode approach, is displayed by figure 4.10. According to the analysis made in section 4.4,

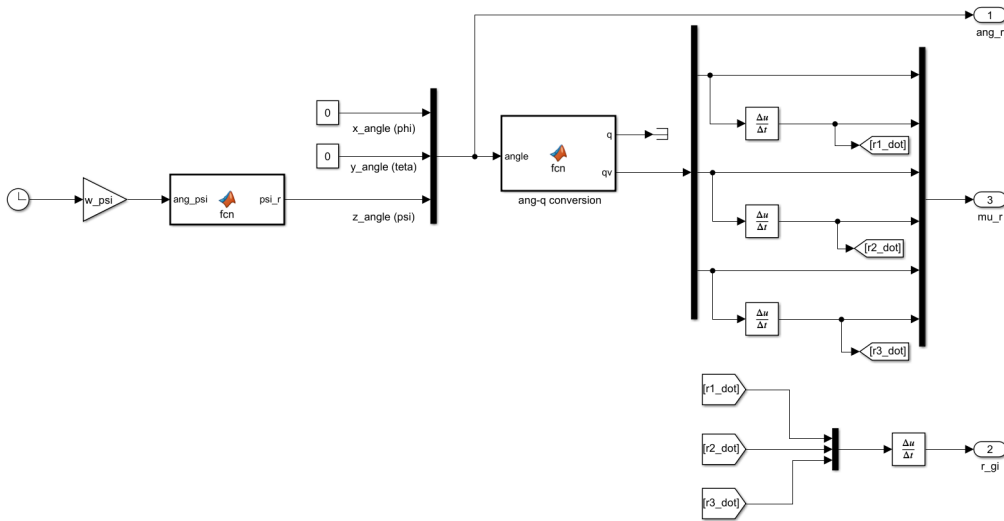


Figure 4.10: Reference generation for the sliding mode approach

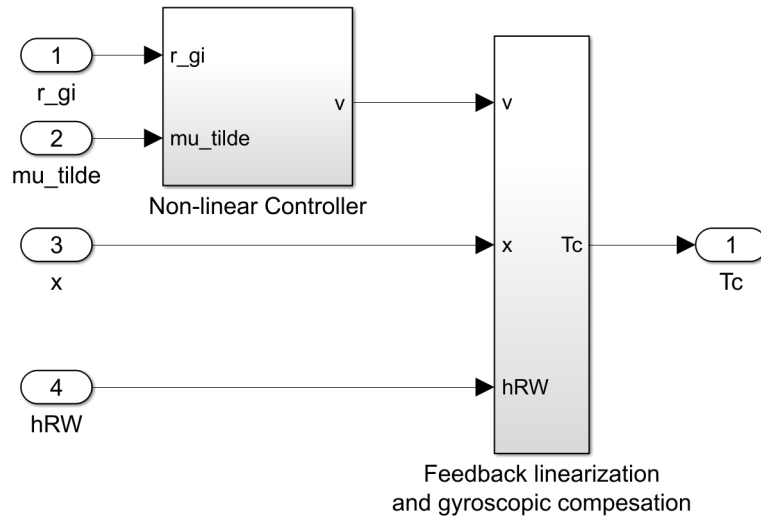
the first step towards the reference computation is the conversion from the Cardan reference angles to the corresponding quaternion. As usual, this operation is carried out by the MATLAB function labelled as *ang-q conversion*. Then, since the desired variables are the components of the vectorial part, a *demux* block is used to split it into its constitutive elements i.e. q_{ref_1} , q_{ref_2}

and q_{ref_3} , according to the notation of section 4.4. Now, the objective is to build the reference variable μ_r expressed by (4.85). Therefore, suitable *derivative* blocks and a *mux* one are used to compute the quaternion components derivatives and to collect them together with the above-mentioned reference component. Moreover, since the second derivatives of each quaternion component is needed to build variable $r^{(\gamma_i)}$ of (4.84) (named r_{g_i} in figure 4.10), the first derivatives are collected through a *mux* and then injected into a *derivative* block. Finally, the output variable ang_r can be noticed, as usual used for the error angles computation.

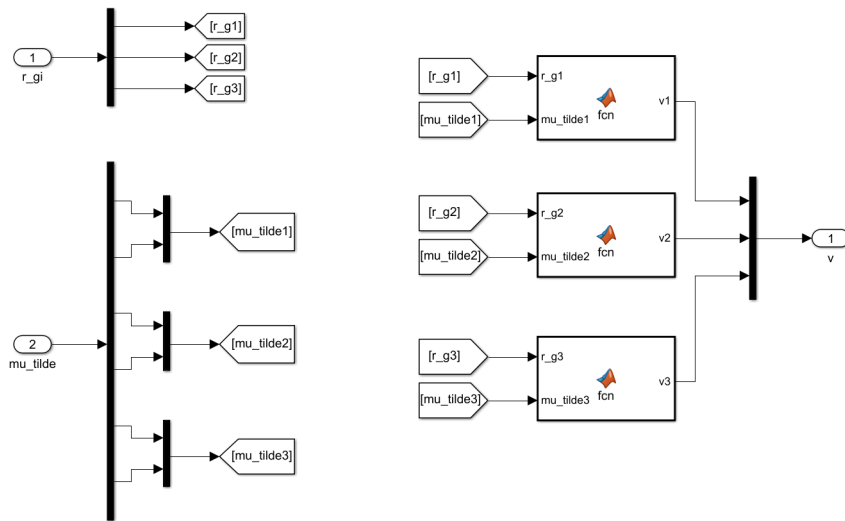
A brief comment must be made about the *Control Inputs* block of figure 4.9. This subsystem is simply responsible for the computation of $\tilde{\mu}$ (named *mutilde* in the above-mentioned figure), as expressed by (4.86). This is the only manipulation required before considering the controller structure, as clearly depicted by figure 4.9.

Controller

Finally, the controller development is considered. Its structure is split in two parts, as shown by figure 4.11: the *feedback linearisation and gyroscopic compensation* and the *non-linear controller*, designed with the sliding mode technique. Since the feedback linearisation structure has already been discussed, the following analysis focuses on the non-linear controller block, shown by figure 4.11 (b). It is clear from the above-mentioned figure that the three MATLAB functions are used to implement relation (4.78), which defines the structure of the control command $v = [v_1 \ v_2 \ v_3]^T$. According to (4.78), to build such vectorial control variable, for each SISO subsystem described in section 4.2, is required the knowledge of $r^{(\gamma_1)}$, $r^{(\gamma_2)}$, $r^{(\gamma_3)}$ (components of the vector given by (4.84) and named r_{g1}, r_{g2}, r_{g3} in figure 4.11 (b)) and variable $\tilde{\mu}$ expressed by (4.86). In particular, this vectorial variable is split into its sub-vectorial components, as mentioned by (4.86), and the latter are injected in the MATLAB functions. It is evident from figure 4.11 (b) that all the necessary splitting and merging operations are performed through *demux* and *mux* blocks.



(a) Complete controller structure



(b) Non-linear controller detail

Figure 4.11: Sliding mode controller

4.6 EICASLAB implementation

This section deals with the implementation of the whole control schemes in the EICASLAB environment. At first, it will be analysed the structure related to the pole placement design. Then, the sliding mode control scheme will be evaluated. Before starting the analyses, some comments must be made. In both the simulation schemes there will be the *AD* and *DA* blocks. As already mentioned in chapter 3 section 3.4, EICASLAB was born with the objective of building professional control schemes, therefore it is not possible to substitute the above-mentioned blocks with a simple sampler and a zero order holder. However, since this work of thesis neglects the contribution coming from the quantization process, the best possible approximation has been implemented. So, the smallest resolution for this two subsystems has been chosen and the quantization effects have been mitigated. It is important to highlight that the resolution value is constrained by the specific values interval of the quantities to be converted and by the available number of bits. Since the two converters can work at most with integer variables of 32 bits, this value represents the maximum number of available bits. Moreover, to know in advance the interval of values assumed by the variables, some Simulink simulation have been used.

Furthermore, it must be pointed out that there will be another difference between the EICASLAB simulation schemes and the Simulink ones. Indeed, in the first ones there will be a specific block that perform an on-line computation of the RMS pointing error, in a specific time interval of observation. Instead, in the Simulink schemes of figures 4.6, 4.9 this block does not appear because there has been the possibility to make the above-mentioned computation off-line by using MATLAB.

Pole placement methodology

Figure 4.12 depicts the overall control scheme used when a pole placement controller is employed. It is quite easy to recognize all the subsystems described in section 4.2 and in chapter 2. As in the Simulink scheme of figure 4.9, there is a specific block responsible for the angles error computation. This block is labelled as *Pointing error and angle error* and it is also respon-

sible for the RMS pointing error, as mentioned at the beginning of section 4.6. In the following parts, the implementation of the *Reference* and *Linear controller* will be analysed. About the *Control inputs* block, it will be briefly analysed in the *Reference generator* section, since it does not require a detailed analysis.

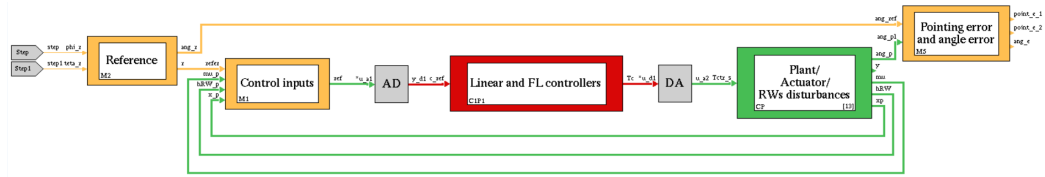


Figure 4.12: Pole placement-based control scheme

Reference generator

The EICASLAB block representing the reference generation structure is shown by figure 4.13. As it is possible to see, it has two inputs given by the reference angles ϕ_{ref} and θ_{ref} and produces as outputs the reference angles variable, labelled as ang_r , and the specific reference signal r , which are injected in the *Control inputs* block. The first output is composed by the above-mentioned angles and the third one computed by this block. To do so, specific C code lines have been written, as mentioned in section 2.4. The second output is the vectorial variable containing the usual reference quaternion components, according to the analysis made in section 4.4. To compute it, the C code of relation (3.1) has been implemented, which simply defines the *angle-quaternion* conversion. Also in this case, only the *Output* function has been used, as already done for the control scheme of chapter 3. Finally, a brief comment on the *Control inputs* block is necessary. As already mentioned, it does not perform any variable manipulation, so the variables are simply merged and injected in the controllers block. These variables are: the reference signal r , the external state μ , the vectorial angular velocity and the actual attitude quaternion ω, q (i.e. the plant state labelled as x_p) and the reaction wheels angular momenta variable h_{RW} , which coincides with the well-known quantity $\mathbf{H}_B^{(w)}$ of chapter 2.

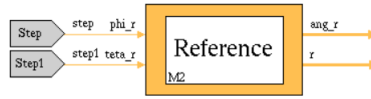


Figure 4.13: Reference generation block

Controller

Finally, figure 4.14 depicts the block of the main part of the whole control scheme i.e. *Linear and FL controllers*. It is characterised by the C code lines needed to implement both the control structures. Also in this case, like the controller of chapter 3, it has been used only one of the three main functions that define the C code structure of any EICASLAB simulation block i.e. the *Output* function. This has been divided in three portions: the *pre-processing* part, the *main computation* section and the *post-processing* portion. This is the same structure used for the PD controller of chapter 3. So, in the same way, the *pre-processing* part is used to implement the *DA* operation on the variable labelled as c_{ref} , in order to work with the *analogic* variables and not with the converted/digital ones. This means that all the manipulations performed by the *main computation* part are done with respect to variables values that are real numbers and not suitable integers coming from the *AD* block of figure 4.12. It is important to remind that c_{ref} is a vectorial variable that contains all the outputs coming from the *Control inputs* block. These quantities have been mentioned before, at the end of the *Reference generator* analysis.

Instead, the *main computation* section is composed by specific C functions to implement relations (4.34) and (4.53), that define the input-output linearisation and the pole-placement control law. As mentioned before, since all the variables subject to manipulations are real number, they are represented by the C variable type *double*.

Finally, the *post-processing* portion is responsible for implementing the *AD* operation on the output produced by the *main computation* part i.e. the vectorial control torque. In this way, the torque command is converted from *double* to *int* (32 bit integer) and injected in the *DA* block shown by figure 4.12. This variable is labelled as T_c , as displayed by figure 4.12 and 4.14.



Figure 4.14: Controller structure

Sliding mode approach

Figure 4.15 shows the complete control scheme used in presence of a sliding mode controller. It is quite easy to see that the scheme is really similar to the one describing the pole placement approach. Therefore, it will be directly described the subsystems that differ from the above-mentioned structure i.e. the *Reference* and *Non-linear and Feedback Linearisation Controllers*. About the *Control inputs* block, also in this case, it will be given a brief analysis, in the *Reference generator* section, since it does not require a detailed discussion.

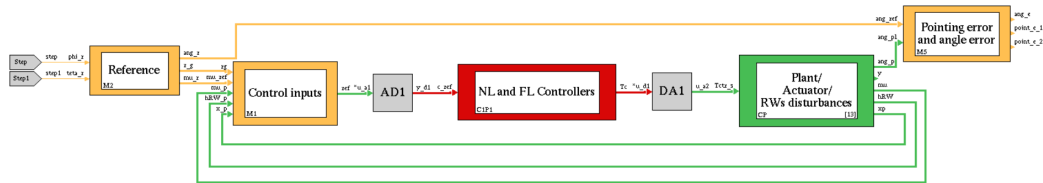


Figure 4.15: Sliding mode-based control scheme

Reference generator

The block responsible for the reference generation is shown by figure 4.16. As it is possible to see, it has the usual two inputs given by the reference angles ϕ_{ref} and θ_{ref} and produces as outputs the reference angles variable, labelled as ang_r , the second derivatives of reference signals r_{gi} , according to the relative degrees of each output analysed in section 4.1, and the reference variable for the external state, labelled as μ_r . All these variables have been analysed in section 4.4. This block contains the C code lines necessary to build all the above-mentioned variables. In particular, it must be pointed out that once the reference angles and the correspondent quaternion have been computed, as usual, the components of the vectorial part are injected into a specific function to compute the first and second derivatives. Then, the

variable r_{gi} has been built with all the second derivatives. Instead, the reference components and their first derivatives are used to define the variable μ_r . It is important to remind that everything is compliant with the theoretical analysis made in section 4.4 and the previous ones. Also in this case, only the *Output* function has been used. Finally, a brief comment on the *Control inputs* block must be done. This structure, as already mentioned, is responsible only for the computation of the variable $\tilde{\mu}$, labelled as μ_t in figure 4.16. Its structure is given by (4.86). The other variables that enter the block are not subject to any manipulation and they are simply merged and injected in the controllers block, after the *AD* conversion. These variables are the second derivatives of the reference signal $r^{(\gamma_i)}$ (labelled as r_{gi} , the vectorial angular velocity and the actual attitude quaternion ω, q (i.e. the plant state labelled as x_p) and the reaction wheels angular momenta variable h_{RW} , which coincides with the well-known quantity $\mathbf{H}_B^{(w)}$ of chapter 2.



Figure 4.16: Reference generation block

Controller

Figure 4.17 displays the key block of the whole scheme i.e. the *Non-Linear (NL) and Feedback Linearisation (FL) Controllers*. It is characterised by the C code lines needed to implement these two control structures. Also in this case, it has been used only the *Output* function, which has been divided in the same three portions described for the pole placement controller. Therefore, since the structure is identical to the previous one, it is only necessary to make a brief comment on the *main computation* section. This portion is basically defined by C functions which implement relations (4.34) and (4.78), that define the input-output linearisation and the sliding mode control law.



Figure 4.17: Controller structure

Chapter 5

Simulation results and comparisons

This is the final chapter of the thesis, which aims to show the simulation results about the attitude control performed with the different control systems analysed in the previous chapters. The discussion of the simulation results will be split in two parts: the first one will refer to the disturbances-free case, in order to study the basic behaviour of the specific control system. In this situation, only the reference signal has been considered as input and the system output response, in presence of different values of the controller parameters, has been studied. So, some comments will be made about the effect of the parameters modification on the output time trend. As already mentioned in the previous sections, the main variables of the attitude control system are the *error angles*, which are used to understand how much the telescope is far from the target star. Moreover, a brief analysis of the control variable will be performed in order to understand if, in some situations, the actuator saturation takes place. It is necessary to evaluate the behaviour of the control system without any disturbance, since it is fundamental to figure out if the specific control law can be suitable for the attitude control of a small satellite. Instead, the second part of the simulation result analysis deals with the control system behaviour when reaction wheels disturbances act on it. It is quite important to highlight that the only disturbance contribution comes from the RWs and all the environmental ones have been

neglected, since the objective of this thesis is to perform an initial analysis of the RWs disturbances impact on the overall control structure and how they can be attenuated through the controller parameters. So, all the obtained results about the telescope pointing error will be in general quite lower than the ones characterizing all the papers related to the RWs disturbances effect. This situation will be analysed in the specific section. Also in this simulation case, it will be evaluated the time trend of the *error angles*, in order to understand how much the oscillations induced by the reaction wheels disturbances affect the pointing stability of the telescope. Moreover, a brief discussion about the disturbances and the control inputs will be performed. Finally, some comments and comparisons will be made about the simulation results obtained with the the three control structures. Before starting the discussion, it is important to highlight that even though the control systems simulations have been performed in both the well-known environments i.e. MATLAB/Simulink and EICASLAB, almost all the figures that will be shown in the following part refer to the Simulink implementation and only some pictures will refer to the EICASLAB one. This situation is simply due to space problems and to avoid making the analysis too redundant.

5.1 Simulations without disturbances

As mentioned in the chapter introduction, this section focuses on the simulation results analysis of the three control systems, previously analysed, when only the reference signal is applied. Therefore, no disturbance has been considered in the following simulations. As mentioned before, it will be shown the time trend of the three error angles defined as the difference between the reference Cardan angles ϕ_{ref} , θ_{ref} , ψ_{ref} and the ones describing the actual satellite attitude ϕ , θ , ψ , expressed in arcseconds, since it is the measurement unit used in this kind of applications. Furthermore, the control torque applied by each reaction wheel to the satellite will be studied. The order that will be followed for the simulations analysis is the same of the previous theoretical description. So, at first the PD controller will be evaluated and, then, the feedback linearisation structure plus the linear and non-linear controller will be analysed.

PD controller

The Proportional-Derivative controller is characterized by a control variable expressed by (3.5) which can be suitably modified by considering the small angle approximation (3.6). Moreover, this control law includes the gyroscopic compensation term, used to remove the non-linearity of equation (2.15). Therefore, the net control torque is expressed by (3.12), which clearly highlights that proportionality to the error angles and their derivatives through the matrix \mathbf{K}'_P and \mathbf{K}'_D . Now, as mentioned before, these matrices are diagonal, so that a decoupled system is obtained, and all the coefficients for each matrix (relation (3.14)) are equal. Now, by recalling that these coefficients have been considered as $k_P = \omega_n^2$ and $k_D = 2\zeta\omega_n$, the following time trend for the error angles are considered, when specific variations of ω_n and ζ take place. It is quite important to highlight that the following figures refer only to the error angle relative to the z-axis of the body frame ψ_e , since the only non-zero reference angle is ψ_{ref} and the initial conditions are related only to the angle ψ , as mentioned in chapter 2. So, the other error angles ϕ_e and θ_e are always null. Figures 5.1, 5.2/5.3 and 5.4 highlight the time trend of the error angle on the body frame z-axis ψ_e , when a variable ω_n and a fixed ζ are considered. It is quite evident that an increase of ω_n makes the error convergence faster and it also reduces its maximum absolute value. Instead, an increase of ζ leads to a more damped behaviour of the error. This situation is well-evident through a comparisons among the scenarios described by figures 5.1, 5.2 and 5.4 (Simulink environment). Figure 5.3 shows the error time trend when the control system simulation is performed in EICASLAB. So, it easy to notice that almost the same results of figure 5.2 have been obtained. The small differences are due to the quantization procedure effects, which have been mitigated as much as possible.

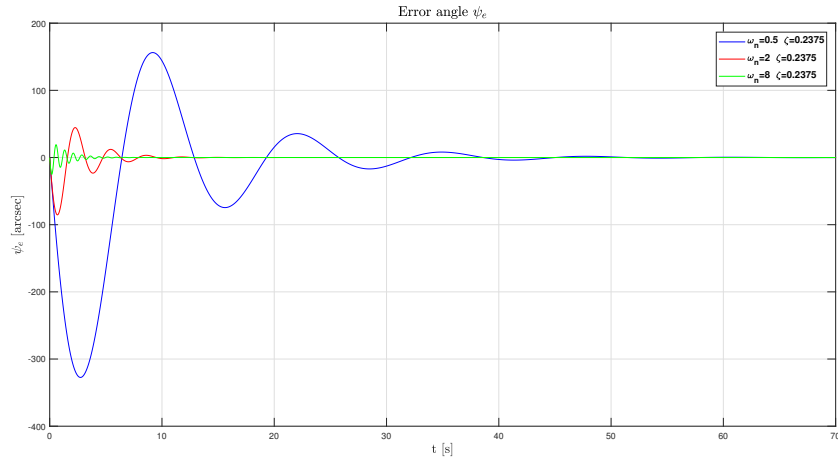


Figure 5.1: Error angle ψ_e when $\omega_n \in \{0.5, 2, 8\}$ and $\zeta = 0.2375$

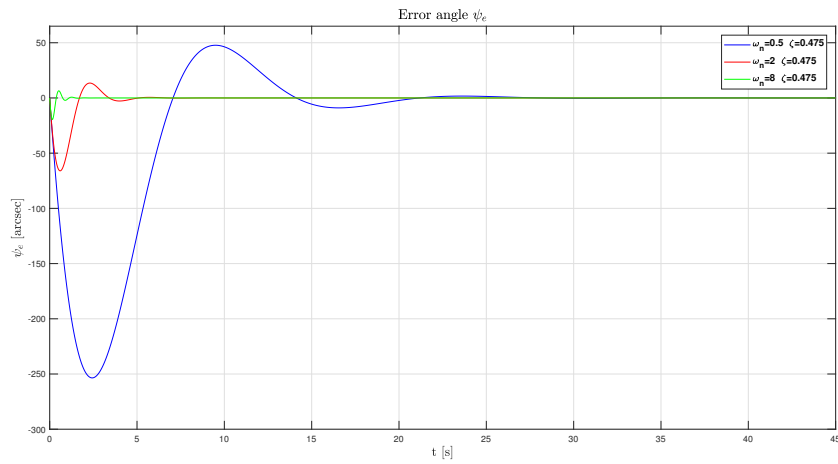


Figure 5.2: Error angle ψ_e when $\omega_n \in \{0.5, 2, 8\}$ and $\zeta = 0.475$

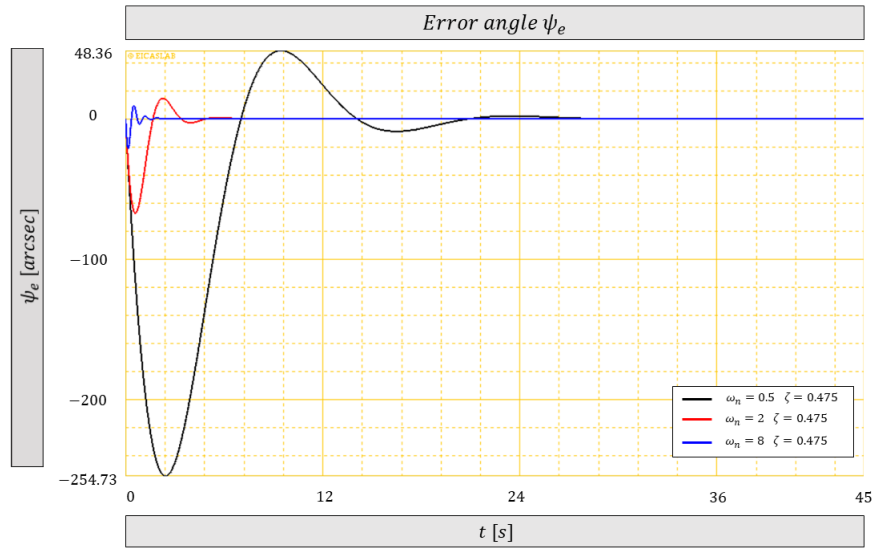


Figure 5.3: EICASLAB simulation results of ψ_e when $\omega_n \in \{0.5, 2, 8\}$ and $\zeta = 0.475$

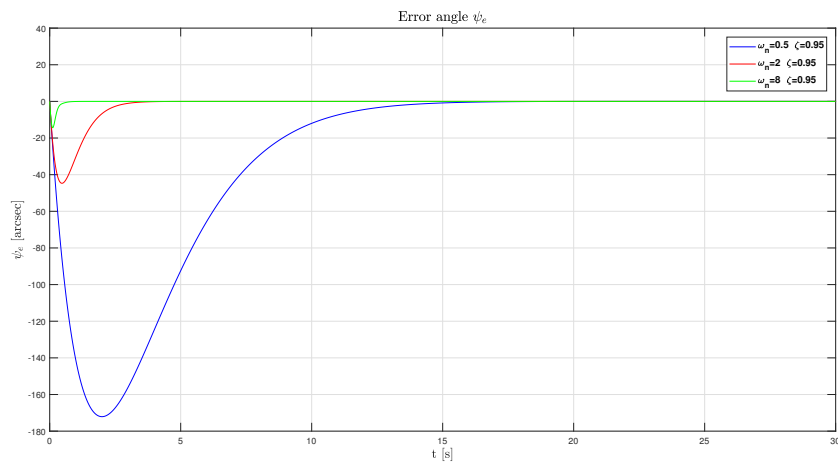


Figure 5.4: Error angle ψ_e when $\omega_n \in \{0.5, 2, 8\}$ and $\zeta = 0.95$

Now, it is really interesting to point out that a particular behaviour takes place when $\omega_n = 8$ and $\zeta = 0.2375$. As it is possible to see from figures 5.1, with the above-mentioned values, the error angles is not as damped as in the cases represented by $\omega_n = 0.5, 2$. This situation is due to the influence of the DC motors dynamics on the overall system. As mentioned in chapter 2, the coefficient K^* has been used to neglect the motor dynamic. This means that in the scenario of figure 5.1 the values of this gain is not high enough to consider negligible the actuator dynamic. Instead, for the other situations this value is quite good and an increase of it does not leads to strong modification of the error angle trend. Therefore, the solution to this problem is to increase the value of K^* . Figures 5.5 and 5.6 display the scenarios before and after the coefficient increment. So, it is evident, from the comparison between these figures, that with a higher K^* the ψ_e trend is more damped and aligned with the other situations.

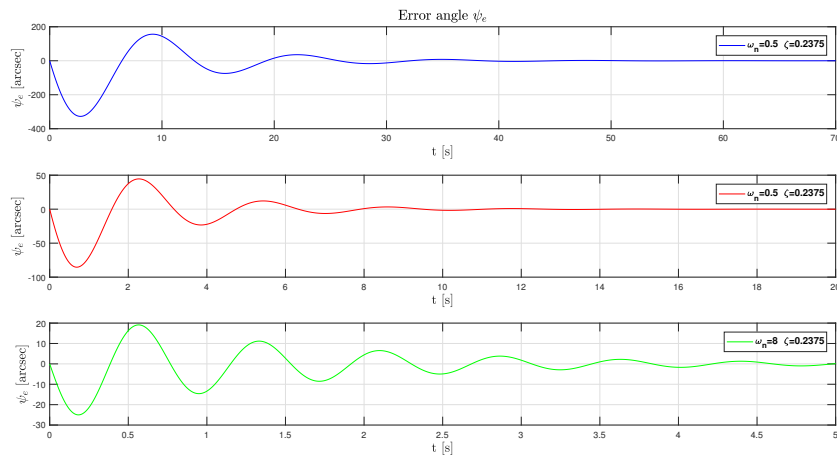


Figure 5.5: Error angle ψ_e when $\omega_n = 8$ and $\zeta = 0.2375$ before the K^* increment

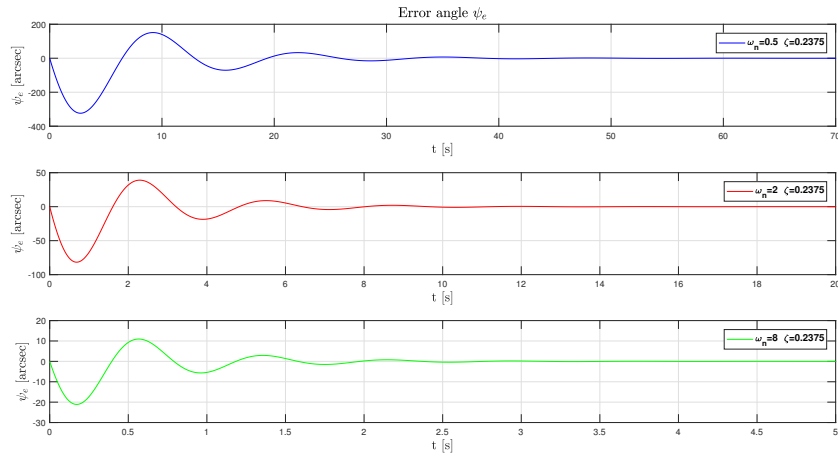


Figure 5.6: Error angle ψ_e when $\omega_n = 8$ and $\zeta = 0.2375$ after the K^* increment

Finally, it is interesting to show that an increase of ω_n produces a quite strong increment of the control command (variable T_c in the Simulink schemes), higher than the one obtained with an increment of ζ for a fixed ω_n . However, due to the limitation of the actuator torque, even if a high K^* is considered, there will be a strong difference between the torque command and the torque produced by the motor if the control command exceeds too much the saturation value of the actuator. Figure 5.7 and 5.8 depict this situation, characterized by an high value of K^* . In particular, figure 5.7 shows the time trend of the torque command when it does not exceed the limit value (fixed at 0.635 mNm) and the correspondent motor torque, which is quite similar the previous one. Instead, figure 5.8 displays the scenario when the torque command exceeds (not too much) the saturation value. In this case, the motor torque starts moving away from the control command, even though the coefficient K^* is quite high.

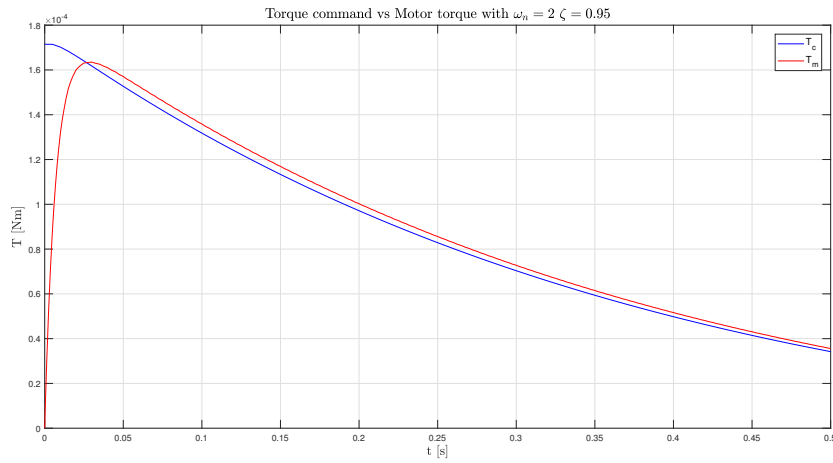


Figure 5.7: Torque command vs motor torque when $\omega_n = 2$ and $zeta = 0.95$

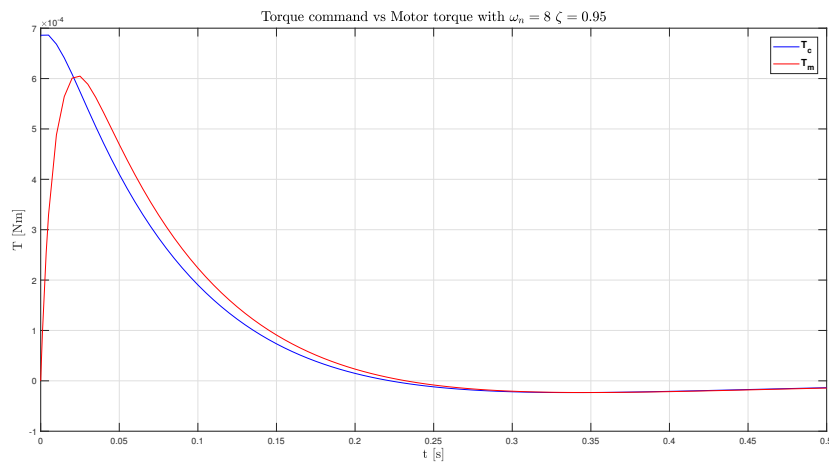


Figure 5.8: Torque command vs motor torque when $\omega_n = 8$ and $zeta = 0.95$

Feedback linearisation approach with a linear controller

This section aims to show the simulation results obtained with a feedback linearisation approach plus a linear controller, designed with the pole placement technique. In this case, as mentioned in section 4.2, the control law for each Cardan angle is characterized by the matrix K_c^i and the gain N^i , as shown by relation (4.53). These two parameters are determined by choosing the desired poles/eigenvalues positions and, in this thesis, they have been defined as $\lambda_{1/2} = -\zeta\omega_n \pm \omega_n\sqrt{1-\zeta^2}$. Therefore, as displayed in chapter 4, the coefficients of K_c^i are equal to ω_n^2 and $2\zeta\omega_n$ and the gain N^i coincides with first element of K_c^i i.e. ω_n^2 . So, also in this case, different graphs will be shown by considering suitable variations of ω_n and ζ . It is quite interesting to remind that the transfer function between reference angle and actual one is very similar to the one determined for the PD controller case. In particular, the following figures will show that, for the situation analysed in this thesis, the two control approaches (PD and FL plus a linear controller) produce the same simulation results. Also in this case, only ψ_e will be shown. Figures 5.9, 5.10/11 and 5.12 clearly show that the time trend of ψ_e is identical to the one obtained with the Proportional-Derivative control. Therefore, the same comments about the effect of ω_n and ζ variation can be made in this situation. Figure 5.11 displays the simulation results obtained by using the EICASLAB environment. They are almost identical to the ones of figure 5.10 and, consequently, of figures 5.2/5.3. Moreover, it is also evident from figure 5.9 the effect of the DC motor dynamic on the angle error when $\omega_n = 8$ and $\zeta = 0.2375$. Also in this case, an increment of K^* leads to a more damped trend, as mentioned in the previous section for the PD control. Finally, the increase of ω_n produces the same time trend for the torque command and motor torque seen before. Therefore, a too high value of this coefficient leads to overcome the actuator saturation level and to determine an augmented discrepancy between the two torques.

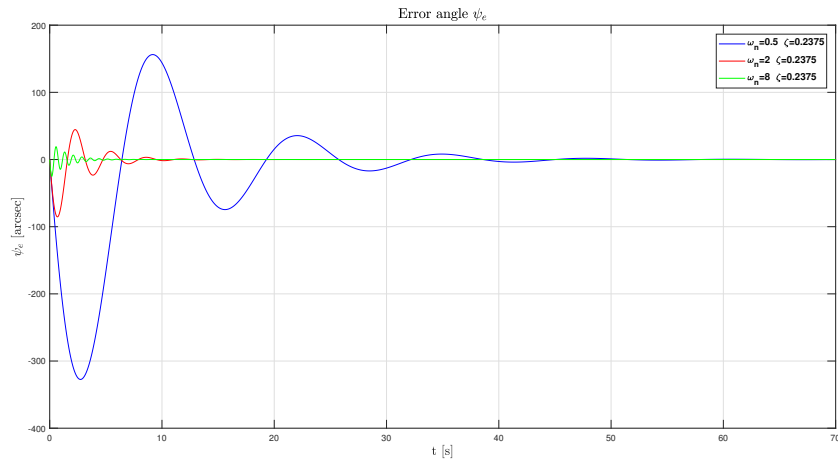


Figure 5.9: Error angle ψ_e when $\omega_n \in \{0.5, 2, 8\}$ and $\zeta = 0.2375$

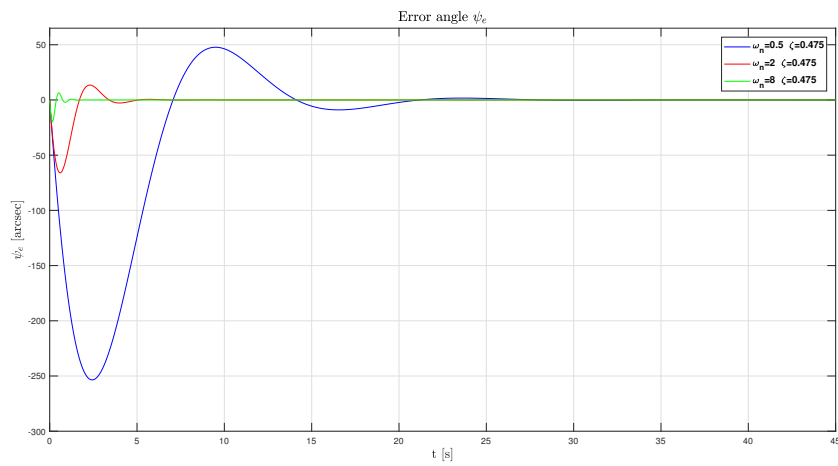


Figure 5.10: Error angle ψ_e when $\omega_n \in \{0.5, 2, 8\}$ and $\zeta = 0.475$

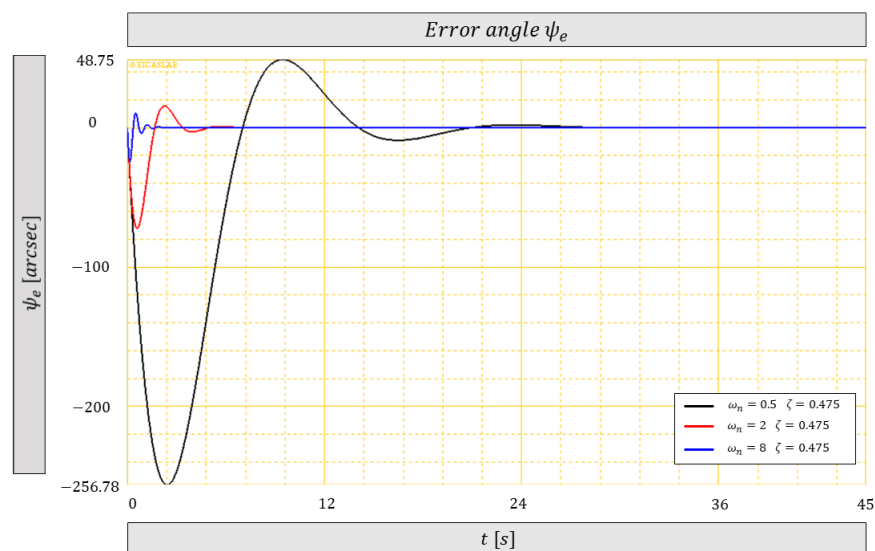


Figure 5.11: EICASLAB simulation results of ψ_e when $\omega_n \in \{0.5, 2, 8\}$ and $\zeta = 0.475$

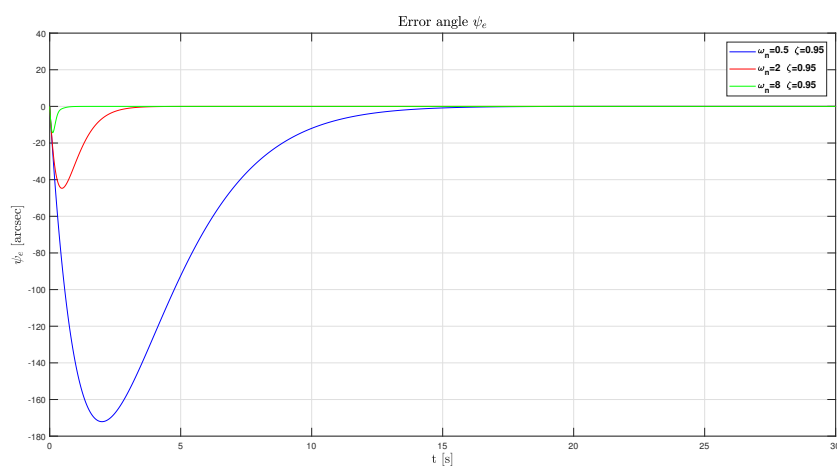


Figure 5.12: Error angle ψ_e when $\omega_n \in \{0.5, 2, 8\}$ and $\zeta = 0.95$

Feedback linearisation method with a non-linear controller

As mentioned in chapter 4, the feedback linearisation approach has been used together with a non-linear controller, developed through the sliding mode methodology. In this case, the specific control law for each Tait-Bryan angles is characterized by three parameters, as mentioned by (4.78): k_1 , k_2 and η . The following figures describe the behaviour of the only variable of interest i.e. ψ_e , when a suitable variation of these coefficients is considered. The first figure (5.13) shows the time trend for the initial scenario, where $k_1 = 0.5$, $k_2 = 0.5$ and $\eta = 1$, and two cases where only a variation is considered. In the first one, only η is modified and set to 10. Instead, the second one is characterized by the variation of k_2 , imposed equal to 4. As it is possible to notice, by modifying η (the parameter that defines the non-linearity) a strong reduction of the maximum absolute value of the error is attained. However, it can be seen a small reduction of the convergence speed. A quite similar behaviour can be obtained through the modification of k_2 . In this situation, the maximum value is a little bit higher than the previous case but, anyway, much lower than the initial one.

Figures 5.14/5.15 depict an augmented analysis of the error trend, by considering other kinds of variation. In particular, two scenarios are added to the previous analysis i.e. the modification of the coefficient $k_1 = 2$ and the contemporary change of $k_1 = 2$, $k_2 = 4$. In the first case, it is easily to notice that the variation of k_1 produces worse results in terms of maximum value, even though it tends to keep unaltered the convergence speed of the initial scenario. Instead, the second case shows a strong improvement with respect to the initial condition and also a better behaviour of the error with respect to all the situations analysed so far. Indeed, the maximum absolute value is lower and also the convergence velocity is a little bit higher. Figure 5.15 shows the EICASLAB results relative to this augmented analysis of ψ_e . It is evident that they are almost equal to the ones displayed by figure 5.14.

Finally, figure 5.16 display the complete analysis of ψ_e , by considering other two double variations and a triple one. The first double modification involves $k_2 = 0.5$ and $\eta = 10$ and shows a reduced maximum value with respect to the

case where $k_1 = 2$, $k_2 = 4$, $\eta = 1$ and an unmodified convergence speed. Instead, the contemporary modification of $k_1 = 2$ and $\eta = 10$ produces an even smaller value of the maximum error, but it is characterized by a very small convergence speed. Finally, the triple variation described by $k_1 = 2$, $k_2 = 4$ and $\eta = 10$ generates the best possible result in terms of maximum error and convergence velocity. From all these simulations, it can be noticed that no tracking problem has been experienced. Therefore, the internal stability of the system, mentioned in chapter 4, can be considered asymptotically stable.

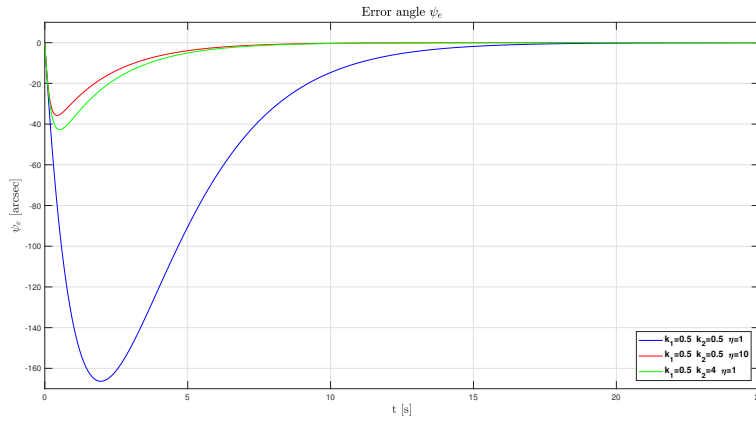


Figure 5.13: First analysis of error angle ψ_e with variation of k_1 , k_2 , η

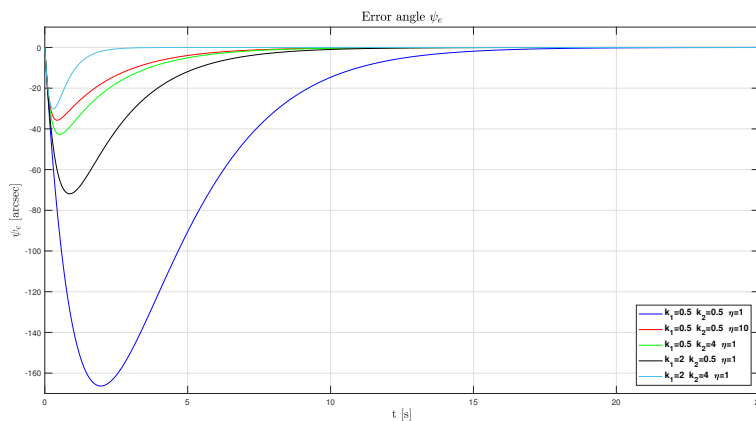


Figure 5.14: Second analysis of error angle ψ_e with variation of k_1 , k_2 , η

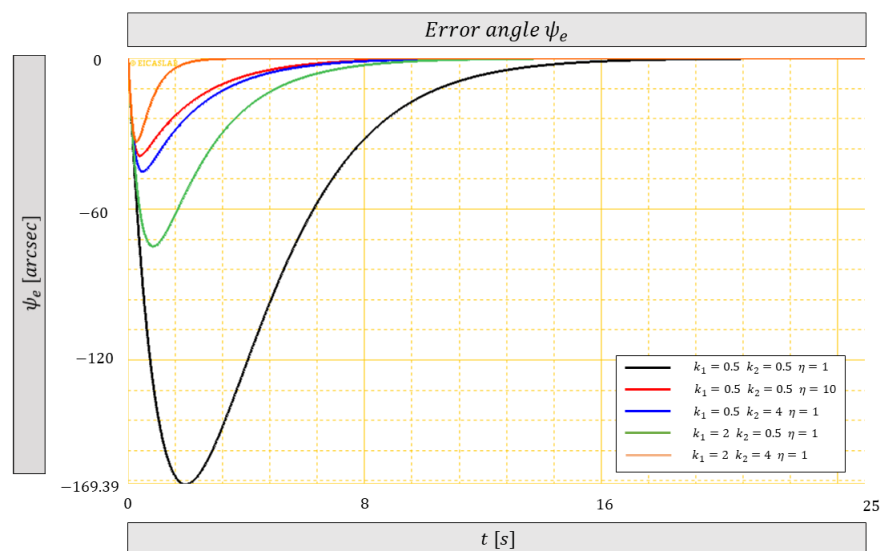


Figure 5.15: EICASLAB second analysis of the error angle ψ_e with variation of k_1 , k_2 , η

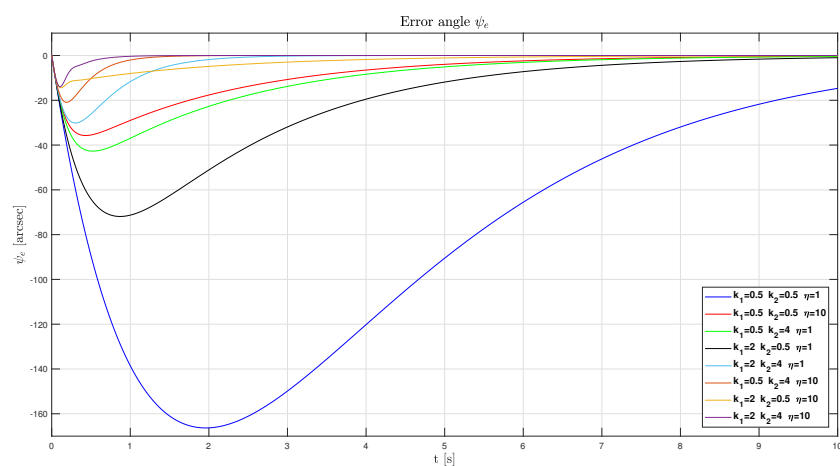


Figure 5.16: Final analysis of error angle ψ_e with variation of k_1 , k_2 , η

Now, it is interesting to notice that for almost all the scenarios, the initial value of K^* is such that the DC motor dynamic does not strongly influence the error trend, since its increment does not lead to consistent modifications. The only exceptions occur when both k_1 and/or k_2 and η are modified. The following figure shows the scenario represented by the triple parameter variation with respect to the initial case.

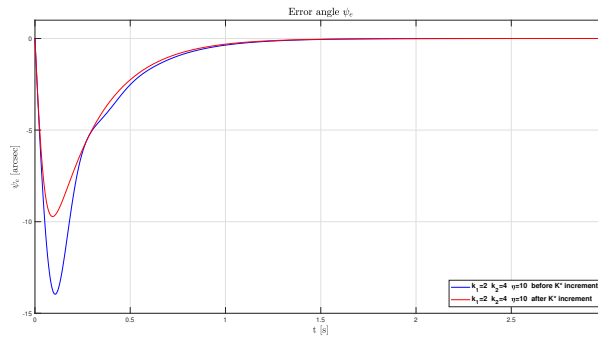


Figure 5.17: ψ_e with $k_1 = 2$, $k_2 = 4$, $\eta = 10$ and different values of K^*

Finally, it is important to highlight that there are two scenarios where the torque command exceeds the limit value and, therefore, a consistent discrepancy between the motor torque and the command one occurs even though the coefficient K^* assumes a very high value. These situations are characterized by: 1) $k_1 = 2$, $k_2 = 0.5$, $\eta = 10$ 2) $k_1 = 2$, $k_2 = 4$, $\eta = 10$. Figure 5.15 depicts the latter situation, when a very high value is considered for K^* .

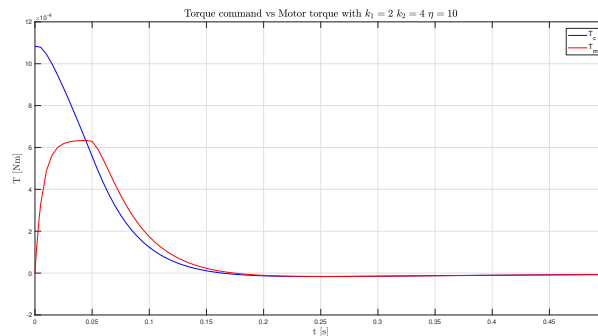


Figure 5.18: Torque command vs motor torque with $k_1 = 2$, $k_2 = 4$, $\eta = 10$ and high value of K^*

5.2 Simulation results with disturbances

This section aims to analyse the effects of the RWs disturbances on the three error angles that characterize the pointing action of the satellite telescope. Figure 5.19 clearly depicts what happens, in general, on the focal plane of the telescope when the spacecraft is subject to the reaction wheels disturbances. It is important to point out that for each wheel the disturbances are expressed by relation (1.15) to (1.18), which highlight the sinusoidal/oscillating trend of these variables. As already mentioned in chapter 1, the only contribution analysed in this thesis comes from the first/fundamental harmonic, which produces the most relevant effect.

The above-mentioned figure shows the equivalent motion of the target star on the focal plane, even though it is clear that the star is still and the element that moves is the satellite. Anyway, it is a good method to represent the impact of the disturbances on the pointing stability. The control system objective is making the target star motion as close as possible to the central point of the focal plane, such that a reliable photometric analysis can be obtained.

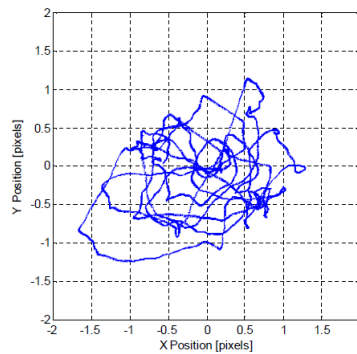


Figure 5.19: Example of the target star motion on the telescope focal plane [10]

In the following parts, it will be shown the time trends of the three Cardan angles errors ϕ_e , θ_e and ψ_e , when different control approaches are considered. The analysis will start with the PD control simulation results and, then, it will focus on the feedback linearisation approach with the addition of the linear and non-linear control. Before starting the discussion, it is fundamental to

highlight that all the obtained results, about the oscillating behaviour of the three error angles, are characterized by values that are quite lower than the ones that can be obtained in general and mentioned in different papers about the reaction wheels impact on a small satellite attitude. The reason of this situation is basically due to total absence of environmental disturbances like gravity gradient, magnetic effects and aerodynamic drag. Indeed, since this work of thesis aims to perform an initial analysis of the RWs disturbances effect on the telescope pointing stability, all the above-mentioned disturbances have been neglected. However, these external disturbances lead to a strong counteraction of the controller command which, in turn, generates a higher rotation speed of the actuator and so disturbances with higher frequency and amplitude. Therefore, in this situation, the values of the three Cardan error angles are much higher than the ones presented in this thesis.

PD controller

As already mentioned in section 5.1, the PD controller is characterized by two matrices whose values are related to the coefficients ω_n and ζ . The following figures shows the time trend of the angle errors ϕ_e , θ_e , ψ_e when different values for these parameters are considered.

Figures from 5.20 to 5.24 depict the error angles associated to the x, y and z axis of the body frame ϕ_e , θ_e and ψ_e at steady state, by considering three plots characterized by a variable value of ζ and ω_n . As it is possible to see, ϕ_e and θ_e have a high frequency oscillating behaviour due to the disturbances effect. In particular, from figures 5.20 and 5.22 it is evident that an increasing of ω_n with $\zeta = 0.95$ (third plots) leads to an attenuation of the maximum error, which is the main objective of the control system. Instead, when fixed values $\zeta = 0.2375$ and $\zeta = 0.475$ are considered, the increment of ω_n from 0.5 to 2 produces a higher maximum value for the error. This situation does not take place when the value of ω_n is equal to 8. Indeed, a strong reduction of the error occurs. All these results are coherent with the specific transfer functions that describe the effect of the disturbances on actual attitude angles. Moreover, from figures 5.21 and 5.23 it can be noticed that with $\omega_n = 0.5$ and variable ζ the maximum value of the errors is almost

the same. A different situation occurs when $\omega = 2$ and $\omega_n = 8$, since an increment of ζ generates an evident reduction of the error values.

Figure 5.24 displays the trend of ψ_e . It is quite clear that this variable is not subject to any variation with respect to the disturbances-free case. This results can be explained in the following way: since the target star lays in the same plane of the orbit and the satellite starts with the body frame z-axis orthogonal to the orbit plane and, so, x and y lay on this plane, the main control action that must be applied to point the telescope towards the star refers to the angle related to the z-axis i.e. ψ . Instead, when disturbances act on the x and y axis, the control action used to take the attitude angles ϕ and θ to the reference values i.e. zero is quite modest. Therefore, the main control action leads to a higher steady state rotational speed of the reaction wheel aligned with the z-axis than the ones related to the other wheels. Subsequently, since the disturbances amplitude is proportional to the square of the wheel rotational speed, as mentioned by relations (1.15) to (1.18), the disturbance that the z-wheel produces on the body frame axes x and y is quite stronger than the ones produced by the x-wheel and y-wheel on the z axis of the body frame, which are basically negligible.

Moreover, it must be pointed out that a higher value of K^* does not lead to consistent modifications of the errors trend. The only exception is the behaviour of ψ_e when $\omega_n = 8$ and $\zeta = 0.2375$, as deeply analysed in section 5.1.

Finally, from the above-mentioned simulation results has been possible to compute the RMS of ϕ_e and θ_e , at steady state. In particular, the RMS of ϕ_e varies from a minimum value of 0.0064 arcsec to a maximum one of 0.0332 arcsec . Instead, the RMS of θ_e spans from 0.0013 arcsec to 0.0064 arcsec . The minimum values for ψ_e and θ_e are obtained with $\omega_n = 8$ and $\zeta = 0.95$. Instead, the maximum ones with $\omega_n = 2$ and $\zeta = 0.2375$. Clearly, for all the other values of the parameters, the RMS assumes a value between the minimum and maximum one.

Furthermore, figures 5.25 and 5.26 depicts the simulation results of ϕ_e and θ_e , obtained with the EICASLAB environment when $\omega_n \in \{0.5 \ 2 \ 8\}$ and $\zeta = 0.475$. These plots are more or less equal to the second graph of figures 5.20 and 5.22 in the time interval $t \in [220 \ 225] \text{ s}$.

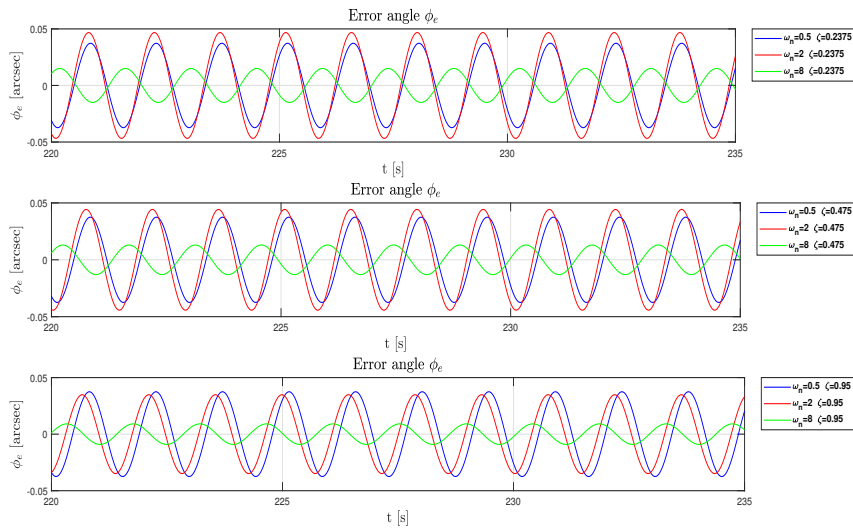


Figure 5.20: Error angle ψ_e with fixed ζ and variable ω_n

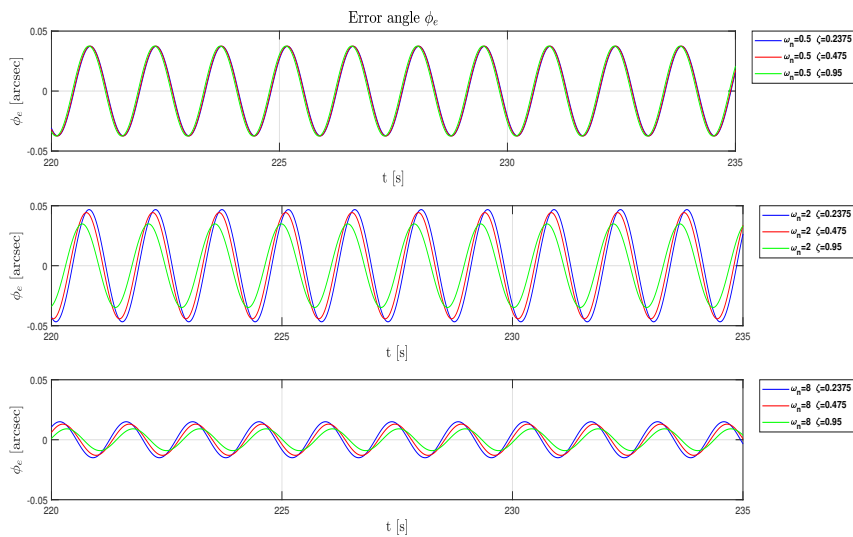


Figure 5.21: Error angle ψ_e with variable ζ and fixed ω_n

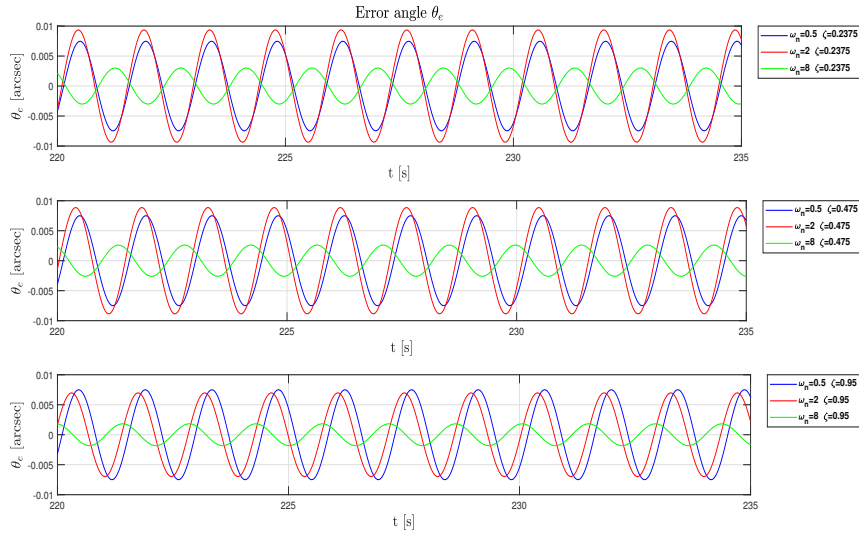


Figure 5.22: Error angle θ_e with fixed ζ and variable ω_n

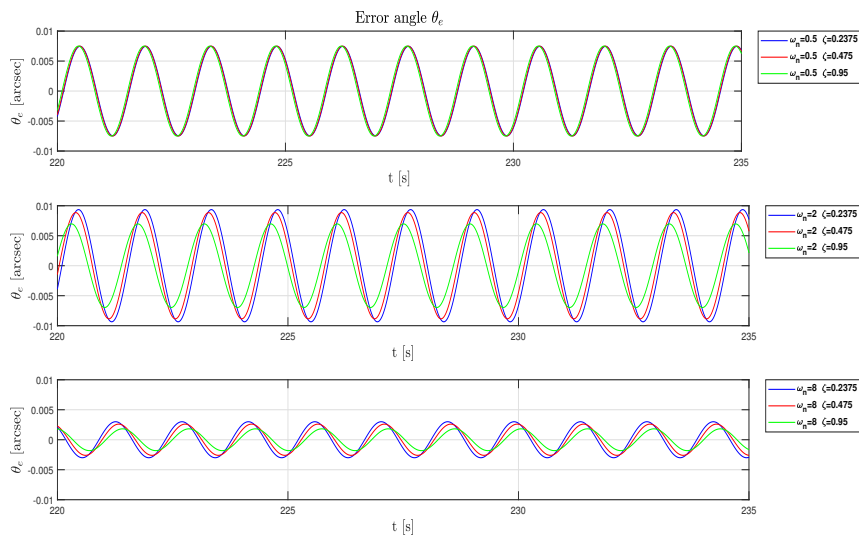


Figure 5.23: Error angle θ_e with variable ζ and fixed ω_n

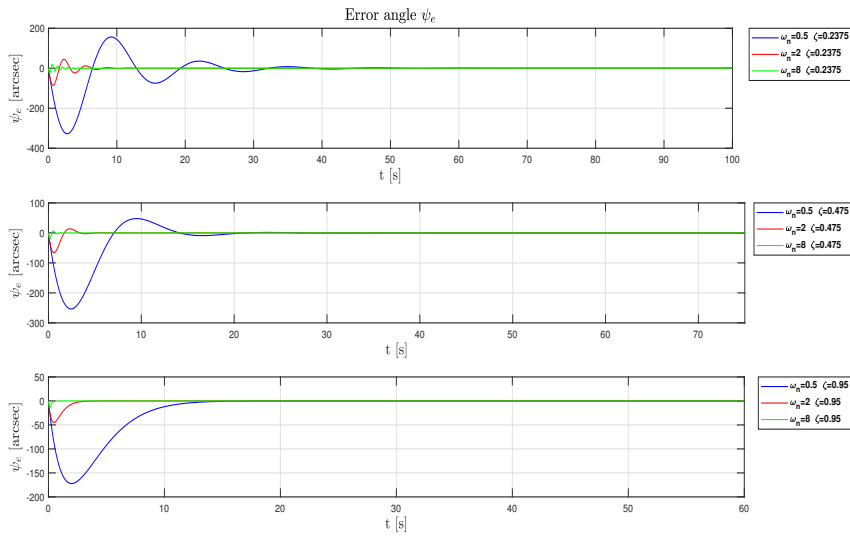


Figure 5.24: Error angle ψ_e

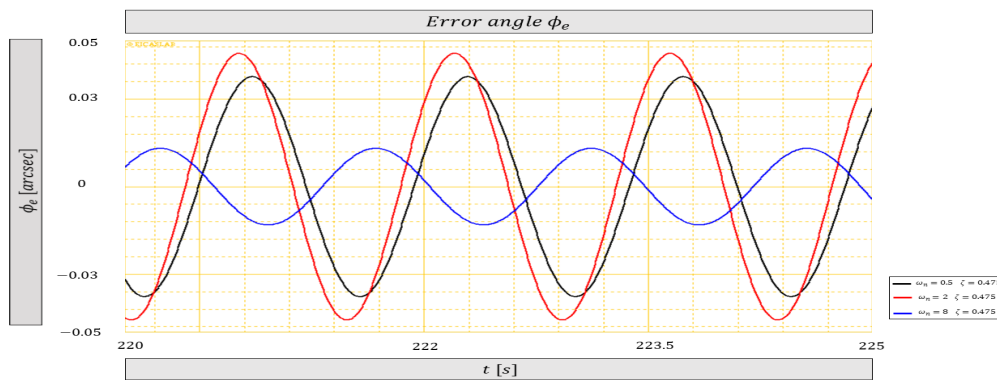


Figure 5.25: EICASLAB results of ϕ_e $\omega_n \in \{0.5\ 2\ 8\}$ and $\zeta = 0.475$

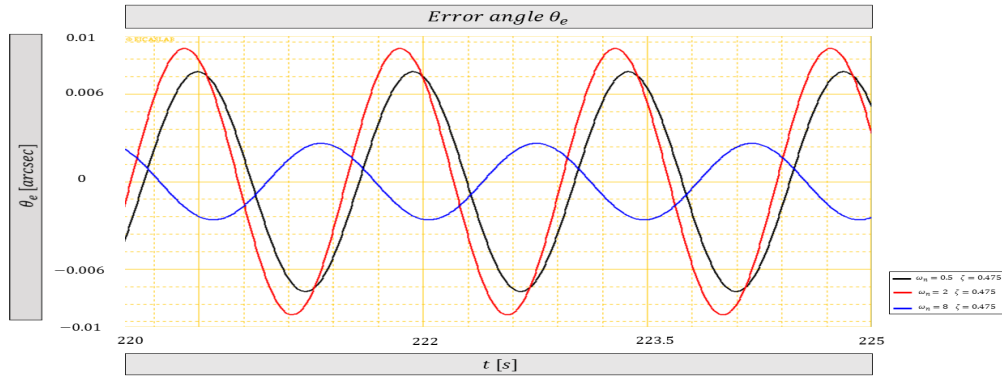


Figure 5.26: EICASLAB results of θ_e when $\omega_n \in \{0.5\ 2\ 8\}$ and $\zeta = 0.475$

Feedback linearisation with the linear controller

As already mentioned in section 5.1, the feedback linearisation method with the linear controller, designed with the pole placement technique, leads to identical results to the PD control ones. So, also in this case will be shown the time trend of the error angles when different values of ω_n and ζ are considered. Then, the comments made in the previous section, about the disturbances attenuation for ϕ_e and θ_e and the invariance of ψ_e with respect to the disturbances-free case, as well as all the other comments, can be re-proposed for this control strategy. Figures 5.27 to 5.31 clearly confirm what has been said. Moreover, the RMS values computed for the PD controller case are the same ones obtained with this control technique. Finally, figures 5.32 and 5.33 display the EICASLAB simulation results of ϕ_e and θ_e when $\omega_n \in \{0.5\ 2\ 8\}$ and $\zeta = 0.475$, as already done for the PD control.

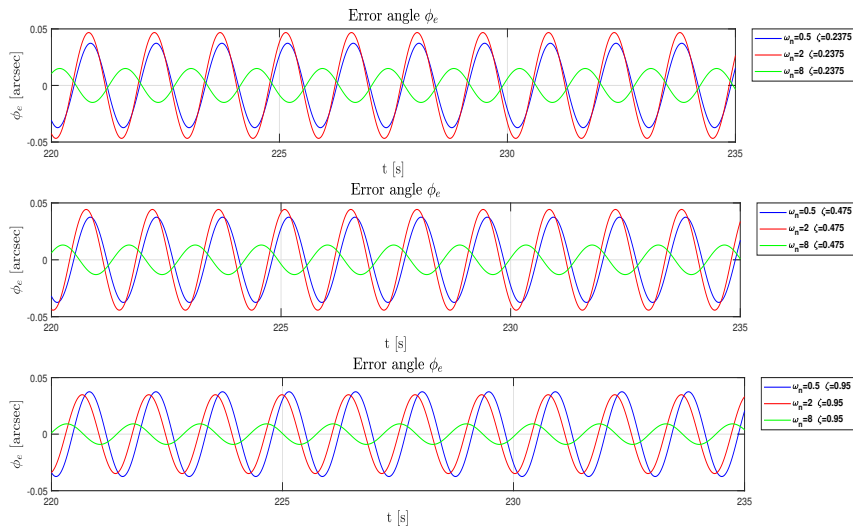


Figure 5.27: Error angle ϕ_e with fixed ζ and variable ω_n

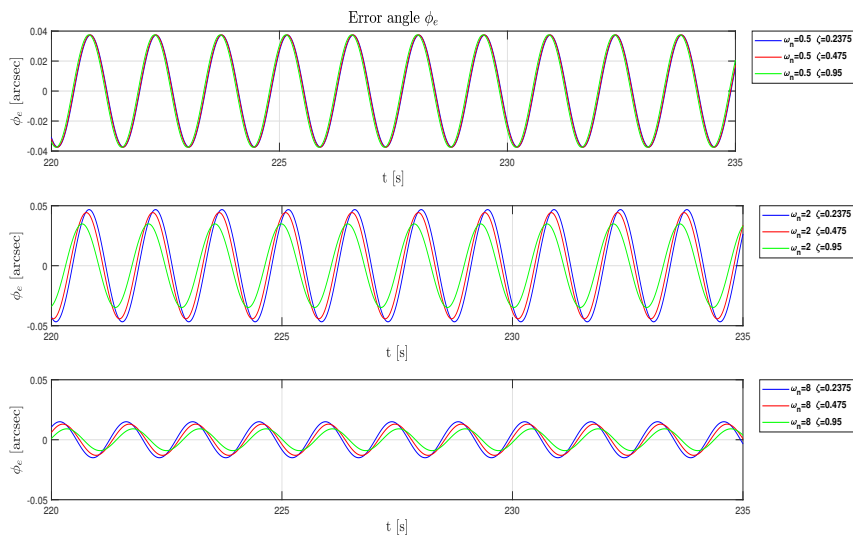


Figure 5.28: Error angle ϕ_e with variable ζ and fixed ω_n

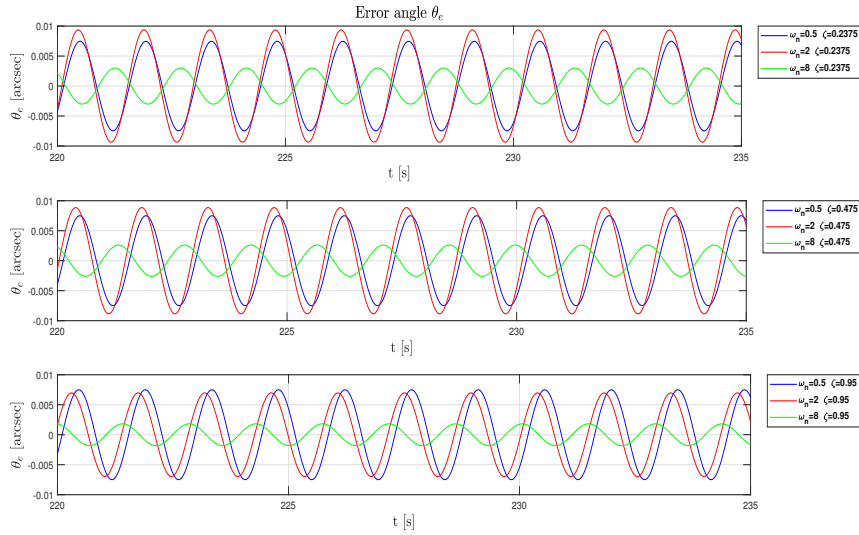


Figure 5.29: Error angle θ_e with fixed ζ and variable ω_n

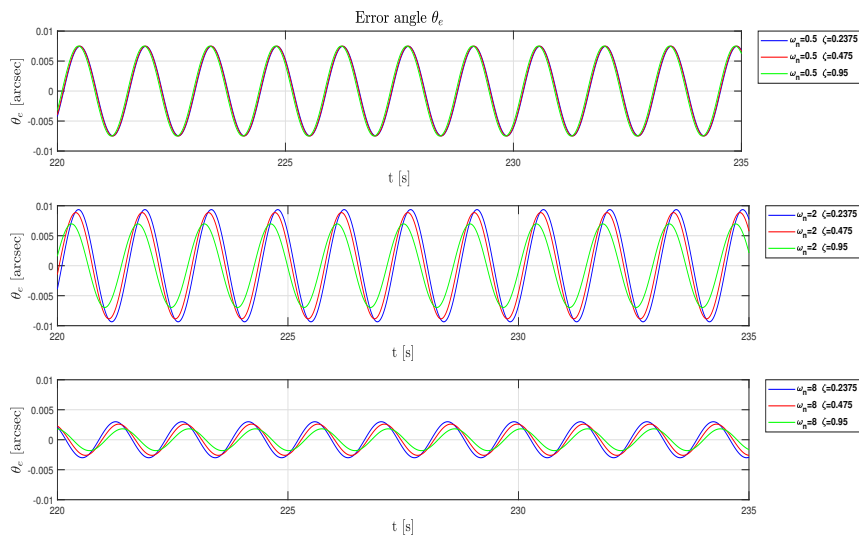


Figure 5.30: Error angle θ_e with variable ζ and fixed ω_n

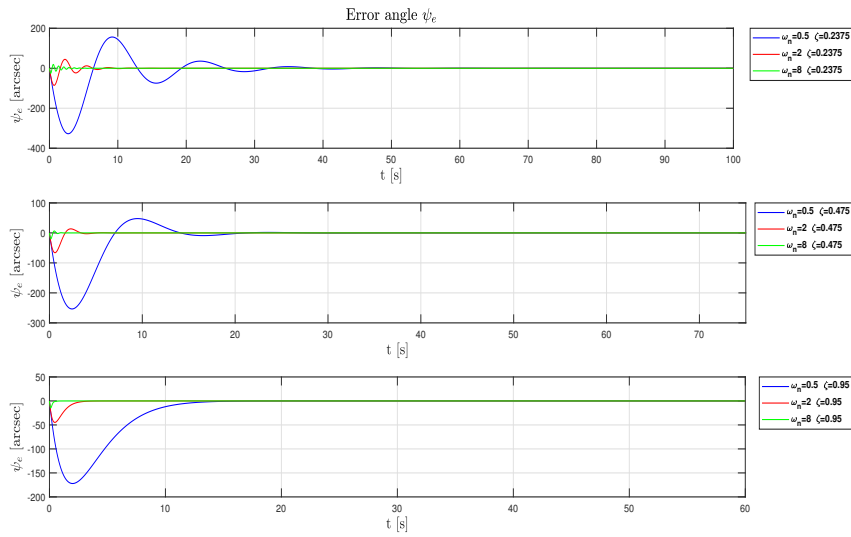


Figure 5.31: Error angle ψ_e

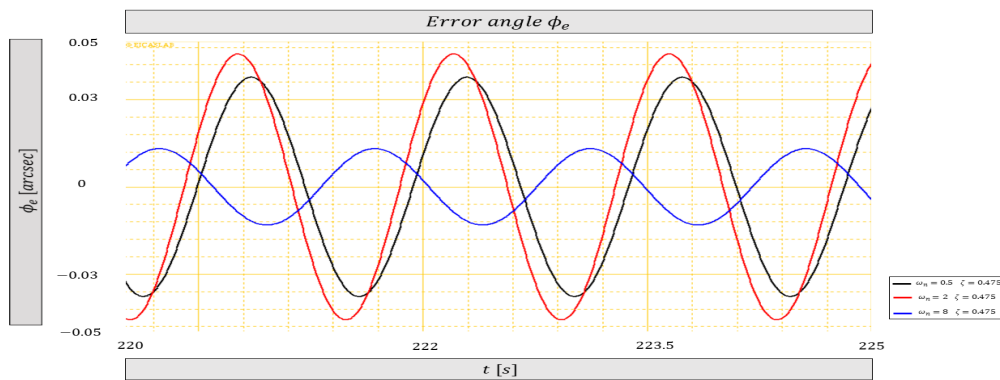


Figure 5.32: EICASLAB results of ϕ_e when $\omega_n \in \{0.5\ 2\ 8\}$ and $\zeta = 0.475$

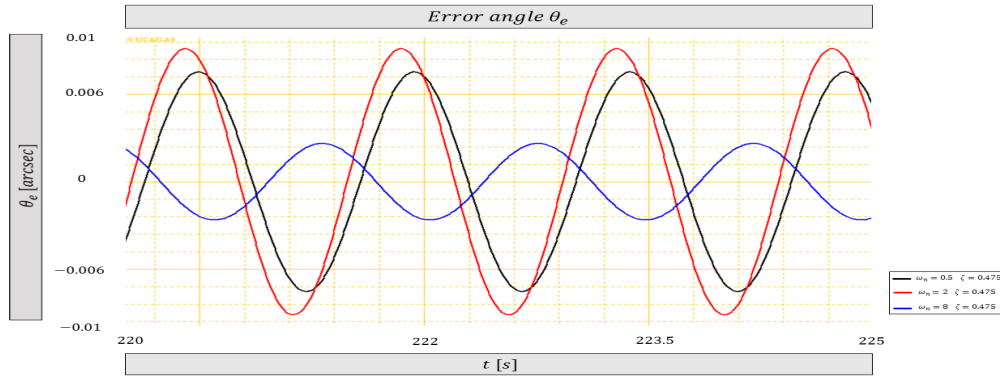


Figure 5.33: EICASLAB results of θ_e when $\omega_n \in \{0.5, 2, 8\}$ and $\zeta = 0.475$

Feedback linearisation with the non-linear controller

Now, the time trend of the error angles ϕ_e , θ_e and ψ_e is analysed, when a feedback linearisation approach with the non-linear controller, developed with the sliding mode methodology, is used. As stated in section 5.1, the main controller parameters for each control law, associated with a Cardan angle, are k_1 , k_2 and η . The following figures put in evidence how these parameters can be chosen to reduce the effect of the RWs disturbances. Also in this case, the steady state behaviour of the error angles will be analysed. Figures 5.34 and 5.35 show the oscillating behaviour of ϕ_e and θ_e , when a suitable combination of the three control parameters is considered. The first plot highlights the maximum value reduction that occurs when the increase of $\eta = 10$ or $k_2 = 4$ takes place, with respect to the initial condition characterized by $k_1 = 0.5$, $k_2 = 0.5$ and $\eta = 1$. So, it is very clear that by increasing η a higher reduction of the error is obtained than the one related to the k_2 increment. Anyway, these two scenarios are not so different.

Instead, the second plot focuses on the increment of $k_1 = 2$ and the double variation of $k_1 = 2$ and $k_2 = 4$. It is important to remind that these variations are referenced to the initial scenario. Therefore, in this case, the value of η is still equal to 1. It is evident that the only increment of k_1 leads to a very small attenuation of the error with respect to the initial case. So, it produces worse results with respect to the cases characterized by $k_1 = 0.5$, $k_2 = 0.5$, $\eta = 10$ and $k_1 = 0.5$, $k_2 = 4$ and $\eta = 1$. Instead, when the double

modification occurs a good attenuation takes place. This situation is quite similar to the one described by the only variation of $\eta = 10$ (actually, it is a little bit worse) and a little better than the scenario given by the $k_2 = 4$ change.

The third plot points out the effects of two double variations and a triple modification. Indeed, in the first case the parameters are $k_1 = 0.5$, $k_2 = 4$, $\eta = 10$, in the second scenario $k_1 = 2$, $k_2 = 0.5$, $\eta = 10$ and in the third situation $k_1 = 2$, $k_2 = 2$, $\eta = 10$. It is immediately evident that the first scenario produces better results than all the previous cases. Then, the maximum error is further reduced by considering the parameters related to the second and third situation. In particular, the results obtained with the triple parameters variation are a bit better than the ones characterizing the double modification $k_1 = 2$, $\eta = 10$.

Instead, figure 5.36 highlights the same situation that occurs with the PD control and the feedback linearisation approach with the linear controller. Indeed, the time trend of ψ_e does not change with respect to the disturbances-free case. The reason behind this situation has been explained in the previous part.

It is important to highlight that an increase of K^* , with respect to the chosen value, does not lead to consistent modifications of the errors trend. The only exception is represented by ψ_e when both k_1 and/or k_2 and η are changed, as discussed in section 5.1.

Moreover, the RMS values of ϕ_e and θ_e , at steady state, have been computed. In particular, the RMS of ϕ_e oscillates from 0.0042 *arcsec* and 0.0262 *arcsec*. Instead, θ_e varies from 0.00084 *arcsec* and 0.0053 *arcsec*. The minimum values are obtained with $k_1 = 2$, $k_2 = 4$, $\eta = 10$. The maximum ones with $k_1 = 0.5$, $k_2 = 0.5$, $\eta = 1$. For all the other simulation scenarios the RMS values are inside the intervals defined by the minimum and the maximum.

Finally, figures 5.37 and 5.38 show the EICASLAB results of ϕ_e and θ_e , when these three scenarios are considered: 1) $k_1 = 0.5$, $k_2 = 4$, $\eta = 10$, 2) $k_1 = 2$, $k_2 = 0.5$, $\eta = 10$, 3) $k_1 = 2$, $k_2 = 4$, $\eta = 10$. These plots are more or less coincident with the ones sketched by the third graph of figures 5.34 and 5.35.

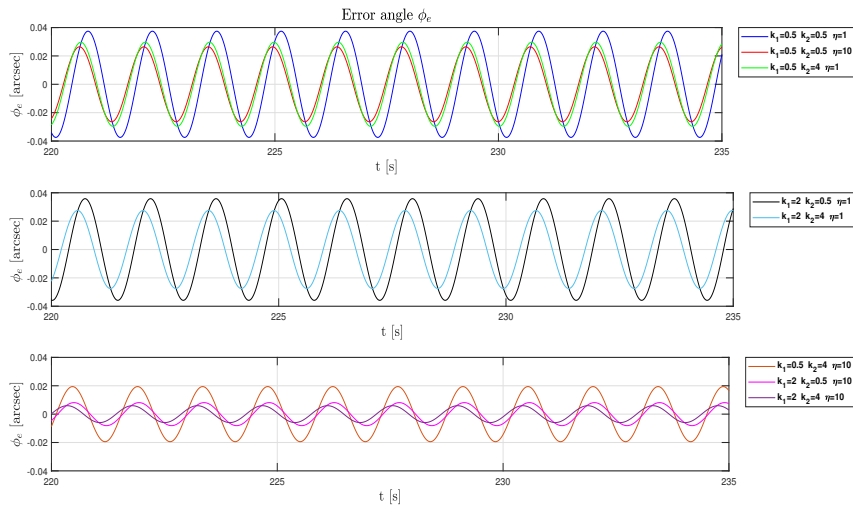


Figure 5.34: Error angle ϕ_e with variable k_1, k_2 and η

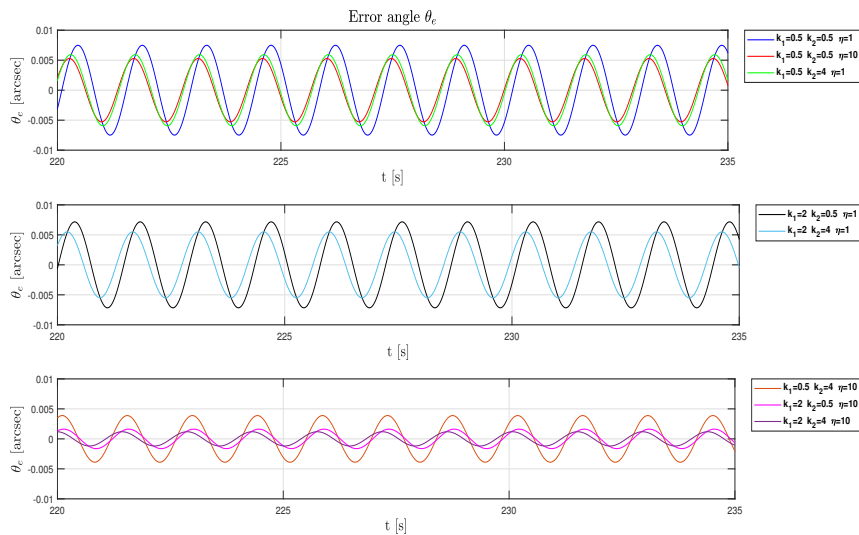


Figure 5.35: Error angle θ_e with variable k_1, k_2 and η

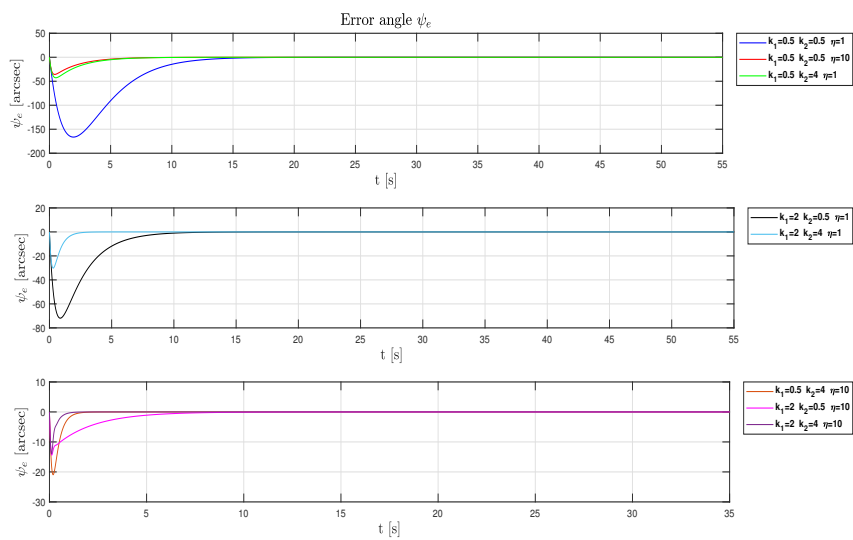


Figure 5.36: Error angle ψ_e with variable k_1 , k_2 and η

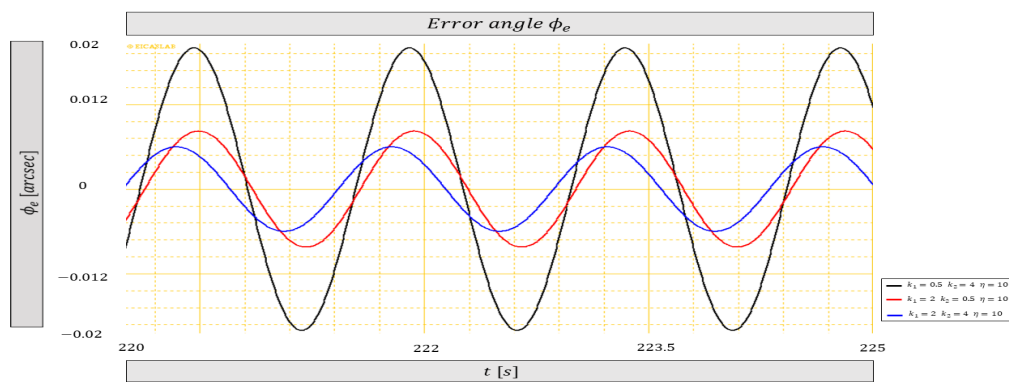


Figure 5.37: EICASLAB results of ϕ_e with fixed $\eta = 10$ and variable k_1 , k_2

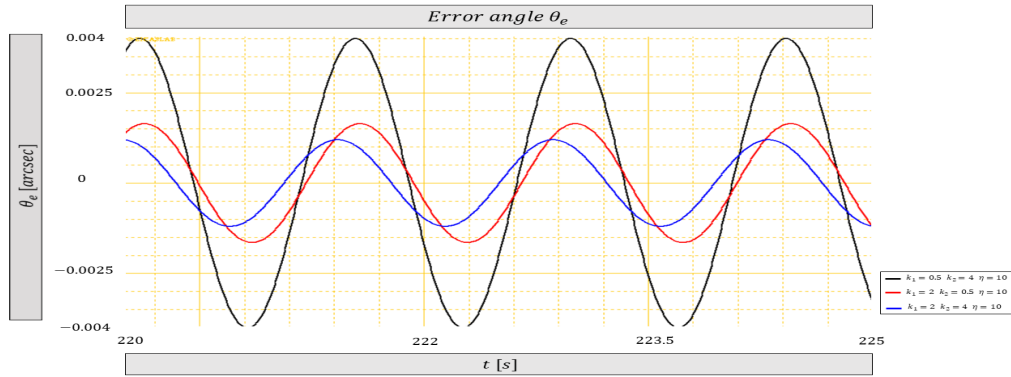


Figure 5.38: EICASLAB results of θ_e with fixed $\eta = 10$ and variable k_1, k_2

5.3 Comments and comparisons

Before making some comments and comparisons about the the results obtained with the three different control approaches, it must be pointed out that the choice of setting the control laws parameters, related to a single Cardan angle, equal to each other has been made to simplify all the simulation operations. It is quite evident, from the theoretical analyses made in chapter 2, 3 and 4, that it is possible to have different values for each of the three control laws. Therefore, by considering the specific set of controller parameters for each Tait-Bryan angle, one of the results shown in the previous figures can be obtained. Moreover, it must be pointed out that for all the simulations the steady state angular speed of the wheel aligned with the z-axis, which is the one related to the most relevant control action, has assumed more or less the same value. This means the disturbances produced by this wheel on the x and y axis of the body frame have been characterized by almost the same amplitude and frequency value.

About the time trend of the error angles, displayed in the previous sections, it can be noticed that in the disturbances-free case, the PD control and the feedback linearisation approach with the linear controller produce in some situations oscillating behaviour during the transient, which can be suitably damped by increasing the coefficient ζ . This situation, instead, never occurs with the FL plus the non-linear controller method. Indeed, it is always obtained a not oscillating time trend of the error angle ψ_e . Anyway, all the

three control systems are able to produce quite good results when suitable sets of parameters are chosen for the control law. This means that the new approach proposed in this thesis can be considered a valid alternative to the classical PD structure. Indeed, with the pole placement approach, the same result of the PD control can be obtained. And, quite good performance can also be attained with the sliding mode technique.

Instead, when the RWs disturbances act on the overall system, it has been noticed that all the three control methodology are able to provide good attenuation of the oscillating time trend of ϕ_e and θ_e , by properly modifying the specific parameters. Therefore, also in this case, the new control approach can be considered as valid as the Proportional-Derivative one, which is in general the most used technique.

Finally, it is important to highlight that the non-linear controller can provide robustness to the control system due to its non-linear term, characterized by the sigmoidal function. This can be a key characteristic that can lead to prefer this control strategy rather than the previous ones, when the knowledge of the satellite inertia matrix is not perfect. As it will be mentioned in the conclusive chapter, it can be a really interesting future work to be developed.

Conclusions and future works

This thesis has been developed with the specific purpose of performing an initial analysis of the reaction wheels disturbances effects on the attitude control system of a small satellite (a 3U CubeSat) and understanding if a new control approach, based on the feedback linearisation, could be as valid as the classical method characterized by the PD control. So, it has been noticed that the reaction wheels produce a sum of sinusoidal disturbances, whose amplitude and frequency increase with the rotational speed, when they are employed for the attitude control. Consequently, the satellite telescope is subject to an oscillating/vibrating motion, known as *jitter*, which can strongly influence the desired photometric analysis. Therefore, the control system must be able to reduce as much as possible the amplitude of the disturbances and so decreasing the amplitude of error angles oscillations. By the way, the classical PD approach is able to achieve the above-mentioned objective, as shown in chapter 5. Moreover, it has been discovered that also this different control strategy ensures as good performance as the one that can be obtained with the classical methodology. In particular, it has been found out that the FL approach with a linear controller, based on the pole placement technique, produces the same results of the Proportional-Derivative method. Therefore, it can be definitely stated that the proposed control structure can be employed for the attitude control of a small satellite, when three reaction wheels are used as actuators.

Now, some future works that can be developed will be analysed.

- **Environmental disturbances:** this work of thesis has neglected any kind of disturbances comes from the environment like gravity gradient, magnetic effects and aerodynamic drag. As already mentioned they

can lead to an augmented control action and, consequently, higher rotational speeds of the RWs, which would produce disturbances with higher amplitude. So, in a future work they must be included in the control system structure.

- **Satellite inertia matrix uncertainty:** another possible element that can be considered is the uncertainty related to the inertia matrix of the spacecraft. So, at first, it is possible to vary all or some elements of the matrix but blinding these variations to the controller, in order to verify potential robustness properties of the control system. By the way, the sliding mode control has been chosen for this reason. Indeed, the non-linear sigmoidal term inside the control law is used to increase the robustness of the controller. Therefore, suitable comparisons between the robustness of a PD controller and the sliding mode one can be developed.
- **A/D and D/A effects:** the effects coming from the conversion operations can also be considered. So, it can be analysed how much the quantization process influences the control performance. Moreover, it is also interesting to evaluate the impact of different sampling time values.
- **Practical implementation:** since with the EICASLAB software the C code of the controller has been written, another interesting future work could be the development of the control law on a specific target board, in order to move towards a real practical implementation. For instance, by exploiting the support given by EICASLAB to Arduino board, it is possible to use it for the controller and a myRio board, by National Instruments, to simulate the plant and all the other subsystems. In this way a Hardware in the Loop procedure can be analysed.

Bibliography

- [1] David S. Bayard. “High-Precision Three-Axis Pointing and Control”. In: 2010.
- [2] Hywel Curtis. *Reaction wheels: an overview of attitude control systems available on the global marketplace for space*. 2019. URL: <https://blog.satsearch.co/2019-07-25-reaction-wheels-an-overview-of-attitude-control-systems-available-on-the-global-market-place-for-space>.
- [3] David Darling. *Reaction Wheel*. 2016. URL: https://www.david-darling.info/encyclopedia/R/reaction_wheel.html.
- [4] Rebecca A. Masterson. “Development and validation of empirical and analytical reaction wheel disturbance models”. In: 1999.
- [5] Gourav Namta. *Let’s talk about CubeSats*. 2018. URL: <https://blog.satsearch.co/2018-11-13-lets-talk-about-cubesats>.
- [6] Carlo Novara. “Feedback linearization”. Slides of *Nonlinear control and aerospace applications* lessons (Politecnico di Torino A.A.2019/2020).
- [7] Carlo Novara. “Sliding mode control”. Slides of *Nonlinear control and aerospace applications* lessons (Politecnico di Torino A.A.2019/2020).
- [8] *Orbital Mechanics for Engineering Students*. Butterworth-Heinemann, 2019.
- [9] Christopher Masaru Pong. “High-precision pointing and attitude estimation and control algorithms for hardware-constrained spacecraft”. In: 2014.

- [10] Christopher Masaru Pong et al. “Achieving high-precision pointing on ExoplanetSat: initial feasibility analysis”. In: *Astronomical Telescopes + Instrumentation*. 2010.
- [11] Christopher Masaru Pong et al. “One-arcsecond line-of-sight pointing control on exoplanetsat, a three-unit CubeSat”. In: 2011.
- [12] Joel Shields et al. “Characterization of CubeSat Reaction Wheel Assemblies”. In: 2017.
- [13] Matthew William Smith et al. “On-Orbit Results and Lessons Learned from the ASTERIA Space Telescope Mission”. In: 2018.
- [14] *Spacecraft dynamics and control: a practical engineering approach*. Cambridge University Press, 1997.